UNIVERSITÀ DEGLI STUDI DI PADOVA

DIPARTIMENTO DI INGEGNERIA CIVILE, EDILE ED AMBIENTALE

CORSO DI LAUREA MAGISTRALE IN INGEGNERIA CIVILE

Tesi di laurea Magistrale in

Ingegneria Civile

Curriculum Strutture

STUDY ON THE SAFETY LEVEL OF FRP REINFORCED CONCRETE BEAMS WITHOUT TRANSVERSE REINFORCEMENT, DESIGN WITH DIFFERENT GUIDELINES

Relatori:

Ch.mo Prof. Joan Ramon Casas

Ch.mo Prof. Carlo Pellegrino

Laureando: Luca Sportiello

Anno Accademico 2014/2015

UNIVERSITÀ DEGLI STUDI DI PADOVA

DIPARTIMENTO DI INGEGNERIA CIVILE, EDILE ED AMBIENTALE

CORSO DI LAUREA MAGISTRALE IN INGEGNERIA CIVILE

Tesi di laurea Magistrale in

Ingegneria Civile

Curriculum Strutture

STUDY ON THE SAFETY LEVEL OF FRP REINFORCED CONCRETE BEAMS WITHOUT TRANSVERSE REINFORCEMENT, DESIGN WITH DIFFERENT GUIDELINES

Relatori:

Ch.mo Prof. Joan Ramon Casas

Ch.mo Prof. Carlo Pellegrino

Laureando: Luca Sportiello

Anno Accademico 2014/2015

Contents

Introduction

The use of Fiber Reinforced Polymer (FRP) composites, as internal reinforcement, for concrete structural elements is a widespread practice in many countries, in substitution of conventional steel reinforcement. Due to their durability, high strength-to-weight ratio, and good fatigue properties, fiber reinforced polymers (FRP) are considered an advantageous alternative to steel for internal reinforcement of concrete structures. However, the FRP reinforcement presents some differences when compared to steel reinforcing bars, such as a lower modulus of elasticity and a linear elastic stress–strain diagram up to rupture, which implies a lack of plastic behavior. Existing experimental programs stressed a reduction of the shear strength of concrete members reinforced longitudinally with FRP bars compared to specimens with the same ratio of steel reinforcement (1). While flexural mechanisms are clearly established, there is not a consensus among the engineers and scientists about how to predict, for design purposes, the shear strength of FRP reinforced concrete beams. It is commonly accepted that the shear strength in a RC beam is composed by the contribution of several mechanisms, which can be summarized in:

a) the shear resisted by the compressed concrete chord;
b) the friction forces developed along the crack length, which are contrary to the relative displacement of both crack faces (*aggregate interlock*);
c) the residual tensile strength existing between inclined cracks, which acts as a tie of the truss mechanism jointly with the compression chord, the tensile reinforcement and the concrete compression struts;
d) the shear strength provided by the longitudinal reinforcement (*dowel action*).

The relative contribution of each mechanism changes as the load increases: in general, c) and d) are small compared to the contribution of the other mechanisms. In the absence of stirrups, the only constrain to the downwards vertical displacement of the longitudinal reinforcement is provided by the concrete cover. For high load levels, splitting of the concrete cover takes place under the vertical component of the concrete struts, dramatically reducing the dowel action and the residual tensile stresses in the web between cracks. Furthermore, cracks width increase as the load increases, reducing the friction along the crack length. In elements without stirrups this effect is especially relevant, since cracks are not crossed by any reinforcement, except the flexural bars, which constrains the relative movements between their surfaces.

In the case of FRP reinforced beams without stirrups, these effects are more remarkable than in steel reinforced ones, since the modulus of elasticity of CFRP and GFRP bars are significantly lower than that of steel bars. Consequently, crack widths are bigger and the bars shear stiffness is lower, thus reducing both the aggregate interlock and the dowel action mechanisms. Therefore, in FRP reinforced elements, the shear strength provided by the longitudinal reinforcement can be neglected. An important mechanism of shear transfer at high load levels is the shear force carry by the compressed concrete zone where the compressive stresses increases as the load increases. Since the lower modulus of elasticity of FRP reinforcing bars influences both the level of concrete compressive stresses and the neutral axis depth under flexure, this parameter must be taken into account in order to evaluate the ultimate shear capacity. Alkhrdaji et al. (2) concluded that the shear strength was proportional to the amount of longitudinal reinforcement. In addition, Tureyen and Frosch (3), El-Sayed et al. (4) (5), and Alam and Hussein (6) observed that the shear strength of FRP reinforced elements is proportional to the axial stiffness of the longitudinal reinforcement.

Shear design equations of FRP reinforced concrete beams without stirrups have been developed and many of them have been included in the shear

provisions of the Codes of Practice. Most of the formulations were developed modifying existing equations for shear design of concrete members with steel, taking into account the difference in modulus of elasticity (CNR-DT 203/2006 (7), ACI440.1R-06 (8), CAN/CSAS6-02 (9) and CAN/CSAS6-06 (10), JSCE (11)). The ACI 440.1R-06 guideline is based on the work of Tureyen and Frosch (3) and considers the axial stiffness of the FRP through the depth of the compression block using a cracked section analysis. Previous analysis of the existing formulations concluded that most of the current guidelines provide conservative values of the concrete shear strength (experimental to theoretical ratios around 2). The CSA S6-06 Addendum contained the best balance of accuracy, the CNR-DT203 produced unreliable results and ACI-440.1R-06 and JSCE are very conservative. The differences between the experimental and theoretical results can be explained by the fact that the shear design equations for elements without transverse reinforcement are not always supported on solid theories that explain the observed behavior, but mainly they are empirically based, by adjustments of equations to experimental results.

Objectives

The purpose of this work is to study the safety level of seven reinforced concrete bridges without shear reinforcement. Analyzed bridges belong to the Spanish catalogue realized by Casado (12) in 1942 with the aim to suggest some standard solutions for cross section geometry and reinforcement amount in order to give a design guideline in a country so far lacking of adequate design codes.

The flexural reinforcement with Carbon Fiber Reinforced Polymer bars, it will be designed according to Italian guideline CNR-DT 203/2006 (7). Then, a simple model for the prediction of the shear strength of FRP reinforced concrete beams and one-way slabs without shear reinforcement is utilized. The method proposed by Marí et al. (13) is based on the principles of structural mechanics and on the experimentally observed behavior of FRP RC beams at shear-flexural failure. Simple design formulation is provided, which explicitly account for those parameters governing the shear strength, such as the concrete tensile strength, the amount of longitudinal reinforcement ratio and the ratio between the elastic modulus of the longitudinal reinforcement and the concrete.

A reliability-based analysis it will be conducted to calculate the probability of failure of the seven reinforced concrete bridges. In order to calculate the probability of failure a Monte Carlo simulation is performed. The aim was to solve the limit state function, which involves all the variables belonging to the general problem $(R - S \geq 0)$ as random variables, each of which with its statistical properties. Monte Carlo simulation allow to simulate a large number of trials. The Marí's formulation is set within the simulation including the basic variables which affects the shear strength. Eventually, the results obtained are compared with those obtained according to Italian guideline CNR-DT 203, and to the American ACI 440.1R-06 .

Chapter 1

Fiber Reinforced Polymer for RC structures

1.1. FRP as internal reinforcement

The use of Fiber Reinforced Polymer (FRP) composites, as internal reinforcement, for concrete structural elements is a widespread practice in many countries, in substitution of conventional steel reinforcement. There are several reasons that make the use of FRP bars preferable to conventional steel ones. The peculiar characteristic of FRP materials of not being susceptible to corrosion phenomena makes their use particularly suitable in different situations, such as for marine structures as well as structures exposed to harsh environments. Furthermore, glass FRP composites (GFRP) are non-conductive and therefore can be used effectively when stray currents are an issue, as in the case of structures serving rail transportation. In the building industry, the use of this technology can be adopted for the construction of building slabs for civil or industrial use. The reasons that lead to choosing FRP in this case can be related not only to durability issues, but also to the possibility of taking advantage of specific properties of composite materials, such as magnetic transparency. The latter is of fundamental importance in the construction of hospital rooms to avoid interference where Magnetic Resonance Imager (MRI) units are located. There are further attractive and promising uses of composites materials in the building of temporary structures and tunnel covering.

Several international guidelines are currently available supporting the design, construction and control of such structures. The main documents are issued by the *fib* ("FRP Reinforcement for reinforced concrete structures", 2005, Task Group 9.3); the *American Concrete Institute* (ACI 440.1R-06, 2006, "Guide

for the design and construction of concrete reinforced with FRP bars"); the two documents published by the *Canadian Standard Association* (CAN/CSA-S6-02, 2002, "Design and construction of building components with Fiber-Reinforced Polymers", and CAN/CSA-S6-06, 2006, "Canadian high bridge design code"); the document of *Japan Society of Civil Engineers* (JSCE, 1997, "Recommendation for design and construction of concrete structures using continuous Fiber Reinforcing Materials") and the most recent document of the *Italian National Research Council* (CNR-DT 203/2006, 2006, "Guide for the design and construction of concrete structures reinforced with Fiber-Reinforced Polymer bars"). From a theoretical perspective, there are no conceptual differences in relation to the classical theory of steel reinforced concrete elements. What does need to be taken into account, is the different mechanical behavior of FRP material, whose constitutive law is fundamentally linear elastic up to failure. Therefore the methods assuming plastic redistribution capability are not applicable. Moreover, the nearly complete lack of ductility displayed by FRP reinforced concrete structures shall be taken into account for applications in seismic field. In such cases, the design spectrum shall be derived from the elastic spectrum by setting the structural factor to an appropriate value to account for the elastic behavior shown by an element reinforced with FRP bars.

1.2. Properties of Composite Materials

Composite materials exhibit the following characteristics:

- They are comprised of two or more materials (phases) different in nature and "macroscopi-cally" distinguishable.
- At least two phases have physical and mechanical properties quite different from one another, such to provide FRP material with different properties than those of its constituents.

Fiber-reinforced composites with polymeric matrix satisfy both characteristics given above. In fact, they consist of both organic polymeric matrix

and reinforcing fibers. For structural applications the most utilized are the glass fibers (GFRP), carbon fibers (CFRP) and aramid fibers (AFRP). FRP bars properties, such as high temperature performances, corrosion resistance, dielectric properties, flammability and thermal conductivity are mainly derived from the properties of their components.

The matrix is considered an isotropic material, while the reinforcing phase (with the exception of glass fiber) is an anisotropic material (different properties in different directions). The defining characteristics of FRP materials are as follows:

- Geometry: shape and dimensions;
- Fiber orientation: the orientation with respect to the symmetrical axes of the material; when random, the composite characteristics are similar to an isotropic material isotropic"). In all other cases the composite is considered an anisotropic material;
- Fiber concentration: volume fraction, distribution (dispersion).

1.3. FRP bars

FRP reinforcement is available in different forms such as; bars, grids, prestressing tendons, and laminates to serve a wide range of purposes. This work focuses on using FRP bars (Fig. 1.1) as an internal reinforcing material for concrete members (FRP-RC). The main characteristics of FRP bars, can be summarized as follows:

- high durability, in particular elevated resistance to corrosion;
- high strength-to-weight ratio;
- good fatigue properties;
- high properties as thermic and electric insulator.

FRP are characterized by a unidirectional array of fibers, generally having a volume fraction ranging between 50% and 70%. Therefore, composites are in most cases a non-homogeneous and anisotropic material.

The fibers exhibit high tensile strength and stiffness and are the main load carrying element. The resin offers high compressive strength and binds the fibers into a firm matrix. The additives help to improve the mechanical and physical properties as well as the workability of composites. The GFRP is the least expensive but has lower strength and significantly lower stiffness compared to other alternatives. CFRP is the stiffest, most durable, and most expensive one. AFRP has improved durability and excellent impact resistance.

Fig. 1-1: *FRP bars available on the market (CNR-DT203/2006).*

Chapter 2

A model for the prediction of the shear strength

2.1. RC shear strength

While flexural mechanisms are clearly established, there is not a consensus among the engineers and scientists about how to predict, for design purposes, the shear strength of FRP reinforced concrete beams. As observed in existing experimental programs, concrete members reinforced longitudinally with FRP bars show a reduction of the shear strength compared to specimens with the same ratio of steel reinforcement.

As is commonly know, the shear strength in reinforced concrete beam is composed by the contribution of several mechanisms whose relative importance changes as the load increases. In general, the residual tensile strength existing between inclined cracks, which acts as a tie of the truss mechanism jointly with the compression chord, the tensile reinforcement and the concrete compression struts, and the shear strength provided by the longitudinal reinforcement (dowel action) are small compared to the contribution of the others mechanisms like the shear resisted in the uncracked compressed zone of the beam, and the interface forces developed along the crack length (aggregate interlock).

In the absence of stirrups, the only constrain to the downwards vertical displacement of the longitudinal reinforcement is provided by the concrete cover. For high load levels, splitting of the concrete cover takes place under the vertical component of the concrete struts, thus drastically reducing the dowel action and the residual tensile stresses in the web between cracks.

Furthermore, cracks width increase as the load increases, reducing the friction along the crack length. In elements without stirrups this effect is especially relevant, since cracks are not crossed by any reinforcement, except the flexural bars, which constrains the relative movements between their surfaces.

In the case of FRP reinforced beams without stirrups, these effects are more remarkable than in steel reinforced ones, since the modulus of elasticity of FRP bars are significantly lower than that of steel bars. Consequently, crack widths are bigger and the bars shear stiffness is lower, thus reducing both the aggregate interlock and the dowel action mechanisms. Therefore, in FRP reinforced elements, the shear strength provided by the longitudinal reinforcement can be neglected.

An important mechanism of shear transfer that becomes relevant at high load levels is the shear force carry by the compressed concrete zone where the compressive stresses increase as the load increases. Since the lower modulus of elasticity of FRP reinforcing bars influences both the level of concrete compressive stresses and the neutral axis depth under flexure, this parameter must be taken into account in order to evaluate the ultimate shear capacity, as will be seen in detail in this chapter.

The main objective of the existing experimental programs on the study of the shear strength of FRP reinforced members without transverse reinforcement is to study\ the effect of the reinforcement amount and stiffness on the shear strength of FRP reinforced elements. Some authors concluded that the shear strength was proportional to the amount of longitudinal reinforcement. In particular, some observed that the shear strength of FRP reinforced elements is proportional to the axial stiffness of the longitudinal reinforcement.

In this chapter is presented a simple model for the prediction of the shear strength of FRP reinforced concrete beams and one-way slabs without shear reinforcement, proposed by A. Marí et al. (13). The method is based on the principles of structural mechanics and on the experimentally observed behavior of

FRP RC beams at shear-flexural failure. Simple design equations are provided, which explicitly account for those parameters governing the shear strength, such as the concrete tensile strength, the amount of longitudinal reinforcement ratio and the ratio between the elastic modulus of the longitudinal reinforcement and the concrete.

2.2. Basis of the proposed method

The main hypothesis, based on experimental observations, of the method presented in this chapter is that just before failure, the main mechanism that contributes to the shear strength of the beam is the shear carried by the concrete compression chord, neglecting, at this stage, the contributions of the rest of mechanism mentioned in Section 3.1.

The studied model is based on the experimental analysis of the behavior of an FRP reinforced concrete beam without transverse reinforcement, subjected to an increasing point load. A typical inclined crack pattern, as well as normal and vertical shear stresses are produced. By increasing the load, cracks propagate and open, and the normal and shear stresses increase and progressively migrate towards the uncracked concrete compression chord (**Fig. 2-1**).

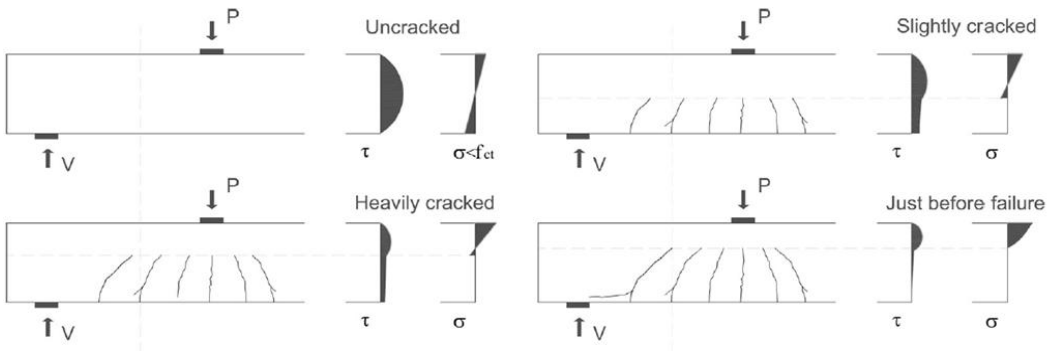

Fig. 2-1: *Evolution of stresses distribution in a cracked section near the support*

The tensional state at any point of this chord is characterized by normal and shear stresses coming from the bending moment. Thus, the principal compressive (σ_{I}) and tensile (σ_{II}) stresses produced by this tensional state are, according to the Mohr's circle for stresses:

$$\sigma_{\mathrm{I,II}} = \frac{\sigma_x}{2} \pm \sqrt{\left(\frac{\sigma_x}{2}\right)^2 + \tau^2} \qquad (2.1)$$

The shear stresses τ_c and τ_t are the shear stresses that take place at the fibers of the concrete chord where the principal stresses reach respectively the concrete compressive and tensile strengths:

$$\tau_c = f_{cd} \cdot \sqrt{1 - \frac{\sigma_x}{f_{cd}}} \qquad (2.2)$$

$$\tau_t = f_{ct} \cdot \sqrt{1 + \frac{\sigma_x}{f_{ct}}} \qquad (2.3)$$

Two failure modes can be defined (according to Park et al. (14)). Tensile failure mode that is considered to take places when the principal tensile stress at any point of the concrete chord reaches the tensile strength ($\sigma_{\mathrm{II}} = f_{ct}$ and $\tau = \tau_{\mathrm{t}}$). Compressive failure mode, instead, is assumed to occur when the principal compressive stress reaches, at any point of the concrete chord, the compressive strength ($\sigma_{\mathrm{I}} = f_{cd}$ and $\tau = \tau_{\mathrm{c}}$). Since the concrete compressive strength takes values more than ten times greater than those of the tensile concrete strength, the load level necessary to produce the compressive failure, in general, is much higher than that necessary to produce tensile failure.

Furthermore, since the normal stresses at any section increase with the bending moment increases, according to Eq. (2.2) and (2.3), in simple supported beams, tensile failure is expected to occur in sections near the support,

while compression failure is expected to occur in sections closer to the center span.

For the reasons above mentioned, in the studied model it is assumed that the ultimate shear capacity in FRP reinforced concrete beams without shear reinforcement is associated to the tensile failure at a critical section placed near the support. Thus, to evaluate the principal tensile stress at any fiber of the compression chord of a section, which depends on the bending moment acting on the section, it's necessary to determine the depth of the compression chord.

For this purpose and in order to obtain at which fiber of the concrete chord the maximum principal compressive and tensile stresses takes place, it is first needed to assume distributions for the normal and shear stresses along the compression chord depth.

It is hence supposed that compressed concrete follows a parabolic stress-strain law with a given modulus of elasticity in the origin, E_c, and horizontal slope for the strain ε_0, when the stress σ reaches the compression strength f_c. The peak strain ε_0 is assumed to be a function of E_c and f_c so that, is sufficiently captured the behavior for low and medium stress levels:

$$\sigma = f_c \cdot \left(\frac{2 \cdot \varepsilon}{\varepsilon_0} - \frac{\varepsilon^2}{\varepsilon_0^2} \right) \quad (2.4)$$

$$\varepsilon_0 = \frac{2 \cdot f_c}{E_c} \quad (2.5)$$

As a consequence of the hypothesis made about the contributions of each mechanism just before failure, the shear stress below the neutral axis must be zero. Furthermore, a parabolic distribution of the shear stress on the concrete compression chord can be assumed, with zero values at both end fibers (**Fig. 2-2**).

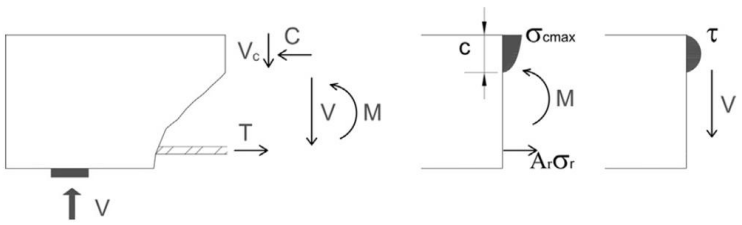

Fig. 2-2: *Distribution of normal and shear stresses at failure at the concrete compression chord.*

2.2.1. Neutral axis depth and compression concrete stresses

In order to evaluate the depth of the concrete compression chord, which is assumed to be equal to the neutral axis depth in flexure in cracked state, a non-linear sectional analysis must be performed and it can be obtained through a iteratively process. For this reason, the neutral axis depth is firstly obtained assuming a linear stress-strain law for concrete in compression, and subsequently corrected by a factor, to account the influence of the non-linear concrete stress-strain. Thus, for sections with only tensile reinforcement the depth of the neutral axis can be written by the following expression:

$$\xi = \frac{c}{d} = F_{\alpha,\mu} \cdot \frac{c_l}{d} \tag{2.6}$$

$$\xi_l = \frac{c_l}{d} = \alpha \cdot \rho_r \cdot \left(1 + \sqrt{1 + \frac{2}{\alpha \cdot \rho_r}} \right) \tag{2.7}$$

Where c_l is the neutral axis depth calculated assuming a linear stress distribution, which depends on the modular ratio $\alpha = E_r / E_c$ and on the reinforcing ratio $\rho_r = A_r / (b \cdot d)$. The subscript *r* indicates the variables referred to the FRP reinforcements, *b* and *d* are the section width and the effective depth, respectively. The neutral axis depth is calculated by multiplying the above-mentioned value by the factor $F_{\alpha,\mu}$. Such correction factor is obtained solving the sectional analysis for different levels of the non-dimensional applied moment $\mu = M / (f_{ct} \cdot b \cdot d^2)$ and for different values of the equivalent modular ratio α.

The higher is the applied moment and the lower is the modular ratio, the higher is the neutral axis correction factor, as shown in **Fig. 2-3**.

Furthermore, a stress correction factor should be calculated to be applied to the concrete stresses obtained assuming a linear behavior for concrete in compression. This factor is lower as the lower is the modular ratio and the higher is the applied moment (**Fig. 2-4**). Thus, for low values of the modular ratio, the depth of the neutral axis increases and the maximum concrete stress decreases in respect of those values obtained by a linear concrete stress distribution, as can be seen in **Fig. 2-5**.

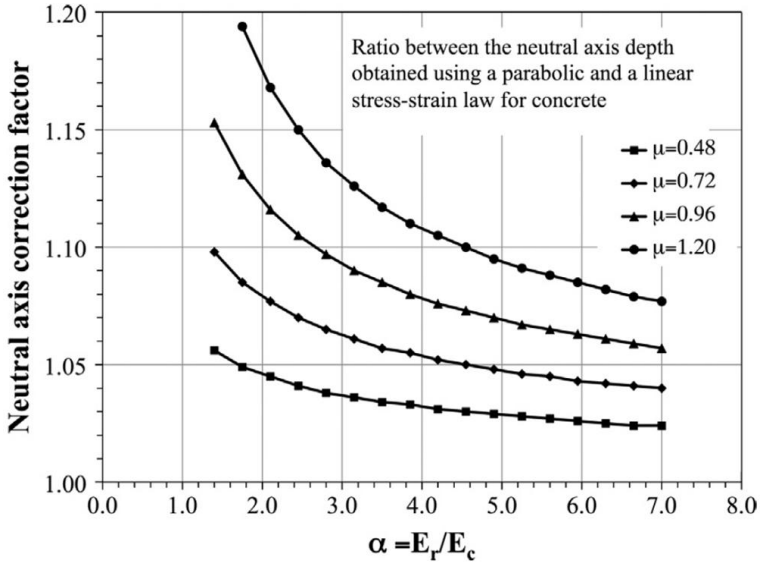

Fig. 2-3: *Neutral axis correction factor* $F_{\alpha,\mu}$.

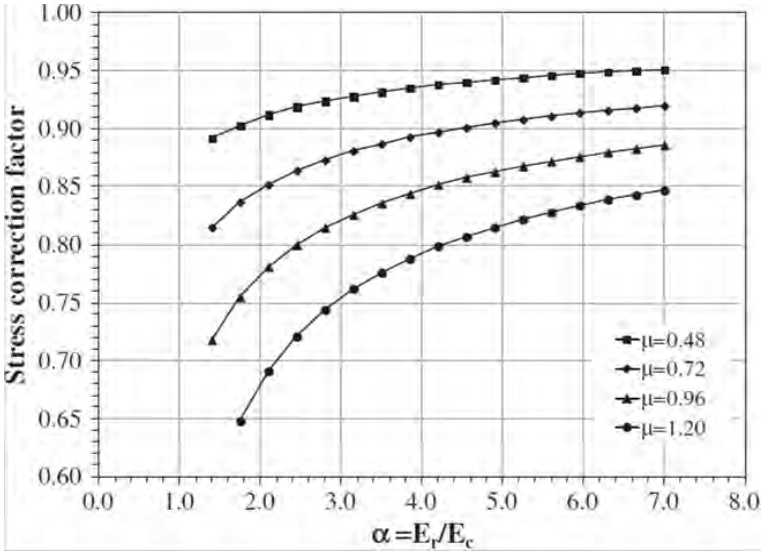

Fig. 2-4: *Concrete stress correction factor.*

Nevertheless, it is possible to see that for the fibers of the concrete compression chord around the mid-height of the neutral axis depth, the concrete stresses are practically equal. Indeed, observing the stress correction factor, obtained for different values of the modular ratio and different applied moment levels, at mid-height of the neutral axis depth, this is practically constant and equal to 1 (**Fig. 2-6**). Such result is relevant since the maximum principal tensile stress in the concrete chord take place at around mid-height of the neutral axis depth and therefore no stress correction is needed.

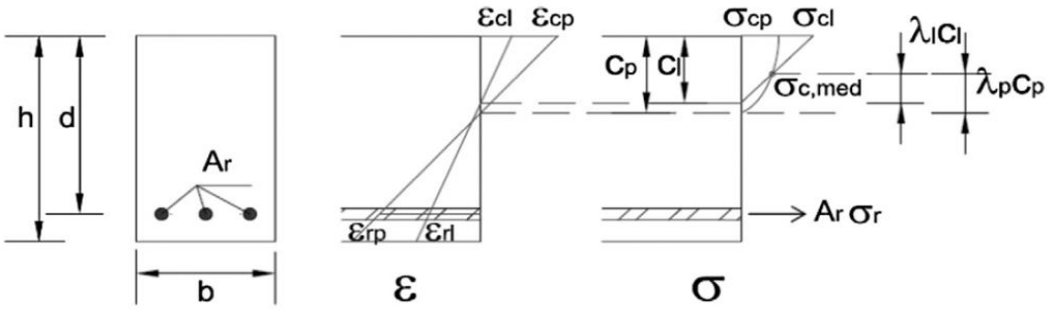

Fig. 2-5: *Neutral axis depth and maximum concrete stress*

2.2.2. Position of the maximum principal tensile stress

The distribution of the principal tensile stresses along the concrete chord (expressed in non-dimensional terms) is shown in **Fig. 2-7**. It can be observed how the position of the maximum principal tensile stress is not very sensitive to the relative distance of the cross section to the support ($d/a = V \cdot d/M$) and tends to takes place at a relative height $y/c = 0{,}45$ as the section approaches the support. A reasonable lower value equal to $y/c = 0{,}425$ is taken into account in the proposed model, which corresponds to the end of the discontinuity region at the support ($d/a = 1$).

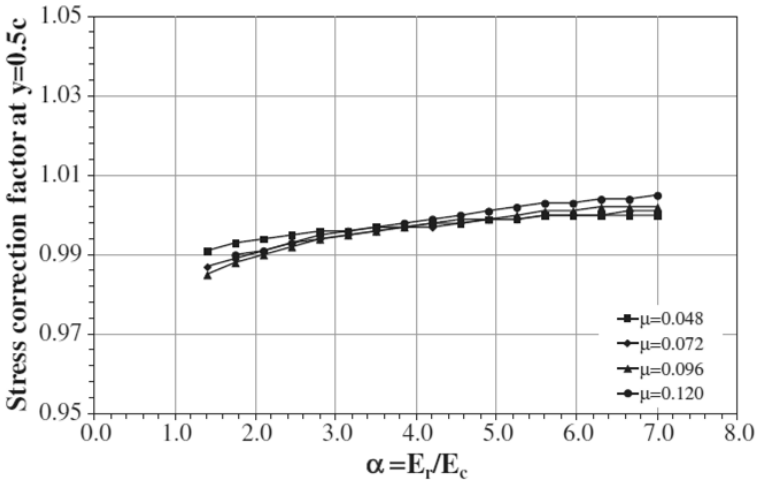

Fig. 2-6: *Stress correction factor at mid height of the neutral axis.*

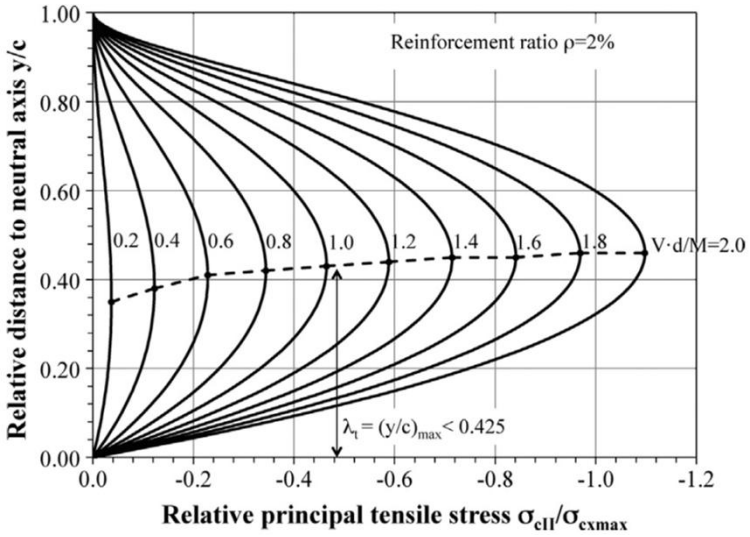

Fig. 2-7: *Distribution of principal tensile stresses at the concrete chord.*

2.3. Shear strength of FRP reinforced concrete beams

Once the position where the maximum principal tensile stress takes place $y = \lambda_t \cdot c$ is know, where the distance y is measured from the neutral axis, it can be written the expression of the parabolic shear stress distribution along the concrete chord:

$$\tau(y) = \frac{\tau_t}{\lambda_t \cdot (1 - \lambda_t)} \cdot \left(\frac{y}{c} - \frac{y^2}{c^2} \right) \qquad (2.8)$$

By integrating the shear stresses along the compression chord and substituting the expression for τ_t (2.3), it can be obtained the value of the shear force carried by the concrete chord when the principal tensile stress reaches the concrete tensile strength f_{ct}:

$$V_{u,t} = \int_0^c \tau(y) \cdot b \cdot dy = \frac{\tau_t \cdot b \cdot c}{6 \cdot \lambda_t \cdot (1 - \lambda_t)} = \frac{f_{ct} \cdot b \cdot c}{6 \cdot \lambda_t \cdot (1 - \lambda_t)} \cdot \sqrt{1 + \frac{\sigma_x}{f_{ct}}} \qquad (2.9)$$

σ_x is the concrete normal stress at a distance $y = \lambda_t \cdot c$ from the neutral axis. For the particular case of $\lambda_t = 0{,}425$, Eq. (2.9) becomes:

$$V_{u,t} = \frac{f_{ct} \cdot b \cdot c}{6 \cdot 0{,}425 \cdot (1 - 0{,}425)} \cdot \sqrt{1 + \frac{\sigma_x}{f_{ct}}} = 0{,}682 \cdot f_{ct} \cdot b \cdot c \cdot \sqrt{1 + \frac{\sigma_x}{f_{ct}}} \qquad (2.10)$$

At the distance $y = 0{,}425 \cdot c$ the normal concrete stress is obtained assuming a linear concrete stress distributions, as follows:

$$\sigma_x = 0{,}425 \cdot \sigma_{x,max}^{c} = \frac{0{,}425 \cdot 2M}{b \cdot c_l \cdot (d - c_l/3)} = \frac{0{,}85 \cdot M}{b \cdot c_l \cdot (d - c_l/3)} \qquad (2.11)$$

where $\sigma_{x,max}^{c}$ is the maximum compressive stress at the top fiber of the section calculated by imposing the rotational equilibrium of the section. At last, the maximum shear force carried by the compression chord is:

$$V_{u,t} = 0{,}682 \cdot f_{ct} \cdot b \cdot F_{\alpha,\mu} \cdot c_l \cdot \sqrt{1 + \frac{0{,}85 \cdot M}{f_{ct} \cdot b \cdot c_l \cdot (d - c_l/3)}} \qquad (2.12)$$

the neutral axis depth is expressed by correcting the value obtained assuming a linear stress distribution with the correction factor, as seen previously.

2.4. Shear design equations

As already mentioned, the failure mode considered occurs in sections near the support and more specifically, the critical section is assumed to be placed at the tip of the crack initiated closer to the support (section "B" in **Fig. 2-8**). The abscissa of the critical section is that corresponding to the point where the first flexural crack starts (x_{cr}), plus the drift of the crack produced by the combination of normal and shear stresses (D). According to experimental observation this

value can be assumed as $D = 0{,}85 \cdot d$, where d represents the effective height of the section.

For the considered simple supported beam subjected to an increasing point load, the value of the bending moment at the critical section will be (**Fig. 2-8**):

$$M = V_{u,t} \cdot (x_{cr} + 0{,}85 \cdot d) \geq M_{cr} + 0{,}85 \cdot V_{u,t} \qquad (2.13)$$

where $M_{cr} = \frac{b \cdot h^2}{6} \cdot f_{ct}$ is the cracking bending moment of the section.

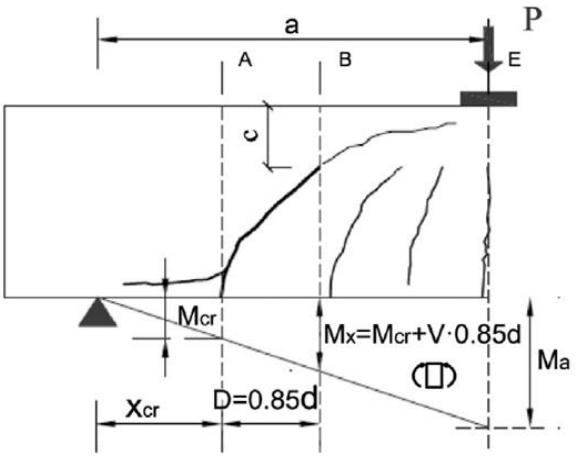

Fig. 2-8: *Position of the critical section in tensile failure mode*

By substituting the expression for the bending moment into Eq. (2.12), which expresses the tensile shear failure condition, and putting it in non-dimensional form, is obtained:

$$v_{u,t} = \frac{V_{u,t}}{f_{ct} \cdot b \cdot d} = 0{,}682 \cdot F_{\alpha,\mu} \cdot \xi_l \cdot \sqrt{1 + \frac{0{,}142 \cdot \left(\frac{h}{d}\right)^2 + 0{,}7225 \cdot v_{u,t}}{\xi_l \cdot (1 - \xi_l/3)}} \qquad (2.14)$$

which results to be a second order polynomial equation.

When shear failure occurs, the bending moment at the critical section is rather low and can be estimated conservatively in about two to four times the cracking moment. In the model utilized is assumed a value of $\mu_{v,t} = 3 \cdot \mu_{crack} \cong 0{,}6$. Solving the second order equation for different values of the neutral axis depth $\xi_l = c_l/d$ and for two different values of the correction factor $F_{\alpha,\mu}$ corresponding to the values of the modular ratio $\alpha = 1{,}4$ and $\alpha = 7$, it can be observed that the non-dimensional shear strength results to be an almost linear function of the relative neutral axis depth in flexure, as shown in **Fig. 2-9**.

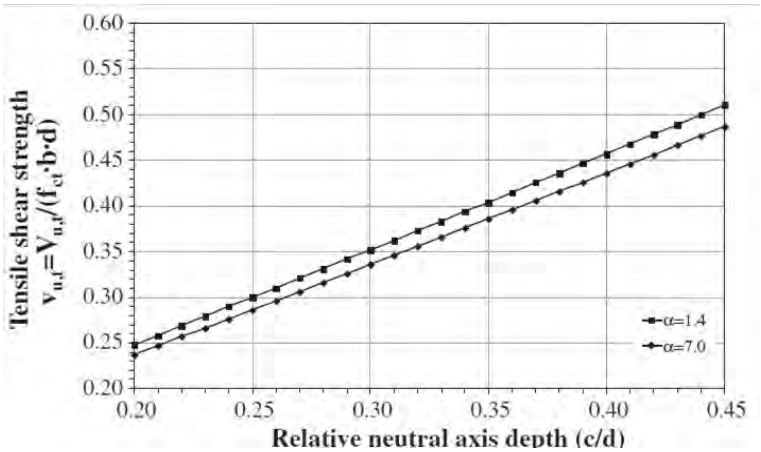

Fig. 2-9: *Non-dimensional shear strength for given values of α*

Therefore, the non-dimensional shear strength can be written as a linear expression that takes into account also the modular ratio α as follows:

$$v_{u,t} = \frac{V_{u,t}}{f_{ct} \cdot b \cdot d} = (1{,}072 - 0{,}01 \cdot \alpha) \cdot \frac{c_l}{d} + 0{,}036 \qquad (2.15)$$

It can be observed, by means Eq. (2.7), that the higher is the reinforcement amount ρ, the higher is the shear strength, since the neutral axis depth increases. The above formulation can be extended to the case of uniformly distributed load by introducing a parabolic bending moment law into Eq. (2.12), since the

assumption made about the critical section in beams subjected to point loads is still valid for a uniformly distributed load. Indeed, in beams subjected to this type of loading, the shear force decreases linearly with the distance to the support, while the bending moment increases according to a parabolic law, so the closer to the center span, the higher is the shear capacity. In the contest of this work, for the sake of simplicity, it will not be taken into account the different distribution of the applied load with respect to the point loads considered in the model and the formulation presented in this chapter will be utilized.

Chapter 3

Description of the studied bridges

3.1. Studied bridges

For the reliability analysis it will be performed a simulation in order to recreate a large number of tests on bridge structures. Seven different reinforced concrete bridges are considered. These are not existing bridges, but they are designed by considering the most common typologies of existing bridges in Spain, built in the 1940's. Indeed these bridges belong to a bridge national catalogue realized by C.F. Casado (12) in Spain in the 1942. The aim of the author was those to suggest some standard solutions for the cross section geometry and reinforcement amount, in order to give a design guideline in a country lacking of adequate design codes. For this reason, nowadays in Spain, existing bridges present, in the most of cases, those suggested characteristic.

For the aims of this work, it has been taken only the geometric characteristic of the cross sections and the concrete properties, while the flexural reinforcement is here designed according to *CNR-DT 203/2006* (7).

Two different typologies of bridges are analyzed:

— four girder bridges;
— three slab bridges.

In order to simply the references to each bridge, the following notion will be utilized. The first letter indicates the typologies of its cross section: "B" stands for "beam" and indicates *girder bridges*; whereas "S" that stands for "slab", indicates *slab bridges*. Then, the first letter is followed by numbers, which represent the span lengths in meters. Two digits are related for simply supported bridges and

four digits for continuous bridges. Eventually the last two letters "RC" state the material of the bridge, which is reinforced concrete. The characteristic compressive strength is taken equal to 20 MPa, which represents a quite low value for compressive strength, this because at that time no better materials were available.

3.2. Girder bridges

The four girder bridges are simply supported and have the same width of the cross section which counts six principal beams. The bridges differ in span length and height of principal and transverse beams. There are three transverse beams, one at the mid span and two at the ends. The common characteristic for girder bridges are resumed in **Table 3-1**.

	Symbol	***Value***	***Unit***
Total bridge width	B	9,35	m
Carriageway width	w	8,00	m
Left sidewalk width	b_l	0,80	m
Right sidewalk width	b_r	0,55	m
Base thickness	t_s	0,20	m
Sidewalk heigth	h_s	0,20	m
Pavimentation thickness	t_p	0,08	m

Table 3-1: *Geometric characteristic of the cross section.*

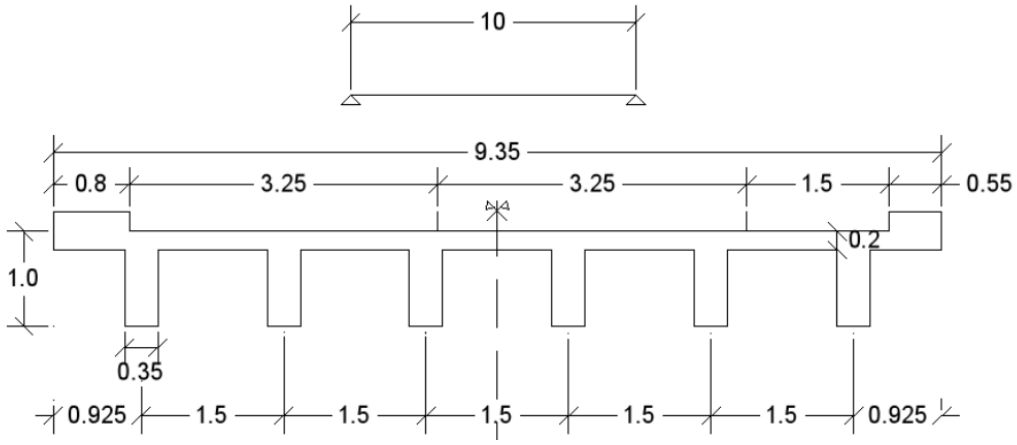

Fig. 3-1: *B10RC (dimensions in m).*

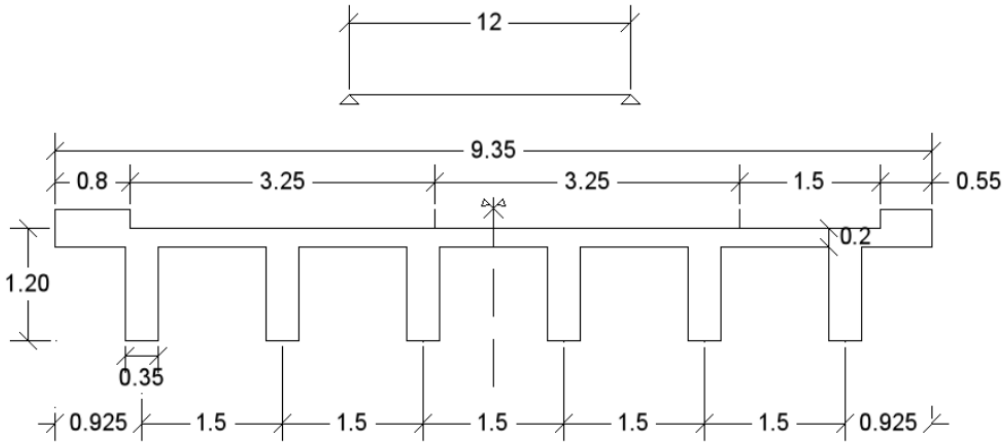

Fig. 3-2: *B12RC (dimensions in m).*

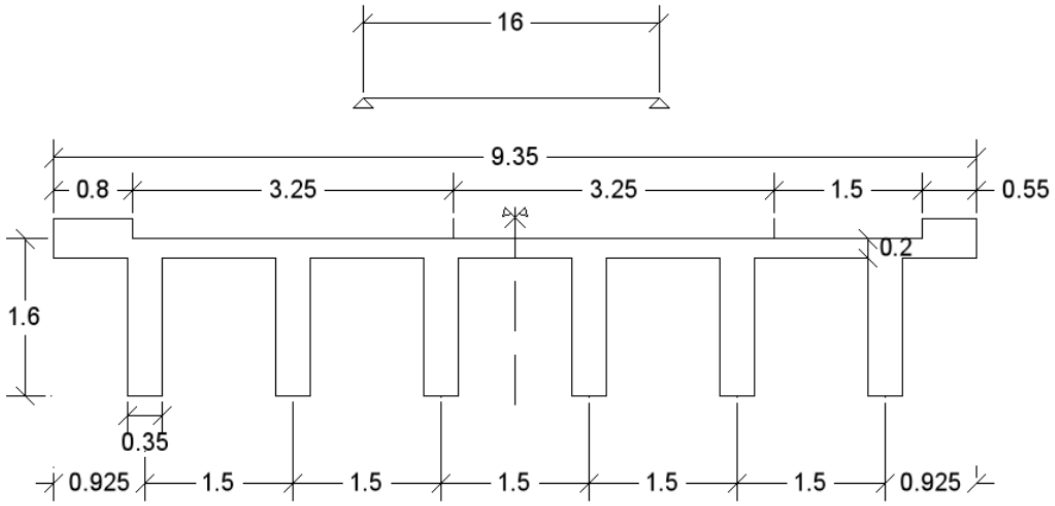

Fig. 3-3: *B16RC (dimensions in m).*

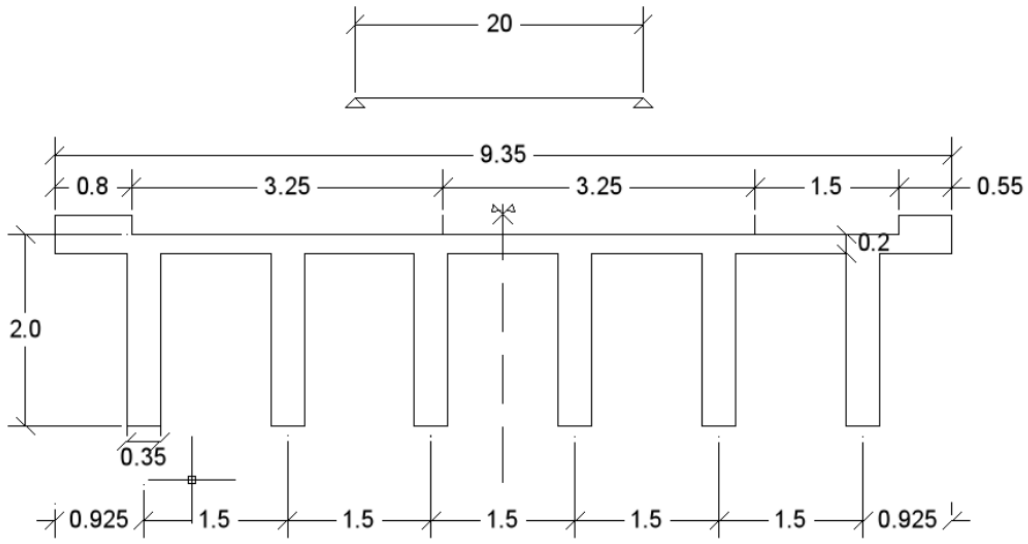

Fig. 3-4: B20RC *(dimensions in m).*

3.3. Slab bridges

Also for slab bridges, the section geometry is taken from the national catalogue by introducing little modifications. Only one of the slab bridges is simply supported, while the others two are continuous bridges with three spans. S10RC and S1015RC differ in cross section only for slab height. S1520RC present some differences on the shape of the cross section.

	Symbol	***Value***	***Unit***
Total bridge width	B	12,00	m
Carriageway width	w	10,00	m
Left sidewalk width	b_l	1,00	m
Right sidewalk width	b_r	1,00	m
Base thickness	t_s	0,15	m
Sidewalk heigth	h_s	0,20	m
Pavimentation thickness	t_p	0,08	m

Table 3-2: *Common geometric characteristics of cross section for S10RC and S1015RC.*

	Symbol	***Value***	***Unit***
Total bridge width	B	11,00	m
Carriageway width	w	10,00	m
Left sidewalk width	b_l	0,50	m
Right sidewalk width	b_r	0,50	m
Base thickness	t_s	0,20	m
Sidewalk heigth	h_s	0,20	m
Pavimentation thickness	t_p	0,08	m

Table 3-3: *Geometric characteristic of cross section for S1520RC.*

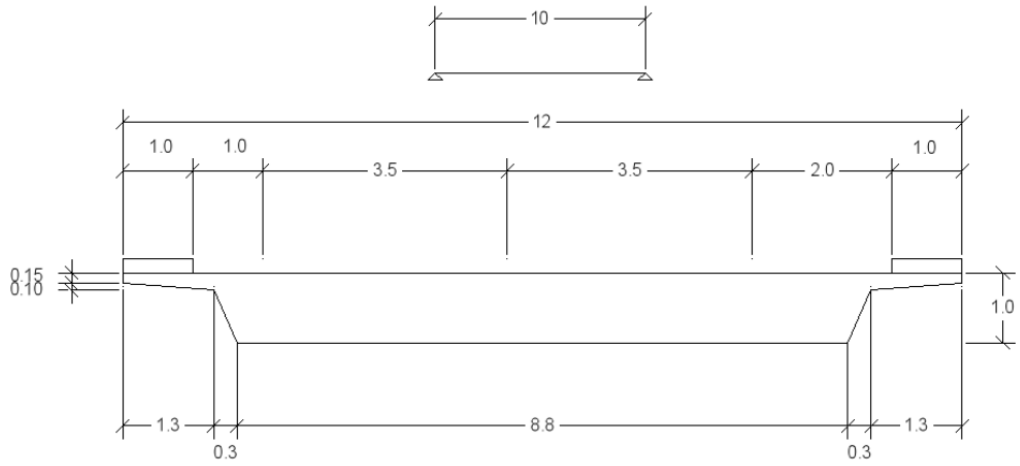

Fig. 3-5: *S10RC (dimensions in m).*

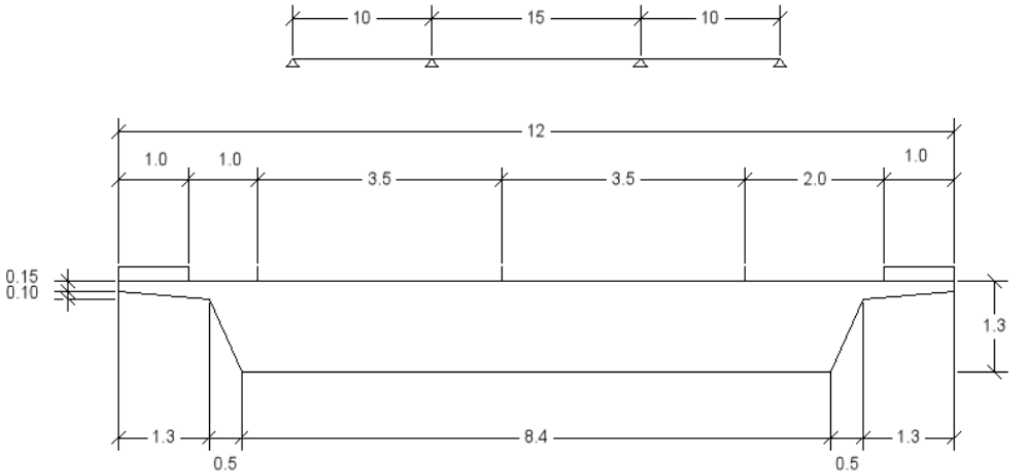

Fig. 3-6: *S1015RC (dimensions in m).*

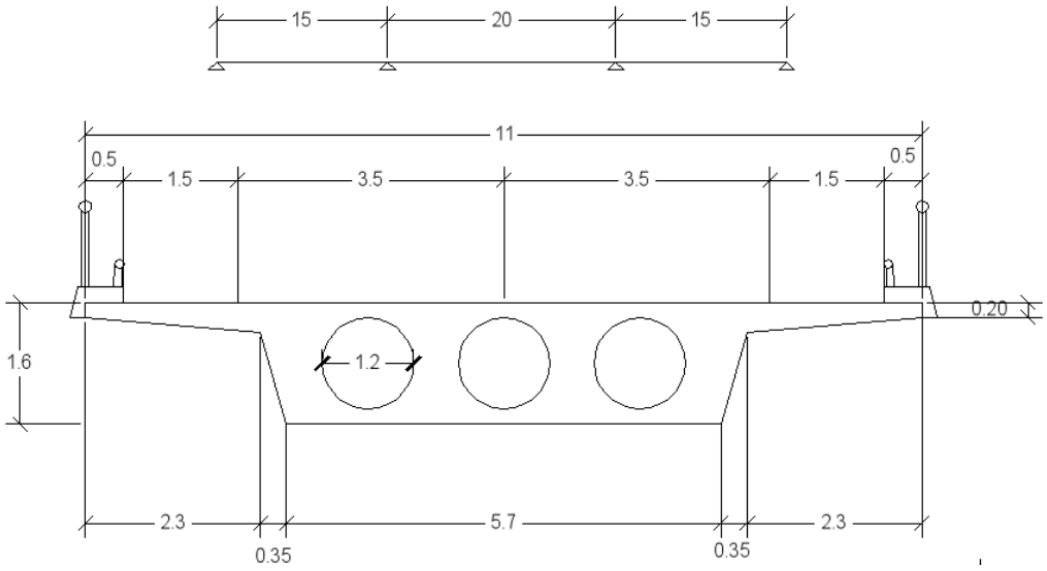

Fig. 3-7: *S1520RC (dimensions in m).*

Chapter 4

Bridges reinforcement design

4.1. Basis of design

Bridges design is conducted according to CNR-DT 203/2006, "Guide for the Design and Construction of Concrete Structures Reinforced with Fiber-Reinforced Polymer Bars". For the flexural design at the ultimate limit state it is required that the factored ultimate moment M_{sd} and the flexural capacity M_{rd} of the FRP reinforced concrete element satisfy the following inequality:

$$M_{sd} \leq M_{rd} \qquad (4.1)$$

The ultimate limit state analysis of FRP reinforced concrete sections relies on the following fundamental hypotheses:

- Cross-beam sections remain plane after deflection so that can be adopted a linear strain diagram;
- Perfect bond exists between the FRP bars and concrete;
- Concrete does not react to tensile stresses;
- Contribution in compression of the FRP bars to the flexural capacity is neglected;
- Constitutive laws for concrete are accounted for according to the current code NTC 08;
- FRP is considered a linear-elastic material up to failure.

It is assumed that flexural failure takes place when one of the following condition is met:

- Concrete in compression reaches the maximum compressive strain ε_{cu}, taken equal to 0,0035 according to NTC 08 (15);
- Tensile FRP bars reach the maximum tensile strain ε_{fd}, computed from the characteristic value, as defined in Section 4.2.2.

Hence, with the reference to the illustrative scheme shown in **Fig. 4-1**, two types of failure may be accounted for, depending upon whether the ultimate FRP strain or the concrete compressive strain is reached:

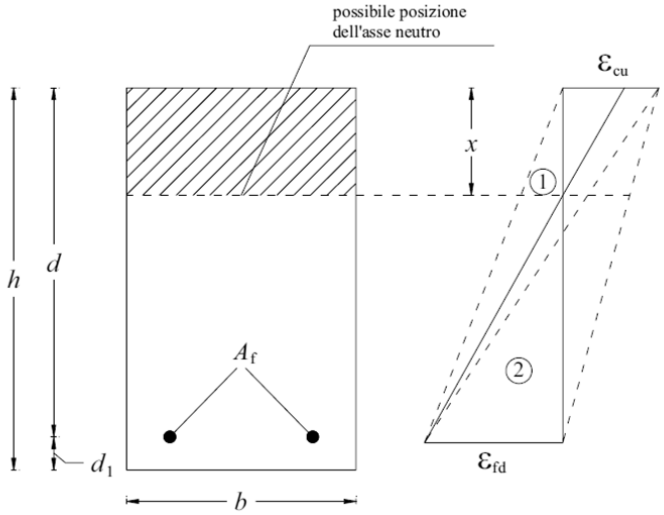

Fig. 4-1: *Failure modes of FRP reinforced concrete section.*

Failure occurring in area 1 is attained by reaching the design strain in the FRP bars: any strain diagram corresponding to such failure mode has its fixed point at the limit value of ε_{fd}. For the hypothesis of linear strain diagram the following relationship can be written:

$$\varepsilon_c = \varepsilon_{fd} \cdot \frac{x}{(d-x)} \leq \varepsilon_{cu} \qquad (4.2)$$

$$\varepsilon_f = \varepsilon_{fd} \qquad (4.3)$$

where, ε_c and ε_f are respectively the concrete strain at compression side and the FRP strain at the centroidal fiber of bars.

Failure occurring in area 2 takes place due to concrete crushing, while the ultimate strain of FRP has not been attained yet: in this case is fixed the maximum concrete compressive strain ε_{cu}. Also in this case, for the linearity of the deformation, it can be written:

$$\varepsilon_c = \varepsilon_{cu} \tag{4.4}$$

$$\varepsilon_f = \varepsilon_{cu} \cdot \frac{(d - x)}{x} \leq \varepsilon_{fd} \tag{4.5}$$

where the symbols are illustrated in **Fig. 4-1**.

The reinforcements for the studied bridges is designed taking into account a failure mode with the neutral axis in area 1, by reaching the designed ultimate strain in FRP bars. The principles are the same than those for ordinary RC beams design. Neutral axis depth x is calculated from strain compatibility and internal force equilibrium, then the resisting moment is obtained by the rotational equilibrium around a certain point of the section.

4.2. Materials

4.2.1. Concrete

According to the current building code (15), design at ULS can be conducted by assuming a simplified distribution of the normal stresses for concrete, such as a "stress-block", either the failure is reached by crushing of concrete or rupture of the FRP bars.

4.2.2. CFRP

Since the FRP bars have a linear elastic behavior up to failure, their stresses may be computed as the product of the pertaining strain by the FRP

modulus of elasticity. The ultimate design strain ε_{fd} is computed from the characteristic tensile strain ε_{fk}, as follows:

$$\varepsilon_{fd} = 0{,}9 \cdot \eta_a \cdot \frac{\varepsilon_{fk}}{\gamma_f} \qquad (4.6)$$

where the coefficient 0,9 accounts for the lower ultimate strain of specimens subjected to flexure as compared to those subjected to standard tensile tests, η_a represents the environmental conversion factor whose values are shown in **Fig. 4-2** and γ_f is the partial factor for FRP bars. For ultimate limit states γ_f shall be set equal to 1,5.

Table 4-1 – Environmental conversion factor η_a for different exposure conditions of the structure and different fiber types.

Exposure conditions	Type of fiber / matrix*	η_a
Concrete not-exposed to moisture	Carbon / Vinylester or epoxy	1.0
	Glass / Vinylesters or epoxy	0.8
	Aramid / Vinylesters or epoxy	0.9
Concrete exposed to moisture	Carbon / Vinylesters or epoxy	0.9
	Glass / Vinylesters or epoxy	0.7
	Aramid / Vinylesters or epoxy	0.8

* The use of a polyester matrix is allowed only for temporary structures.

Fig. 4-2: *Table 4-1 CNR-DT 203/2006, values for the environmental conversion factor.*

4.3. Design calculations

For the resolution of the equilibrium equations necessary to solve the design problem, a spreadsheet has been utilized.

FORCES EQUILIBRIUM

$$N_c - N_f = 0 \qquad (4.7)$$

where N_c and N_f represent compressive and tensile forces in concrete and FRP bars, respectively. The two unknowns are the position of the neutral axis x and the area A_f of FRP bars. Thus, the neutral axis depth is calculated for increasing values of FRP reinforcement amount.

ROTATIONAL EQUILIBRIUM

The flexural capacity can be determined by imposing the rotational equilibrium at any point of the section. In

$$M_{Rd} = \frac{1}{\gamma_{Rd}}[A_c f_{cd}(d - \psi x)] \quad (4.8)$$

where:

- $\gamma_{Rd}$is a partial factor covering uncertainties in the capacity model; in this case such factor shall be set equal to 1;
- A_c is the area of concrete in compression and f_{cd} the compressive strength;
- d is the effective depth and ψ is a coefficient which indicates the position of the compressive force compared to the neutral axis depth x.

Once the neutral axis depth x is calculated, the resistant moment is easily determined. The design amount of FRP reinforcement is that for which $M_{Rd} \geq M_{Sd}$.

4.3.1. Minimum reinforcement

The amount of longitudinal FRP reinforcement in tension shall not be less than the minimum value that satisfies the equation $M_{Rd} = 1{,}5 \cdot M_{cr}$, where M_{cr} is the cracking moment. Moreover, for elements without transverse reinforcement, sufficient longitudinal FRP reinforcement in tension shall be provided such that:

$$\rho_l = \frac{A_f}{b \cdot d} \geq 0{,}01 \qquad (4.9)$$

While the former results always satisfied due to the very low value for M_{cr}, the latter is much more restrictive with respect to the flexural reinforcement amount previously determined.

4.4. Shear strength

The shear verifications of FRP reinforced concrete members shall be carried out at ultimate limit state only. The shear strength for the analyzed bridges is determined according to Italian guideline CNR-DT 203/2006, to the American one ACI 440.1R-06 and according to the model proposed by A. Marí et al.

4.4.1. CNR-DT 203/2006

Shear capacity of FRP reinforced members without stirrups can be evaluated as follows:

$$V_{Rd} = min\{V_{Rd,ct}, V_{Rd,max}\} \qquad (4.10)$$

where $V_{Rd,ct}$ represents the concrete contribution to shear capacity, and $V_{Rd,max}$ is the concrete contribution corresponding to shear failure due to crashing of the web, as reported by NTC 2008 (15). The latter always assumes much higher values, hence only the $V_{Rd,ct}$ will be considered here.

$V_{Rd,ct}$ can be computed as follows:

$$V_{Rd,ct} = 1.3 \cdot \left(\frac{E_f}{E_s}\right)^{1/2} \cdot \tau_{Rd} \cdot k \cdot (1.2 + 40\rho_l) \cdot b \cdot d \qquad (4.11)$$

with the limitation $1.3 \cdot \left(\frac{E_f}{E_s}\right)^{1/2} \leq 1.0$.

The following symbols have been introduced in the equation (4.11):

- E_f and E_s, represent the Young's modules of elasticity of the FRP and steel bars, respectively, expressed in N/mm^2;
- τ_{Rd} is the design shear stress, in N/mm, defined as $\tau_{Rd} = 0.25 f_{ctd}$;
- k in the case where no more than 50% of the bottom reinforcement is interrupted, shall be assumed as $(1.6 - d) \geq 1$, where d is in m;
- the parameter $\rho_l = A_f/(b \cdot d)$ shall not be assumed larger than 0.02.

4.4.2. ACI 440.1R-06

According to the American guideline approach, a strength reduction factor Φ is given for reducing nominal shear capacity. Such factor of 0.75 is taken by *ACI 318-05* for steel reinforced concrete members and can be used also for FRP reinforcement:

$$\Phi V_n \qquad (4.12)$$

For FRP reinforced members the nominal shear strength V_n is equal to the shear resistance provided by concrete V_c. *ACI 440.1R-06* in its formulation takes into account the influence of the axial stiffness on the concrete shear strength.

The concrete shear capacity of flexural members using FRP reinforcement can be evaluated according the following expression:

$$V_c = \frac{2}{5}\sqrt{f_c'} \cdot b_w \cdot c \qquad (4.13)$$

where f_c' is the specified compressive stress of concrete, corresponding to characteristic value; b_w is the width of the web in *mm*, and c is the neutral axis depth in cracked sections, computed as:

$$c = kd \tag{4.14}$$

$$k = \sqrt{2\rho_f n_f + (\rho_f n_f)^2} - \rho_f n_f \tag{4.15}$$

Equation (4.13) accounts for the axial stiffness of the FRP reinforcement trough the neutral axis depth *c*, which depends on the reinforcement ratio ρ_f and on the modular ratio $n_f = E_f/E_C$.

Chapter 5

Structural reliability analysis

5.1. Reliability and probability of failure

A number of definitions of the term "reliability" are used in literature and in national and international documents. Reliability can be defined as the ability of a structure to comply with given requirements under specified conditions during the intended life, for which it was designed.

For structures or structural components, the requirements which must be satisfied are termed by a limit state, that can be defined as (*Eurocode 0, sections 3.1-3.5* (16)):

- *Ultimate limit state (ULS)*. It aims to the capacity for avoiding collapses, equilibrium loss and serious full or partial failures that could affect safety of people or lead to important economics losses, as well as relevant environmental and social damages.
- Serviceability limit state (SLS). It assures performances referred to operating conditions and it concerns the functioning of the structure or structural members under normal use, the comfort of people and the appearance of the construction works.

The "violation" of a limit state corresponds to the reaching of an undesirable condition for the structure. The aim of *structural reliability analysis* consists indeed in the calculation and prediction of the probability of this limit state violation, that is the probability of failure P_f, here understood in a very general sense which denotes simply any undesirable state of a structure.

Therefore, in quantitative sense reliability *r* may be expressed as the complement of the probability of failure and thus can be defined as the probability of survival:

$$r = 1 - P_f \qquad (5.1)$$

In this work, it will be referred to the probability of failure, in terms of the probability of breaching of the ultimate limit state (as defined above, according to Eurocode 0)

5.2. The limit state function

It is assumed that the limit state can be defined by means of a limit state function, which involves, in its simplest form, two terms, the load effects *S* and the resistance *R*, as follows:

$$G = R - S = 0 \qquad (5.2)$$

Thus, the safety of a structure is represented in terms of its resistance and load effects, which are two uncertain quantities, described by random variables with a known probability density function: $f_R(\,)$ and $f_S(\,)$ respectively. In this sense, as well know, a structure or a structural member is considered to fail when its resistance *R* is less than the load effect *S* acting on it. Therefore, the probability of failure can be expressed as:

$$P_f = P(R - S \leq 0) \qquad (5.3)$$

f_R and f_S, together with the joint density function $f_{RS}(r, s)$ are shown in **Fig. 5-1** in which, the failure domain *D* is represented, so that the probability of failure becomes:

$$P_f = P(R - S \leq 0) = \iint_D f_{RS}(r,s)\, dr ds \qquad (5.4)$$

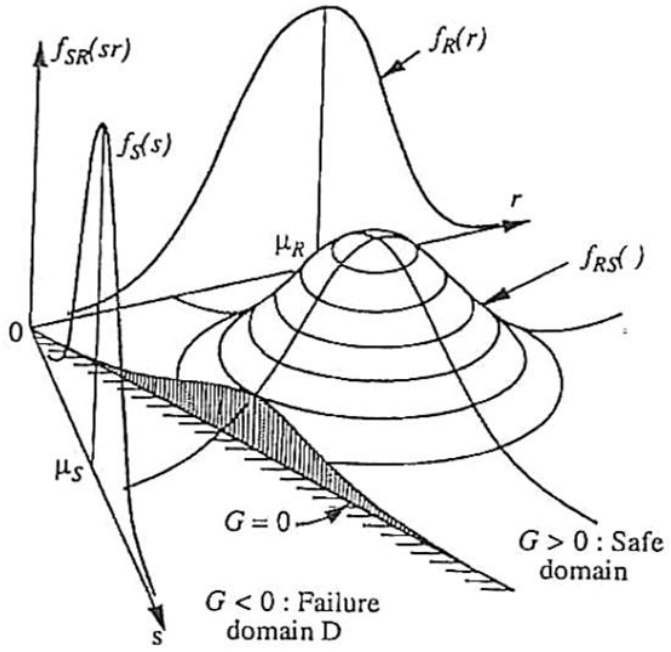

Fig. 5-1: *Joint density function* $\boldsymbol{f_{RS}(r,s)}$*, marginal density function* $\boldsymbol{f_R}$ *and* $\boldsymbol{f_S}$ *and failure domain D, (Melchers* ***(17)****)*

When R and S are independent $f_{RS}(r,s) = f_R(r) f_S(s)$. If $G > 0$ the structure is in the safe domain, otherwise it is in the unsafe and fails.

In a generalized form, if $\boldsymbol{X}$ is the vector of the basic variables, then resistance and loads can be expressed as $R = G_R(\boldsymbol{X})$ and $S = G_S(\boldsymbol{X})$, so that the limit state function became:

$$G(\boldsymbol{X}) = R - S = G_R(\boldsymbol{X}) - G_S(\boldsymbol{X}) \qquad (5.5)$$

.

Particularly, when the random variables defining the problem are many:

$$P_f = P[G(\boldsymbol{X}) \leq 0] = \int \ldots \int_{G(\boldsymbol{X})\leq 0} f_X(\boldsymbol{X}) dX \qquad (5.6)$$

where $f_X(\boldsymbol{X})$ is the joint probability density function for the n vector $\boldsymbol{X}$ of basic variables.

In reality, resistance and loads are generally functions of time. This implies that the uncertainty of prediction of both R and S increases with time and the probability density functions $f_R(r)$ and $f_S(s)$ change. Since the parameter standard deviation (σ) increases, their curves become wider and flatter. Moreover, the mean value may change with time, because resistance tends to decrease, while loads tend to increase (**Fig. 5-2**).

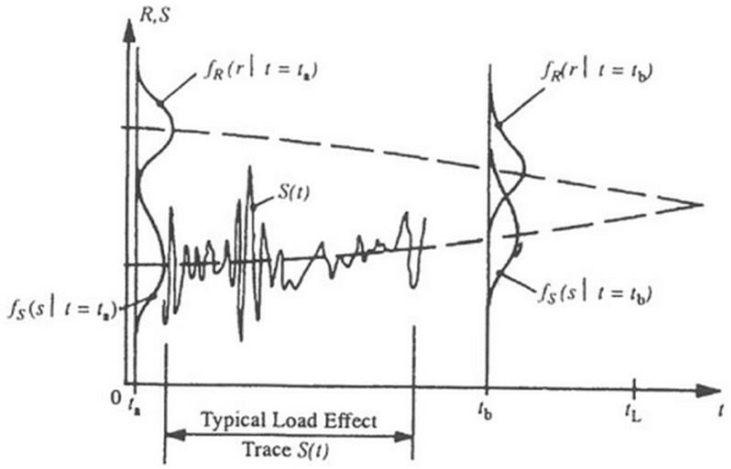

Fig. 5-2: *Schematic time dependent reliability problem (Melchers **(17)**).*

Usually it is assumed that neither R nor S is a function of time and the behavior of the structure is observed under a single load application. However, since there are loads, as the live load, that are applied more than once, their effect over the time should be considered by assuming for example a Gumbel or Frechet distribution. This allows to neglect the time effect in the reliability calculations, even if this simplification is not always possible.

5.3. The reliability index

An equivalent standard reliability measure is the reliability index β which is related to the probability of failure by the following relationship:

$$P_f = \Phi(-\beta) \qquad (5.7)$$

where Φ is the cumulative distribution function of the Standardized Normal distribution, so that the relation between P_f and Φ can be easily determined. Indeed, if the limit state function follows a normal distribution, as it is generally possible to assume thanks to the central limit theorem, the probability of failure can be written as:

$$P_f = P(R - S \leq 0) = P(Z \leq 0) = \Phi\left(\frac{0 - \mu_Z}{\sigma_Z}\right) \qquad (5.8)$$

and thus, the reliability index can be defined as:

$$\beta = \frac{\mu_Z}{\sigma_Z} \qquad (5.9)$$

where μ_Z is the mean value of the limit state function and σ_Z the standard deviation.

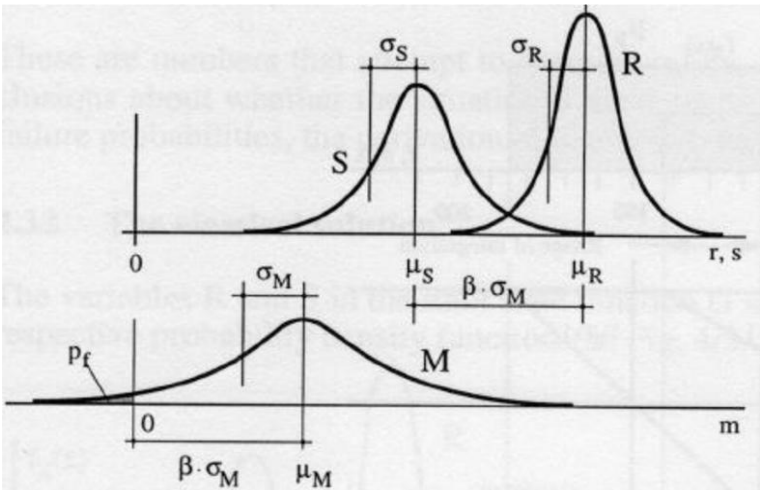

Fig. 5-3: *Reliability index β (Schneider, J.* ***(18)****).*

In **Fig. 5-3**, where the notation σ_M is utilized in place of σ_Z , it can be seen as index β represents how many time the standard deviation of the variable limit state function Z (also called *safety margin*) sets between zero and the mean value of the function. When the standard deviation σ_M is higher than the mean value, the safety margin is crossed and the structure or structural component fails.

It should be emphasized that the failure probability P_f and the reliability index β represent equivalent reliability measures with one to one mutual correspondence given by (5.7) and numerically illustrated in **Table 5-1**.

P_f	10^{-1}	10^{-2}	10^{-3}	10^{-4}	10^{-5}	10^{-6}	10^{-7}
β	1,3	2,3	3,1	3,7	4,2	4,7	5,2

Table 5-1: *Relationship between the failure probability P_f and the reliability index β.*

In EN 1990 (Eurocode 0) the basic recommendation concerning a required reliability level is often formulated in terms of the reliability index β related to a certain design working life.

5.4. Evaluation of the structural reliability

Equation (5.6) can be solved by different methods, which are mainly grouped into two categories:

- Integration and simulation methods;
- Second-moment and transformation methods.

5.4.1. Integration and simulation methods

The principal hypothesis is that the probability density function of each basic variable is known and not approximated. If R and S follow a normal

distribution, then the integration region can be represented by a linear limit state function and the integral of equation (5.6) can be solved even if n-dimensional.

$$G(x) = Z = 0 = a_1 x_1 + a_2 x_2 + \cdots + a_n x_n \qquad (5.10)$$

Most of the time, limit state functions are not linear, therefore it is preferable to proceed with another method, called Monte Carlo simulation. This method introduces approximate numerical solutions to the probability integral and can be applied to problems with limit state functions $G(x)$, which may have any form. Monte Carlo simulation will be later illustrated in detail, being chosen for the calculation of the probability of failure of the studied bridges.

5.4.2. Second-moment and transformation methods

This time, the principle hypothesis is that the probability density function itself is simplified. In the so-called First Order Second Moment method (FOSM), each variable appearing in the limit state function is expressed by its two first moments (mean value and standard deviation of its probability distribution). Therefore, it is assumed to be a Normal distribution even if it is not (in fact, the only distribution that can exactly be represented by its mean value and standard deviation is the Normal distribution). This leads to the calculation of a probability of failure that is "nominal", precisely because to assume a variable described only by its two first moments, unless it has a normal distribution, means to make an approximation. The procedure is iterative and consists mainly in to approximate the limit state function $G(x)$ with a linear function, after transforming all the basic variables to their standardized form $N(0,1)$ (**Fig. 5-4**).

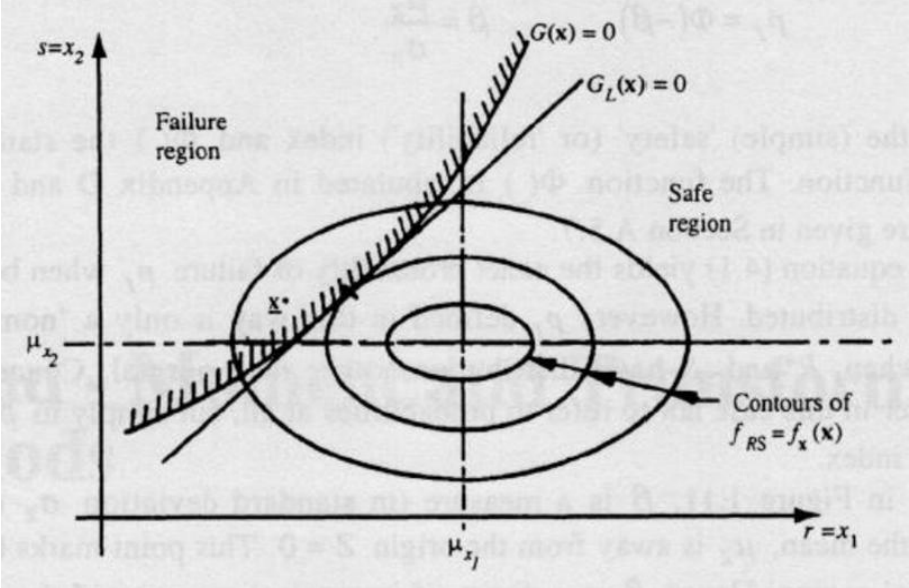

Fig. 5-4: *Limit state function G(x) and linearized state function $G_L(X)$in the domain of basic variables.*

The transformation or First Order Reliability method (FORM) differs from the former because more information about the basic variables are known. These information should be incorporated in the reliability analysis and this can be done by transforming non normal distributions into equivalent normal-distributions. It is done transformed at the so called "design point" and the procedure is more complex than that of the FOSM method.

Eventually there is the so-called Second Order Reliability method (SOR) which is basically equal to the FOR method, with the difference that the limit state function $G(x)$ is approximated with a second order function and no more simply linearized.

5.5. The Monte Carlo simulation

The two physicists John von Neumann and Stanislaw Ulam were investigating in radiation shielding at Los Alamos scientific laboratory (1946) when they had the idea to solve a problem of lack of data by inventing the so

called Monte Carlo simulation, which takes its name from the famous Monte Carlo Casino.

This method is largely used for structural reliability. It consists in sampling each random variable X_i that appears in the limit state function to give a sample value x_i that is briefly to simulate artificially a large number of experiments. Indeed in the limit state function, resistance and loads are assumed as random values with a specific statistical distribution. Depending on their combination the function will result greater or lower than zero. To apply the Monte Carlo simulation means to simulate a certain number N of hypothetical trials, so that the probability of failure can be easily calculated as:

$$P_f = \frac{n(G \leq 0)}{N} \qquad (5.11)$$

where n is the number of trials which $G \leq 0$. Number N depends on the wanted accuracy.

5.5.1. Generation of random numbers

Generally basic variables acting in the structural reliability problem follow a non-uniform distribution. Their sample values are called "*random varieties*" and can be found by different mathematical techniques. The most common procedure used is the "*inverse transform"* method. It is known that the cumulative distribution function $F_X(x_i)$ of a basic variable X_i assumes a value between zero and one. The inverse transform method consists in generating a uniformly distributed random number r_i included in the interval (0,1) and equating this to $F_X(x_i)$:

$$F_X(x_i) = r_i \qquad (5.12)$$

If the inverse function $F_X(x_i) = r_i$ exists, the sample value x_i can be found, as shown in **Fig. 5-5**:

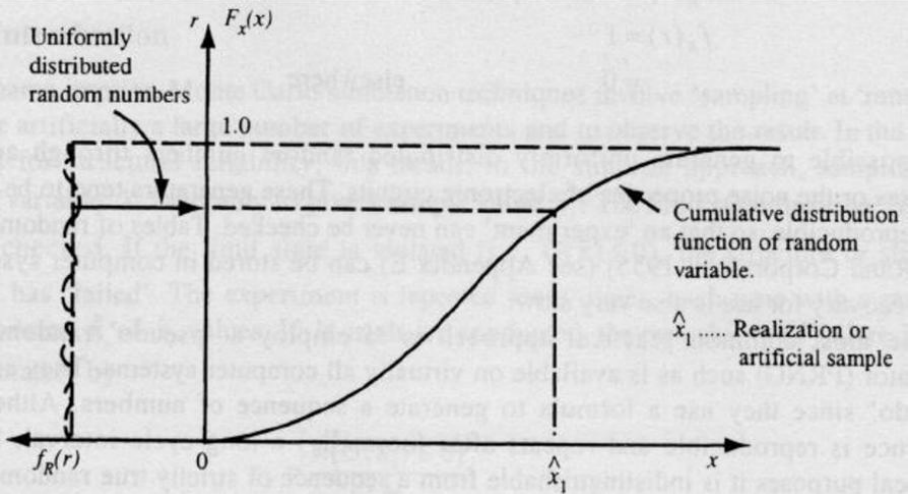

Fig. 5-5: *Inverse transform method for generation of random varieties* ***(17)****.*

In order to generate the random variable , a pseudo random generator (*PRNG*) can be used, that is available in all computers systems. The word "pseudo" indicates that numbers are generated by a formula ant therefore they are not properly random values, even if they follow a sequence which repeats after a long cycle interval.

Hence Monte Carlo methods using PRNG are called more correctly "Quasi Monte Carlo methods".

5.6. Basic variables

Basic variables concurring in the structural reliability problem can be divided, as already seen, into:

— resistance variables;
— load variables.

5.6.1. Resistance variables

Structural resistance can usually be expressed in the following form:

$$R = M \cdot F \cdot D \cdot R_n \qquad (5.13)$$

where:

- R_n is the nominal resistance;
- M indicates the model uncertainty variable and it is called "professional" or "modelling" factor. This term summarizes the effect of the simplifications introduced by the mathematical model assumed in order to evaluate the resistance of the structure or structural component. For good models it results $M \approx 1$, but generally developed models are conservative, so that usually $M > 1$. Moreover the coefficient of variation is of a few percent if the model is good (e.g. bending resistance models), whereas for poor models (e.g. shear resistance models) its value sets between 10% and 20%;
- F indicates material properties (strength, elastic modulus,…) . They should generally be derived from standardized tests (mostly tension and compression tests), performed under specified conditions. These tests have to be planned in order to get a realistic description of the material performance in real applications. The frequency of negative values is normally zero, hence material variables can be generally represented by a log-normal distribution;
- D indicates dimensions and derived quantities. This term can be important in concrete, because it is more easy to introduce dimensional variability, for example in the concreting phase. Generally dimensional variables can be modeled by normal or log-normal distributions. The standard deviations are of the order of magnitude of the dimensional tolerances, therefore the coefficient of variation (mean value/standard deviation) is higher for smaller dimensions.

5.6.2. Load variables

Loads are the most uncertain variables in structural reliability, thus, appropriate model should be developed in order to represent their values. Loads, as already mentioned, are assumed to vary with time and so, they should be represented as a stochastic process. Loads can be divided into two groups: those due to natural phenomena (wind, waves, snow, earthquakes, ...), and those due to man-imposed effects (dead loads and live loads). For the former are usually available observations of the phenomena over a period of time and maxima values are generally identified and used for modeling extreme value distributions. For the latter, long term data are often insufficient and statistical properties of the load distribution must be determined mathematically. In this work, it will be dealt the loads due to man-imposed effects, which will take part into the simulation.

Dead loads are the sum of self-weight and permanent loads. The self-weight is essentially constant during the life of the structure and there is just a small tendency to increasing because of some factors, such as deformation of the shuttering, tolerances, etc.. Generally self-weight in concrete elements is represented by a Normal distribution with a bias of 1,05 and a coefficient of variation of about 5%. Permanent loads are constant during a long time period too, but their coefficient of variation is usually higher than that of self-weight, mainly because changes may occur during the lifetime of a structure.

Live loads in buildings are generally of moderate extent and peaks showed by their distributions are mainly due to possible presence of crowds of people. The so-called accompanying loads, of low intensity, assume a Lognormal distribution. The leading live loads instead, such as the crowd load or traffic load for bridges, can well represented by an extreme value distribution (Gumbel, Frechet, …).

Chapter 6

Statistical properties of basic variables

6.1. Introduction

In order to initiate the MONTE CARLO simulation it is firstly necessary define the main statistical properties of all the variables within in the analysis. Statistical properties discussed in this chapter, are taken from a previous thesis work (19) except for the elastic modulus of FRP bars, whose characteristics are found in the literature (20).

6.2. Statistical properties of the resistance variables

6.2.1. Concrete compressive strength

The concrete compressive strength will appear, in the simulation, in the expression of the shear strength of the model formulation. It follows a *Lognormal* distribution:

Lognormal distribution	
Characteristic value f_{ck} [MPa]	20,00
Bias ϑ	1,40
Coefficient of variation *COV*	0,15
Mean value μ [MPa]	28,00
Standard deviation σ [MPa]	4,20

Table 6-1: *Main statistical properties of the concrete compressive strength*

The mean value μ and the standard deviation σ are calculated as follows:

$$\mu = \vartheta f_{ck} \quad (6.1)$$

$$\sigma = \mu COV \quad (6.2)$$

A random variable x has a lognormal distribution if the transformed variable $n = log(x)$ follows a normal distribution. The mean value and variance of the x distribution are defined by (6.3) and (6.4):

$$\mu_x = exp\left(\lambda + \frac{1}{2}\xi^2\right) \quad (6.3)$$

$$\sigma_x^2 = \mu_x^2\left(e^{\xi^2} - 1\right) \quad (6.4)$$

Where λ and ξ are respectively, the mean value and the standard deviation of the normal distribution of $n = log(x)$.

The value of λ and ξ can be found by inverting the previously equation (6.3) and (6.4):

$$\lambda = ln(\mu_x) - \frac{1}{2}\xi^2 \quad (6.5)$$

$$\xi = \sqrt{ln\left(\left(\frac{\sigma_x}{\mu}\right)^2 + 1\right)} \quad (6.6)$$

It is obtained:

Normal distribution	
Mean value λ [ln(MPa)]	3,321
Standard deviation ξ [ln(MPa)]	0,149

Table 6-2: *Mean value and standard deviation of normal distribution of* $\boldsymbol{n = log(x)}$

The probability density function results:

$$f(x) = \frac{1}{\sqrt{2\pi}x\xi} exp\left[-\frac{1}{2}\left(\frac{lnx - \lambda}{\xi}\right)^2\right] \qquad 0 \leq x < \infty \qquad (6.7)$$

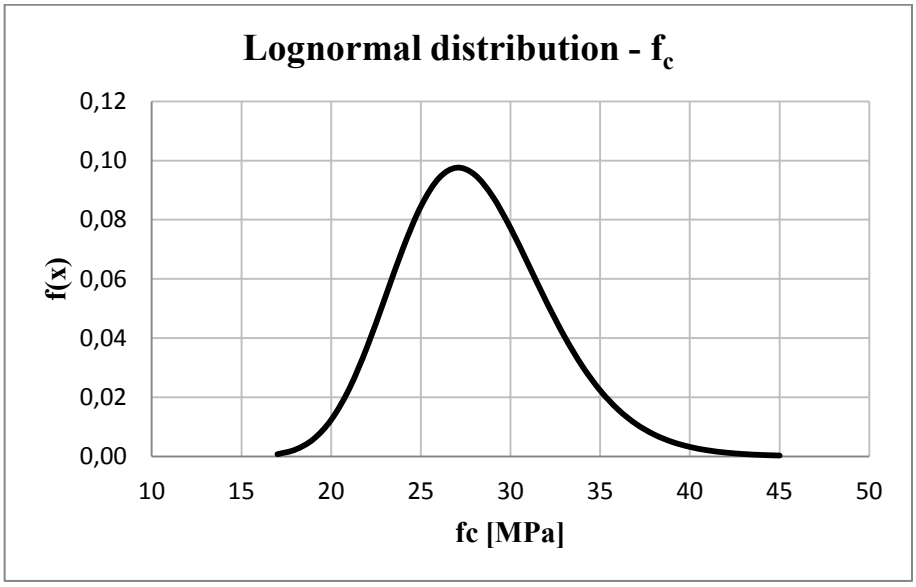

Fig. 6-1: *Probability density function of the concrete compressive strength of f_c.*

6.2.2. Modulus of elasticity of FRP

The CFRP elastic modulus follows a Normal distributions. The characteristic parameters are taken from Pilakoutas et al. (20):

Normal distribution	
Coefficient of variation *COV*	0,05
Mean value μ [MPa]	115000,00
Standard deviation σ [MPa]	5750,00

Table 6-3: *main statistical properties of the CFRP elastic modulus.*

The mean value of the elastic modulus met in literature would be slightly smaller than the value adopted for the FRP bars at the design stage, but no betters data are found.

The probability density function is described in (6.8) and it is shown in **Fig. 6-2** :

$$f(x) = \frac{1}{\sqrt{2\pi}\sigma_x} exp\left[-\frac{1}{2}\left(\frac{x-\mu_x}{\sigma_x}\right)^2\right] \qquad -\infty \leq x < \infty \qquad (6.8)$$

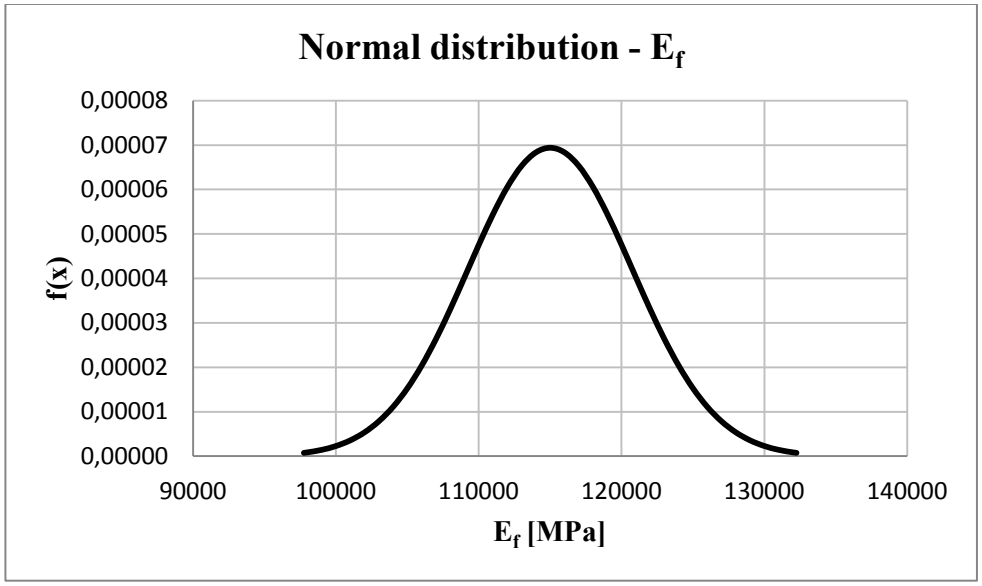

Fig. 6-2: *Probability density function of E_f.*

6.3. Statistical properties of the load variables

6.3.1. Dead loads

Dead load refers to self-weight of the materials and to all other permanent installations and hence they do not vary significantly during the lifetime of the structure. Dead loads can generally be approximated by a *Normal* distribution. The mean is typically almost equal to the nominal load; in this case a bias λ=1,05 is taken, according to Ellingwood et al. (21). The coefficient of variation generally

assumes a value between 0,05-0,10 (18). It is chosen for this work a value of COV=0,08.

In girder bridges the flexural design with FRP reinforcement bars is performed by considering a medium acting moment on the single beam, therefore the effects of the dead loads that will be considered are those acting on the beam. The characteristics values shown in **Table 6-4** and **Table 6-5**, are referred to the shear force acting at the supports. For continuous bridges, there are two values representing the shear force acting at the middle and lateral supports (**Table 6-5**).

GIRDER BRIDGES	**B10RC**	**B12RC**	**B16RC**	**B20RC**
Characteristic value *Vpk* [kN]	92,75	121,80	190,40	273,00
Bias ϑ	1,05	1,05	1,05	1,05
Coefficient of variation *COV*	0,08	0,08	0,08	0,08
Mean value μ_x [kN]	97,39	127,89	199,92	286,65
Standard deviation σ_x [kN]	7,79	10,23	15,99	22,93

Table 6-4: *Statistical properties of dead load acting on girder bridges.*

SLAB BRIDGES	**S10RC**	**S1015RC**		**S1520RC**	
	lateral support	**lateral support**	**middle support**	**lateral support**	**middle support**
Characteristic value *Vpk* [kN]	1356,87	1109,24	2507,85	1200,06	2225,00
Bias ϑ	1,05	1,05	1,05	1,05	1,05
Coefficient of variation *COV*	0,08	0,08	0,08	0,08	0,08
Mean value μ_x [kN]	1424,71	1164,70	2633,24	1260,06	2336,25
Standard deviation σ_x [kN]	113,98	93,18	210,66	100,81	186,90

Table 6-5: *Statistical properties of the dead load acting on slab bridges.*

The equation which describes the probability density function is those already seen for Normal distribution of E_f (6.8).

The probability density function of the dead load acting on B10RC is represented in *Figure 6.9*.

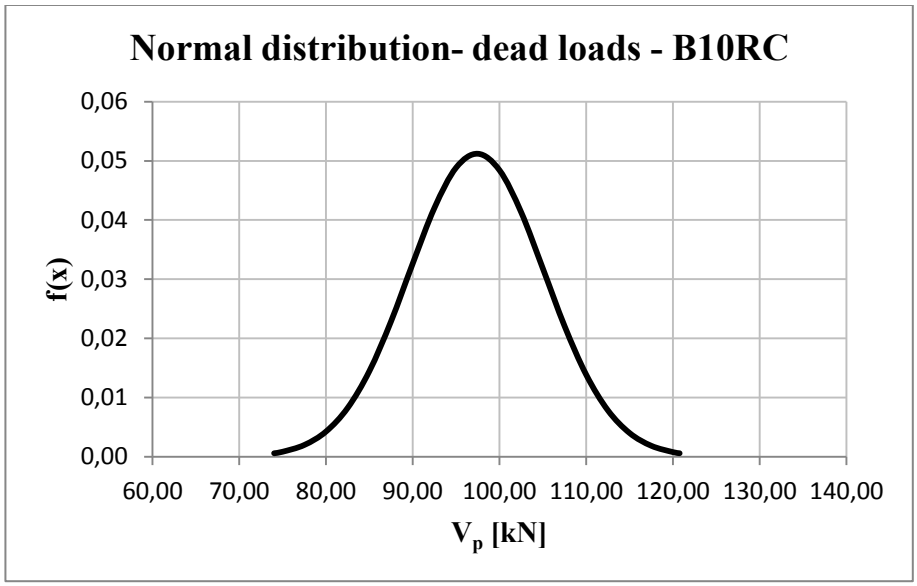

Fig. 6-3: *Probability density function of V_p [B10RC].*

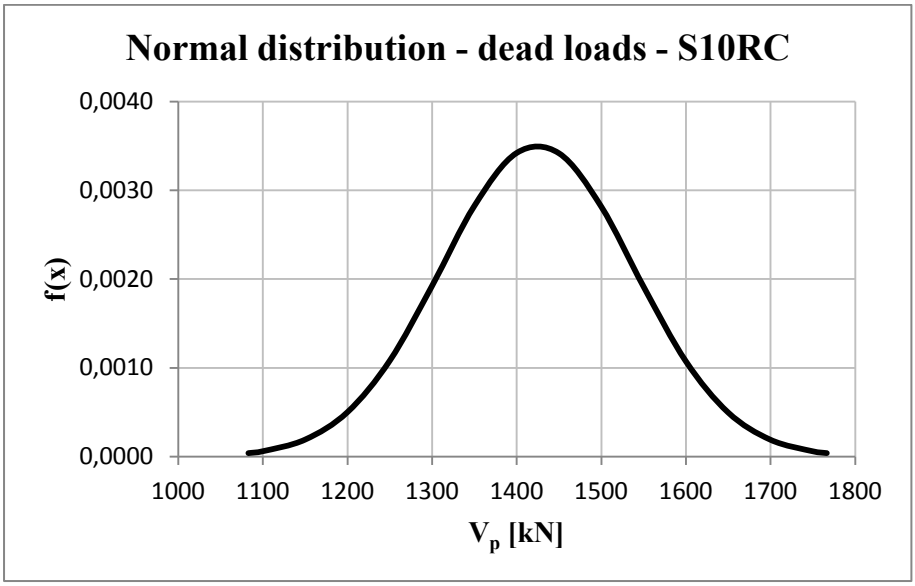

Fig. 6-4: *Probability density function of V_p [S10RC].*

6.3.2. Live loads

For traffic loads the important random variable is the magnitude of the largest extreme load that occurs during a specified reference period for which the probability of failure is calculated. For the analyzed bridges the reference period is of 50 years and the largest extreme follows one of the asymptotic extreme value distributions (Gumbel, Frechet). A Gumbel distribution is chosen.

The Gumbel distribution is also called Extreme value distribution type I and its cumulative distribution function is expressed as follows:

$$F_Y(x) = exp\left[-exp\left(-\alpha(x-u)\right)\right] \qquad -\infty \leq x < \infty \qquad (6.9)$$

The distribution is characterized by two parameters: the mode u and a measure of the dispersion α. Such parameters are related to the mean value μ_x and to the standard deviation σ_x:

$$u = \mu_x - \frac{\Upsilon}{\alpha} \qquad (6.10)$$

Where $\Upsilon = 0{,}5772156649$ ... is the Euler's constant.

α can be defined by the following:

$$\alpha = \frac{\pi}{\sqrt{6}\sigma_x} \qquad (6.11)$$

In this case, only the nominal value and the COV are known. Thus, the mean value and standard deviation can be defined in a way a slightly more laborious, as explained below.

Nominal value is those calculated according to the Eurocode, which corresponds to the 95% fractile for a 50 years reference period (return period of 1000 years). According to (22) is taken $COV = 0{,}2$. The high value of the COV takes into consideration the traffic variability, which depends on the type of

studied road (e.g. a second class road, a local road, etc.), together with eventual amplifications of the loads and the girder distribution. Once the COV is known, the value of the bias ϑ can be extrapolated from the equation of the cumulative probability of the Gumbel distribution:

$$F_Y(x) = 0{,}95 = exp\left[-exp\left(-\alpha(x-u)\right)\right] \qquad -\infty < x < \infty \qquad (6.12)$$

$$0{,}95 = exp\left[-exp\left[-\frac{\pi}{\sqrt{6}\cdot 0{,}2\cdot\mu_x}\left(V_{llk} - \left(\mu_x - \frac{\Upsilon}{\pi}\left(\sqrt{6}\cdot 0{,}2\cdot\mu_x\right)\right)\right)\right]\right] \qquad (6.13)$$

It is obtained a bias equal to $\vartheta = 0{,}723$. Once defined this values, it is easy to determine $\sigma_x = 0{,}2\mu_x = 0{,}2(0{,}723V_{llk})$ and eventually u and α.

GIRDER BRIDGES	**B10RC**	**B12RC**	**B16RC**	**B20RC**
Characteristic value *Vtk* [kN]	184,06	194,26	212,38	228,96
Bias ϑ	0,723	0,723	0,723	0,723
Coefficient of variation *COV*	0,20	0,20	0,20	0,20
Mean value μ_x [kN]	133,08	140,45	153,55	165,54
Standard deviation σ_x [kN]	26,62	28,09	30,71	33,11
Dispersion α [1/kN]	0,048	0,046	0,042	0,039
Mode u [kN]	121,10	127,81	139,73	150,64

Table 6-6: *Statistical properties of the traffic loads acting on girder bridges.*

SLAB BRIDGES	**S10RC**	**S1015RC**		**S1520RC**	
	lateral support	**lateral support**	**middle support**	**lateral support**	**middle support**
Characteristic value *Vtk* [kN]	1137,50	1268,12	1534,54	1414,80	1664,71
Bias ϑ	0,723	0,723	0,723	0,723	0,723
Coefficient of variation *COV*	0,20	0,20	0,20	0,20	0,20
Mean value μ_x [kN]	822,41	916,85	1109,47	1022,90	1203,59
Standard deviation σ_x [kN]	164,48	183,37	221,89	204,58	240,72
Dispersion α [1/kN]	0,008	0,007	0,006	0,006	0,005
Mode *u* [kN]	748,39	834,32	1009,61	930,83	1095,25

Table 6-7: *Statistical properties of the traffic loads acting on slab bridges.*

For illustrative purposes, the probability density function of the traffic load acting on B10RC and S10RC is represented in .

$$f_Y(x) = \alpha \cdot \exp\left[-\alpha(x-u) - exp\left(-\alpha(x-u)\right)\right] \qquad -\infty < x < \infty \qquad (6.14)$$

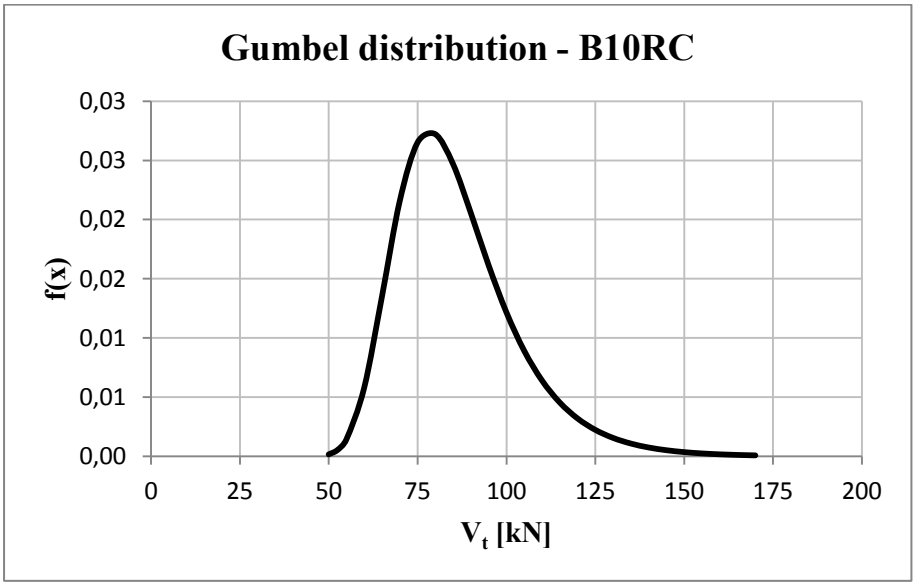

Fig. 6-5: *Probability density function of V_t for B10RC.*

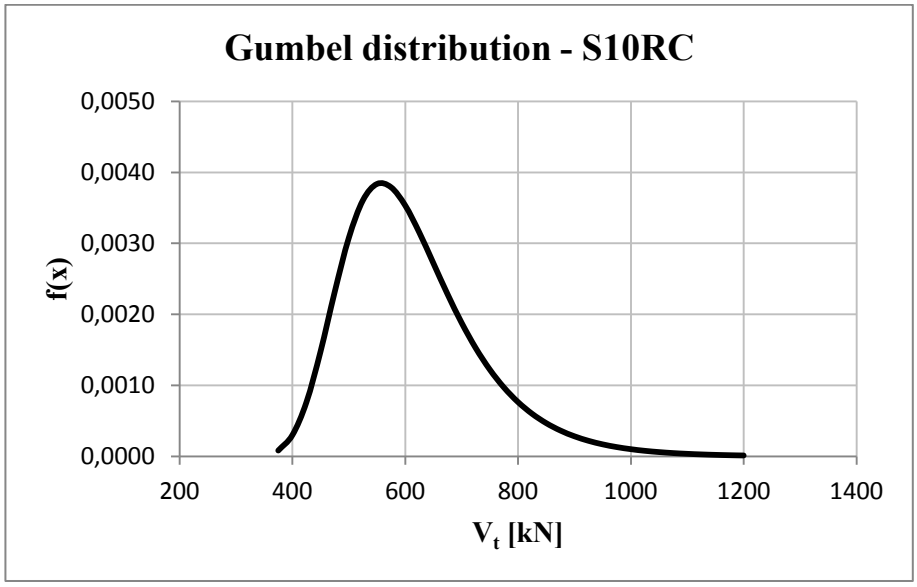

Fig. 6-6: *Probability density function of Vt for S10RC.*

6.4. Statistical properties of the model error

The accuracy of the proposed model (13) has been verified by comparing the model predictions with the results of 144 tests on CFRP and GFRP reinforced concrete beams or one-way slabs. According to Collins (23), the authors considerer asymmetric the distribution of the values V_{test}/V_{model} and a *Lognormal* distribution is assumed.

The results obtained by the proposed method for the prediction of the shear strength are very good, in terms of mean value and coefficient of variation of the ratio between the experimental and the predicted values. Such correlation is shown in **Fig. 6-7.**

Similarly to what was seen earlier for the Lognormal distribution of the concrete compressive strength, by (6.5) and (6.6), can be defined the mean value λ and the standard deviation ξ of the normal distribution $n = log(x)$, where x is the model error variable.

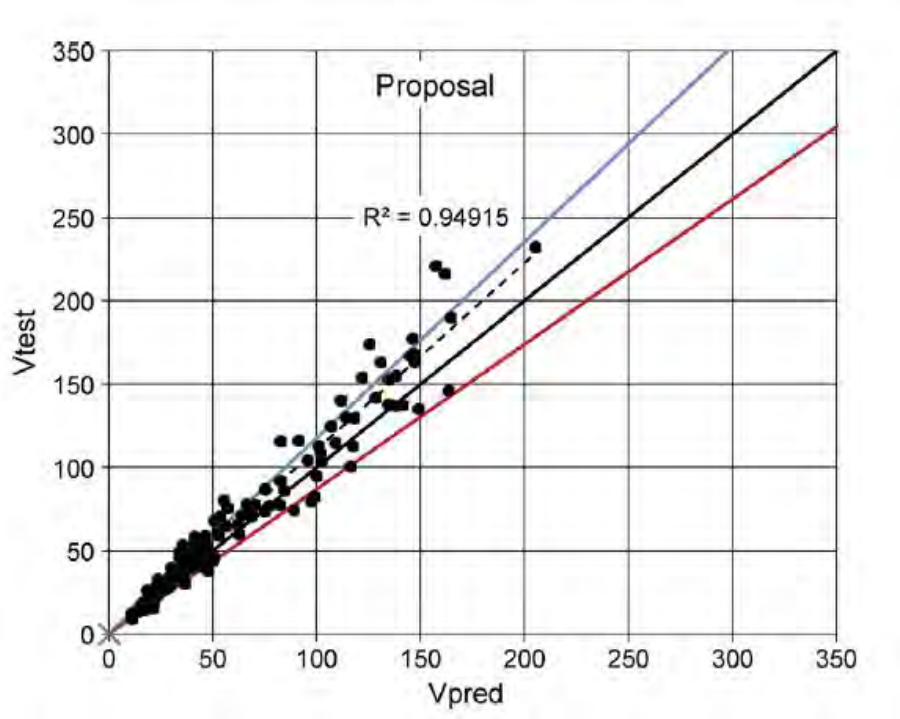

Fig. 6-7: *Correlation between the test value and the prediction value by the studied model (13). A tolerance of 15 % has been represented.*

In **Table 6-8** are presented the main statistical characteristics of the model error:

Lognormal distribution	
Coefficient of variation *COV*	0,15
Mean value μ [MPa]	28,00
Standard deviation σ [MPa]	4,20
Mean value λ	0,15
Standard deviation ξ	0,08

Table 6-8: *Statistical properties of the model error ρ.*

Thereby, the probability density function results (**Fig. 6-8**):

$$f(x) = \frac{1}{\sqrt{2\pi}x\xi} exp\left[-\frac{1}{2}\left(\frac{lnx - \lambda}{\xi}\right)^2\right] \qquad 0 \leq x < \infty \qquad (6.15)$$

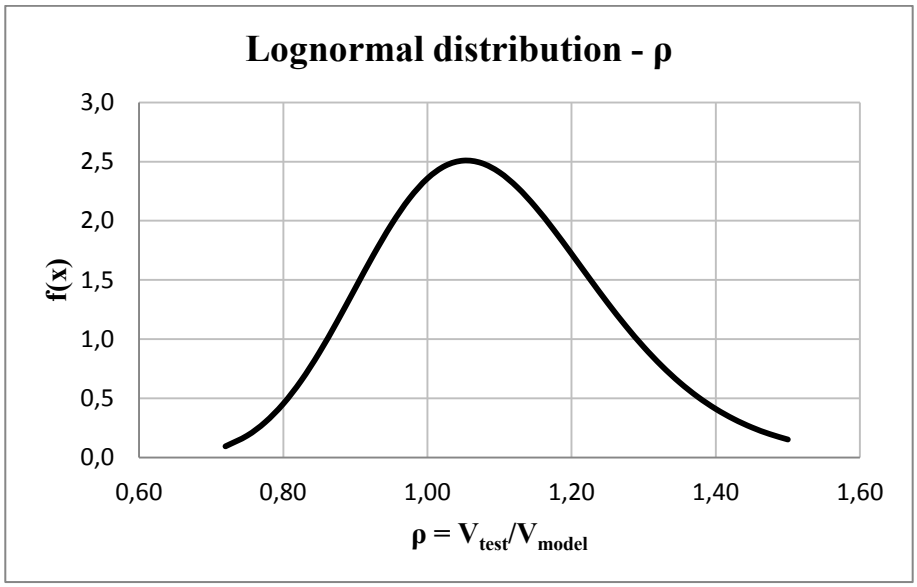

Fig. 6-8: *Probability density function of the model error ρ.*

Chapter 7

Setting of the Monte Carlo simulation

7.1. The general Limit State Function

To calculate the probability of failure of the bridges longitudinally reinforced with FRP bars, a Monte Carlo simulation is performed. Once defined *R* as the resistance and *S* as the load effects acting on the sections, the limit state equation can be written in a generic form as:

$$G = R - S = \rho \cdot V_{model} - (V_p + V_t) \quad (7.1)$$

Resistance and loads are assumed as random variables with a specific probability distribution, whose statistical properties are discussed in detail in Chapter 6. In particular:

- V_{model} is the shear strength calculated according to the formulation proposed by the studied model (13);
- ρ is the model error (discussed in section 6.4);
- V_p is the shear force due to dead load (as sum of the self-weight and no structural permanent loads), acting on the bridges cross-sections closely to the support;
- V_t is the shear force due to the traffic load acting at the support.

The shear strength results to be a function of the two basic variable f_c and E_f, respectively, the concrete compressive strength and the Young's modulus (7.2):

$$G = \rho \cdot V_{model}(f_c, E_f) - (V_p + V_t) \quad (7.2)$$

According to the formulation proposed by Marí (2.15), the modulus of elasticity of the reinforcing bars affects considerably the shear strength. The higher is the modular ratio between the FRP and the concrete modulus, the higher is the shear strength, because the neutral axis c_l depth increases with the parameter $\alpha \cdot \rho_f$ (2.7).

$$v_{u,t} = \frac{V_{u,t}}{f_{ct} \cdot b \cdot d} = (1{,}072 - 0{,}01 \cdot \alpha) \cdot \frac{c_l}{d} + 0{,}036$$

$$\xi_l = \frac{c_l}{d} = \alpha \cdot \rho_f \cdot \left(1 + \sqrt{1 + \frac{2}{\alpha \cdot \rho_f}}\right)$$

α is the modular ratio between the FRP and the concrete modulus:

$$\alpha = \frac{E_f}{E_c} \quad (7.3)$$

E_f is a basic variable, whose statistical properties are described in section 6.2.2. Instead, the concrete modulus is computed, according to the relation provided by the Eurocode (Table 3.1, Eurocode 2), which allows to define the secant modulus of elasticity as a function of the mean value of compressive strength. Substituting the value of the random varieties of the variable f_c in place of the mean value, a series of random values of the elastic modulus are obtained:

$$E_c = 22 \cdot \left(\frac{f_c}{10}\right)^{0,3} \quad (7.4)$$

7.2. Implementation of the Monte Carlo simulation

Once all the variables taking part into the simulation are known, it is generate from them a series of random varieties, which simulates a certain number of fictitious trials. Since the principal parameters of each variable distributions are known, a random value of each variable defined in the previous sections can be generated artificially.

The simulation is performed in a spreadsheet: it is possible to reproduce fictitious values assumed by the cumulative distribution function of each variable by means of the function "*CASUAL*", which allows to simulate uniformly distributed numbers between zero and one. Then, by using an inverse cumulative distribution function, it can be calculated a value of the random variety. This method takes the name *Inverse transform method*. This is done automatically by *Excel* for some distributions such as the Normal and Lognormal, once the principal parameters are introduced as input data (the mean value μ and the standard deviation σ). For the Gumbel distribution instead, it is necessary to manually derive the inverse cumulative function.

It is obtained:

$$x = \frac{\left[\alpha u - ln\left(F_y(x)\right)\right]}{\alpha} \qquad 0 \leq F_y(x) \leq 1 \qquad (7.5)$$

where $F_y(x)$ is the cumulative distribution function (6.12).

Once defined these basic steps, it is possible to calculate the model shear strength, as schematically illustrated in **Fig. 7-1**.

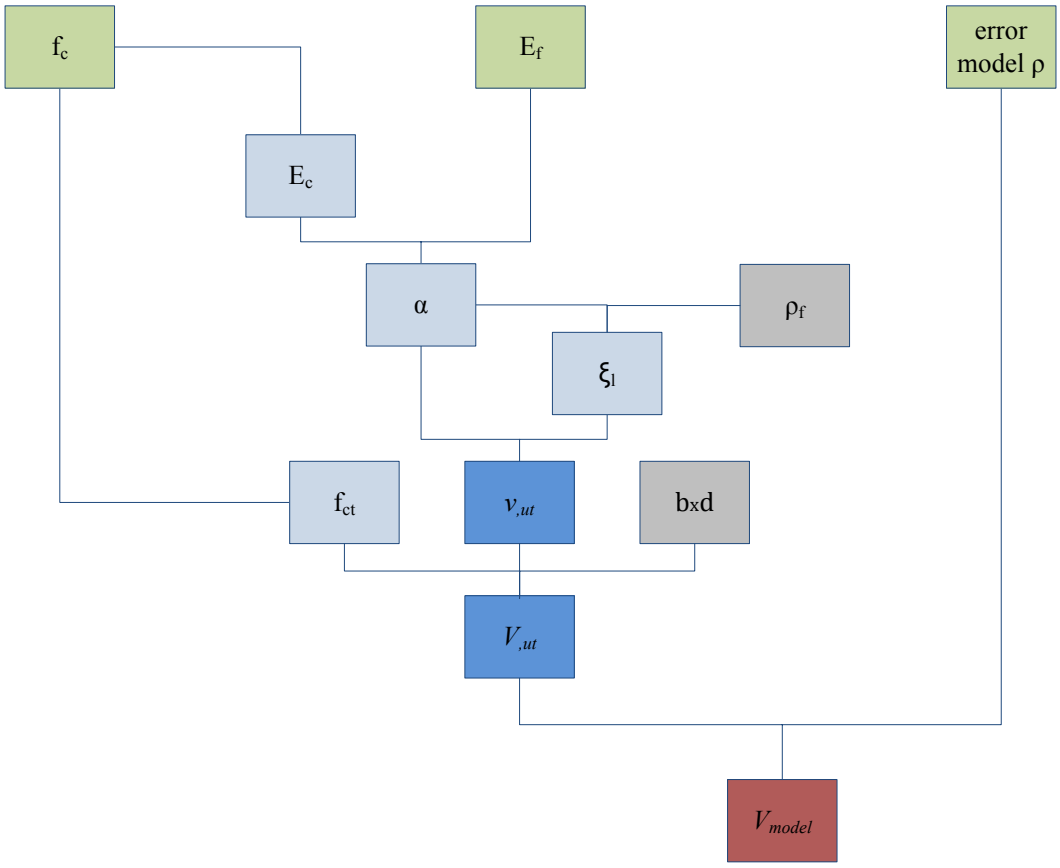

Fig. 7-1: *Basic variables and steps for the computation of the shear strength provided by the model.*

When the shear strength are calculated and random varieties of the load variables are generated, it is possible to set the limit state function (7.1) and thus, performs the simulations:

$$
\begin{aligned}
G' &= \rho' \cdot V'_{model}(f'_c, E'_f) - (V'_p + V'_t) \\
G'' &= \rho'' \cdot V''_{model}(f''_c, E''_f) - (V''_p + V''_t) \\
G''' &= \rho''' \cdot V'''_{model}(f'''_c, E'''_f) - (V'''_p + V'''_t) \\
&\vdots \\
&\vdots \\
G^N &= \rho^N \cdot V^N_{model}(f^N_c, E^N_f) - (V^N_p + V^N_t)
\end{aligned}
\qquad (7.6)
$$

N simulations are performed. If the limit state function is bigger than zero, then the structure is in the safe domain $G \geq 0$, otherwise it is in the unsafe domain $G \leq 0$.

In order to count how many times a failure occurs, the Excel IF function is used: the function returns a value equal to 1 if $G < 0$, 0 if $G \geq 0$. Eventually all the failures are summed, so that the probability of failure can be calculated:

$$P_f = \frac{n}{N} \qquad (7.7)$$

where *n* is the number of failures and *N* the number of trials performed.

7.2.1. Convergence of the simulation

The accuracy of the probability estimates, needless to say, depends heavily on the number of simulations. To assess this accuracy, it should be noted that the estimated probability, *P*, is a random variable itself whose mean, μ_P, and coefficient of variation *COV* are related to the theoretically correct probability P_{true}, by (Nowak and Collins, 2000 (24)):

$$\mu_P = P_{true}; \qquad COV = \sqrt{\frac{1 - P_{true}}{N(P_{true})}} \qquad (7.8)$$

Knowing that P_{true}, although unknown, is relatively small and assuming that the sample size *N*, is large enough so that $P \approx P_{true}$, Equations (7.7) and (7.8) can be combined as:

$$COV \approx \frac{1}{\sqrt{N_f}} \qquad (7.9)$$

Which is used as the indicator of accuracy in this study. Strictly, to calculate the probability of failure, each simulation should be repeated until 400 events of failure are recorded (N_f=400) which corresponds to a $COV = 0{,}05$, a variation deemed small enough to ensure an adequate precision of the calculations. The total number of required simulations hence, should vary approximately from $N = 4 \times 10^4$ (if $P = 1 \times 10^{-2}$) to $N = 4 \times 10^6$ (if $P = 1 \times 10^{-4}$), certainly increasing as the probability of failure decreases. Nonetheless, it has been verified the convergence of P_f for one of the bridges analyzed (*B10RC*), reinforced with the minimum amount of longitudinal reinforcement ($\rho_{min} = 0{,}01$) according to *CNR-DT 203* provisions. It has been calculated the probability of failure on increasing the number of simulations up to $N = 5 \times 10^6$ (**Table 7-1** and **Fig. 7-2**). It has been chosen to perform the simulations up to 5×10^5 trials, obtaining a good accuracy of the results due to the magnitude of the probability of failure.

B10RC - A_{min}	
Number of simulation *N*	Probability of failure P_f
10000	1,260%
50000	1,324%
100000	1,346%
500000	1,279%
1000000	1,279%
5000000	1,291%

Table 7-1: *Values of the probability of failure for B10RC (with minimum reinforcement) on increasing the number of simulations N.*

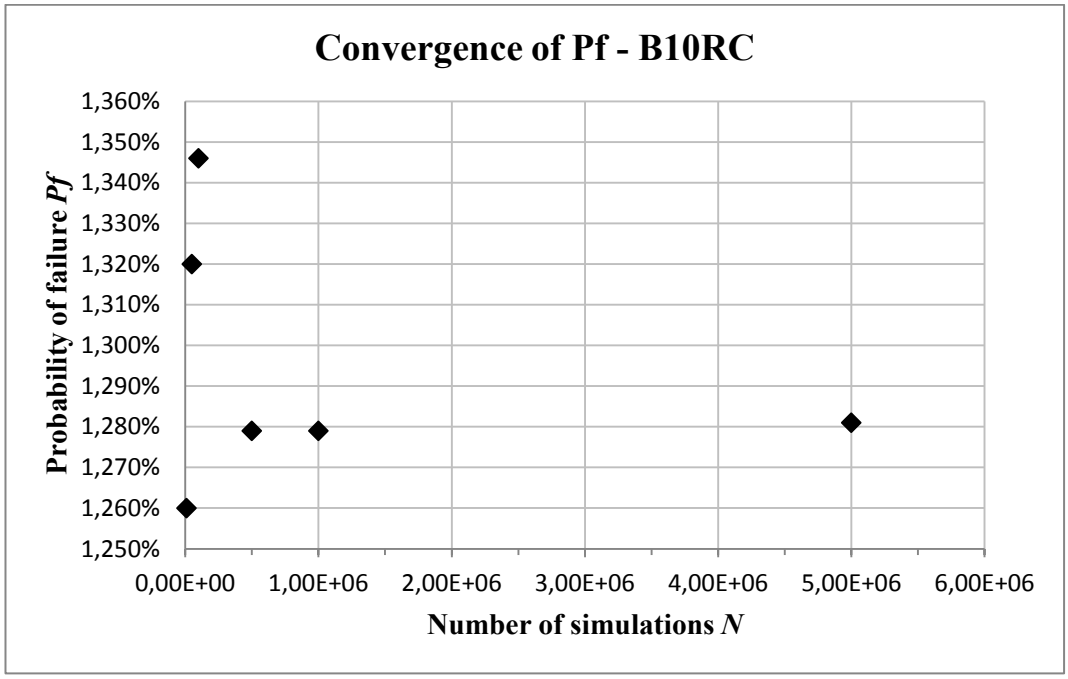

Fig. 7-2: *Convergence of P_f on increasing of number of trials N.*

7.3. Probability of failure

The probability of failure for each analyzed bridge is calculated both considering bridges reinforced with flexural reinforcing FRP bars, and bridges reinforced with the minimum amount required by CNR-DT 203 for elements within shear reinforcement ($\rho_{min} = 0{,}01$).

7.3.1. Girder bridges

In **Table 7-2** are shown the values of probability of failure for girder bridges reinforced with the two different amount of FRP reinforcement. Results obtained are rather different: indeed, probability of failure differs by one or two orders of magnitude in the two cases analyzed. This result is quite obvious, since the

minimum amount of FRP reinforcement provided by the Italian guideline is far greater than that obtained by a flexural design **Table 7-3**.

Girder bridges	*Probability of failure*	
	Flexural reinforcement	*Minimum reinforcement*
B10RC	18,56%	1,28%
B12RC	25,92%	1,14%
B16RC	18,57%	0,52%
B20RC	25,85%	0,36%

Table 7-2: *Probability of failure for girder bridges.*

		Flexural reinforcement	*Probability of failure*	*Minimum reinforcement*	*Probability of failure*
B10RC	**ρ**	0,0062	18,56%	0,0111	1,28%
	A [mm^2]	1990		3582	
	n° of bars	10		18	
B12RC	**ρ**	0,0051	25,92%	0,0102	1,14%
	A [mm^2]	1990		3980	
	n° of bars	10		20	
B16RC	**ρ**	0,0052	18,57%	0,0105	0,52%
	A [mm^2]	2388		5572	
	n° of bars	12		28	
B20RC	**ρ**	0,0046	25,85%	0,0104	0,36%
	A [mm^2]	3184		6766	
	n° of bars	16		34	

Table 7-3: *Probability of failure and amount of FRP reinforcement for girder bridges.*

Probability of failure for bridges reinforced with flexural reinforcement assumes values immoderately high, for this seems reasonable the minimum reinforcement amount provided by the CNR-DT 203; nonetheless, such limit does not provide a sufficient safety level. Indeed girder bridges present a probability of failure on the order of $P_f = \frac{1}{10^2} \div \frac{1}{10^3}$, which is lower, taking into account the type of the structures, for which a reasonable value of the reliability can be assumed around the order of magnitude of $P_f = \frac{1}{10^4} \div \frac{1}{10^5}$.

7.3.2. Slab bridges

Results show nonuniform values of the probability of failure for the three types of slab bridges analyzed. For continuous bridges, (*S1015RC, S1520RC*) probability of failure is calculated for both sections corresponding to the lateral and middle support (**Table 7-4**).

Slab bridges		*Probability of failure*	
		Flexural reinforcement	*Minimum reinforcement*
S10RC		0,08%	0,00%
S1015RC	lateral support	0,08%	0,00%
	middle support	8,49%	0,00%
S15200RC	lateral support	42,27%	0,22%
	middle support	92,40%	23,83%

Table 7-4: *Probability of failure for slab bridges.*

In general, it can be observed that probability of failure assumes values lower than those obtained for girder bridges, except for S1520RC. Even, S10RC

and S1015RC reinforced with the minimum amount, present a zero probability of failure. According to this, it would be tempted to state that slab bridges provide a higher shear strength than girder bridges. Indeed, shear strength provided by the formulation of the studied model is related to the dimensions of the cross section, and for this reason high values of shear strength are obtained. Such issue could be confirmed observing the results obtained for S1520RC. The latter presents a lightened cross-section, and this may be the reason for which the probability of failure is very high.

7.3.3. Further considerations

The values of probability of failure are graphically compared with the ratios V_{Sd}/V_{Rd} , where V_{Sd} and V_{Rd} are respectively the shear force acting on the supports of each beams, calculated according to the Eurocode, and the shear strength calculated according to the two different guidelines and to the model analyzed. It is know that, the inverse of the above ratio is taken as a safety factor.

Therefore, representing in a graph, where the x-axis shows the probability of failure and the axis of ordinates the ratio V_{Sd}/V_{Rd}, it is expected that the higher is the probability of failure P_f the higher is the ratio V_{Sd}/V_{Rd}.

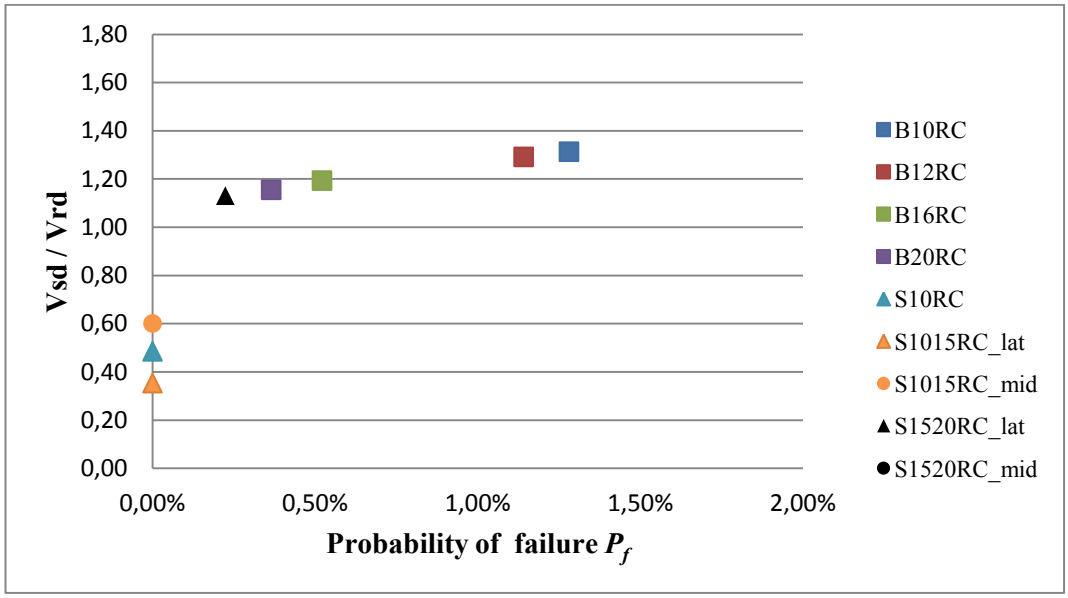

Fig. 7-3: $P_f - (V_{Sd}/V_{Rd})$, *where* V_{Rd} *is calculated according to the model formulation.*

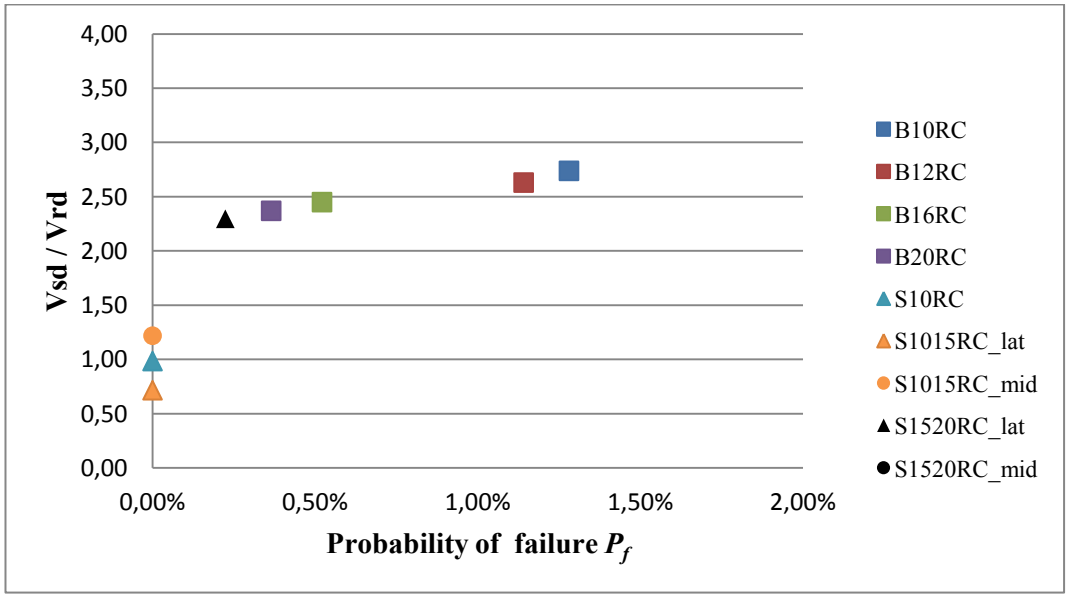

Fig. 7-4: $P_f - (V_{Sd}/V_{Rd})$, *where* V_{Rd} *is calculated according to CNR-DT203/2006.*

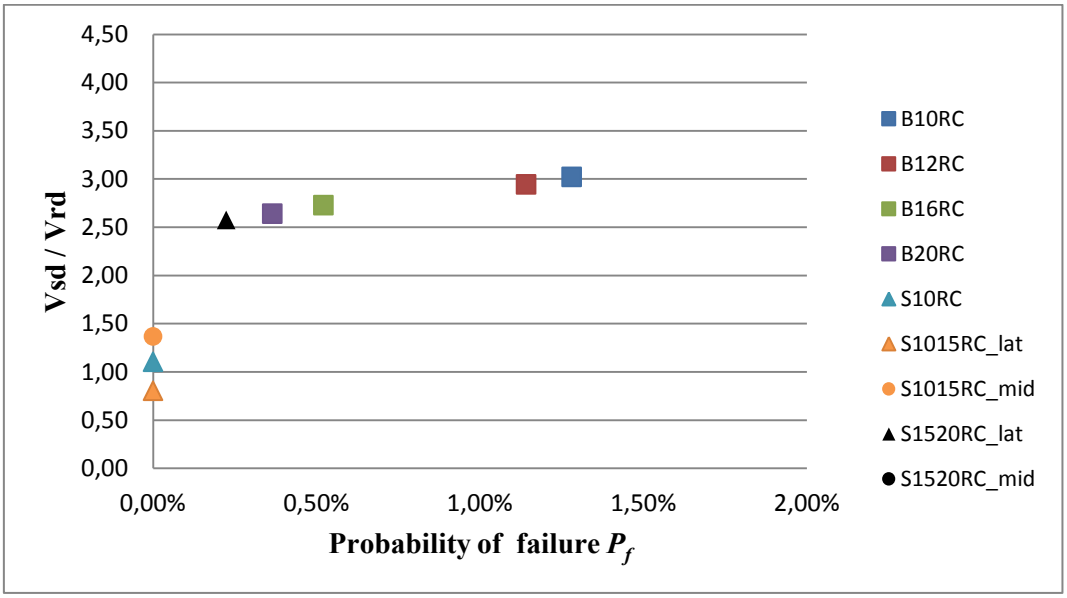

Fig. 7-5: *$P_f - (V_{Sd}/V_{Rd})$, where V_{Rd} is calculated according to ACI440.1R-06.*

The trend shown in the three graphs confirms what supposed above. What changes is the value of the ratio V_{Sd}/V_{Rd}. Values of the shear strength V_{Rd} determined with the American guideline are the lower, as it can be seen by the higher values of V_{Sd}/V_{Rd}. The model provides values closer to unity.

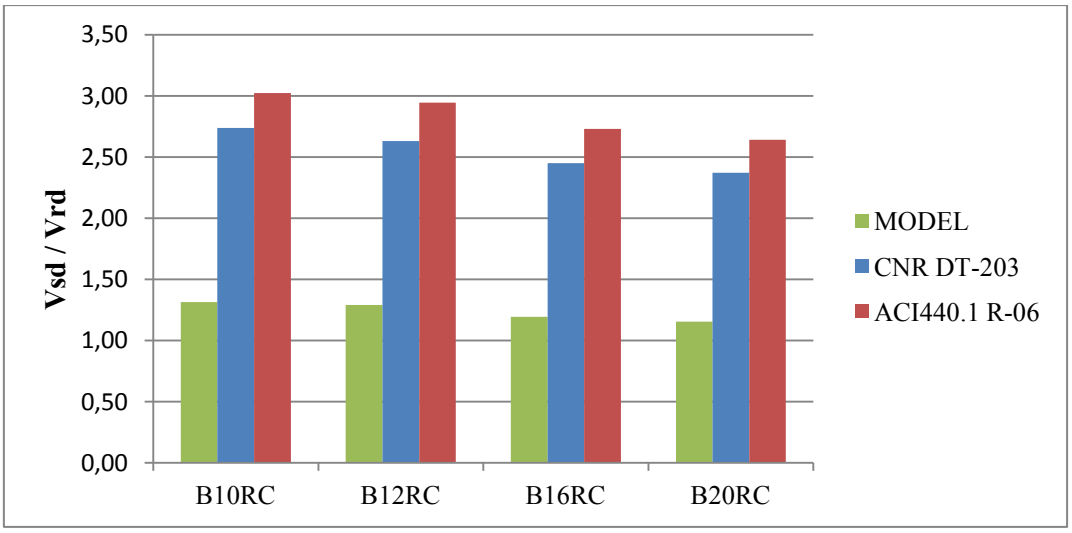

Fig. 7-6: *Shear strength calculated according the two Guideline and to the model formulation.*

Conclusions

A reliability-based analysis was performed to calculate the probability of failure of seven reinforced concrete bridges without shear reinforcement. The bridges analyzed belong to the Spanish catalogue in which are described the most common typologies of existing bridges in Spain. This catalogue was realized with the aim to suggest some standard solutions for cross section geometry and reinforcement amount in order to give a design guideline in a country so far lacking of adequate design codes. Here only the geometric characteristics are taken.

The flexural reinforcement has been designed “ex novo”, by utilizing Carbon Fiber Reinforced Polymer bars, according to Italian guideline CNR-DT 203/2006. The latter provides a minimum amount of longitudinal reinforcement for elements that no present transverse reinforcement. Such provision seems consistent with the results obtained. Indeed, the shear strength offered by studied bridges reinforced with only flexural reinforcement, calculated both according to CNR-DT 203, to the American ACI 440.1R-06 or to the formulation proposed by Marí et al, is much lower than acting shear forces. Nonetheless, providing the minimum amount of longitudinal reinforcement required, which results in all of cases far greater than the flexural amount, a higher shear strength is obviously obtained, but not sufficient, with the exception of some cases. The formulation of the model appears to be the most sensitive to the amount of reinforcement and thus is one which provides the higher values of the shear strength, as states the ratio V_{Sd}/V_{Rd}. Indeed, the main assumption of the model is to consider that, just before failure, the shear force is primarily resisted by the un-cracked concrete compression head. Therefore, the higher is the reinforcement amount, the higher is the shear strength of the beam, because the depth of the concrete compression chord increases with the increment of reinforcement. The lower values of the

shear strength instead, are provided by the American ACI440.1R-06, which confirms to be the more conservative, in line with the experimental results presented in the studied model.

Reliability-based analysis states what has been said so far. In order to calculate the probability of failure a Monte Carlo simulation is performed. The aim was to solve the limit state function, which involves all the variables belonging to the general problem ($R - S \geq 0$) as random variables, each of which with its statistical properties. The Marí's formulation is set within the simulation including the basic variables which affects the shear strength. It has been performed the simulation for the two amounts of reinforcement corresponding to the simply flexural reinforcement and the minimum amount. Probability of failure obtained for the bridges reinforced with the former assumes values unacceptable, in line with what has been said before, that no make sense to comment. From here, the imposition of CNR-DT 203 to provide a minimum amount of longitudinal reinforcement.

Girder and slab bridges reinforced with the minimum amount present different values of the probability of failure. The reliability level offered by the former is not sufficient, above all taking into account the typology and its related importance of the structures at issue. Instead, slab bridges with solid cross-section present a probability of failure close to zero. In fact, for these bridges, the shear strength was much greater than acting shear force. Differently, the slab bridge with lightened cross-section presents a probability of failure extremely high although the section is reinforced with the minimum amount. This is due to the fact that it has been taken into account an effective width of the cross-section which is quite small and this may be the reason why the probability of failure is so high. In conclusion, it is not possible to utilize slab bridges with lightened cross-section without shear reinforcement. The same applies to girder bridges which no offer a sufficient level of safety, related to the class of such structures for which a higher reliability level is required. Instead, the solid slab sections are very safe to shear, even without reinforcement.

Bibliography

1. *Prediction of shear strength of FRP-reinforced cocncrete beams without stirrups based on genetic programming.* **Kara, I. F.** 2011, Advances in Engineering Software, Vol. 42, pp. 295-304.

2. *Shear strength of RC beams and slabs.* **Alkhrdaji, T., et al.** Porto : s.n., 2001, Composite in Construction, pp. 409-414.

3. *Shear tests of FRP-reinforced beams without stirrups.* **Tureyen, A. K. and Frosch, R. J.** 4, 2002, ACI Structural Journal, Vol. 99, pp. 427-434.

4. *Shear strength of FRP-reinforced.* **El-Sayed, A. K., El-Salakawy, E. F. and Benmokrane, B.** 2, 2006, ACI Structural Journal, Vol. 103, pp. 235-243.

5. *Shear capacity of high-strength.* **El-Sayed, A. K., El-Salakawy, E. F. and Benmokrane, B.** 3, 2006, ACI Structural Journal, Vol. 103, pp. 383-389.

6. *Experimental investigation on the effect of longitudinal reinforcement on shear strength on fibrereinforced polymer reinforced concrete beams.* **Alam, M. S. and HusseiN, A.** 3, 2011, Canadian Journal of Civil Engineering, Vol. 38, pp. 243-251.

7. **Advisory Commitee on Techincal Recommendation for Construction.** Guide for the Design and Construction of Concrete Structures Reinforced with Fiber-Reinforced Polymer Bars. Rome, Italy : CNR National Research Council, 2006. CNR-DT203/2006.

8. **ACI Committee 440.** Guide for the Design and Construction of Structural Concrete Reinforced with FRP Bars. s.l. : American Concrete Institute, 2006. ACI4401.R-06.

9. **Canadian Standard Association.** Design and construction of building components with Fiber-Reinforced Polymers. 2002. CAN/CSA S6-02.

10. —. Canadian Highway Bridge Design Code. 2006. CAN/CSA S6-06.

11. **Japan Society of Civil Engineers (JSCE).** Recommendation for design and construction of concrete structures using continuous Fiber Reinforcing Materials. *Concrete Engineering series.* Tokyo, Japan : s.n., 1997. 23.

12. **Casado, C. F.** *Colección oficial de puentes de tramos recto. Tramos de un vano simplemente apoyados.* Madrid : Ministerio de Obras Públicas, 1942.

13. *Shear design of FRP reinforced concrete beams without transverse reinforcement.* **Marí, Antonio, et al.** s.l. : ELSEVIER, 2014, Composites Part B: Engineering, Vol. 57, pp. 228–241.

14. *Strain-based shear strength model for slender beams without web reinforcement.* **Park, H. G., Choi, K. K. and Wight, J. K.** 6, s.l. : ELSEVIER, 2006, ACI Structural Journal, Vol. 103, pp. 783-793.

15. Norme Tecniche per le Costruzioni (NTC 2008). Rome, Italy : s.n., 2008. D.M. 14 gennaio 2008.

16. **European Committee for Standardization (CEN).** Eurocode 0: Basis of Structural Design. Brussels, Belgium : s.n., 2002. EN1990:2002.

17. **Melchers, R. E.** *Structural reliability analysis and Prediction.* 2nd. s.l. : Wiley, 1999.

18. **Schnieder, J.** *Introduction to Safety and Reliability of Structures.* 2nd. Zurich : International Association for Bridge and Structural Engineering (IABSE),, 2006.

19. **Trentin, Caterina.** *Reliability-based calibration of partial safety factors for CFRP strengthening in bending of RC bridges.* Padua : Thesis defenced at Faculty of Civil Engineering of Padua, 2014.

20. *Design philosophy issues of fiber reinforced polymer reinforced concrete structures.* **Pilakoutas, K., Neocleous, K. and Guadagnini, M.** 3, Sheffield : American Society of Civil Engineers (ASCE), 2002, Journal of Composites for Construction, Vol. 6, pp. 154-161.

21. *Development of a probability based load criterion for American National Standard A58.* **Ellingwood, B. R., et al.** Washington : National Bureau of Standards, U.S. Department of Commerce, 1980, NBS Special Publication 577.

22. *Load rating of highway bridges by proof-loading.* **Casas, J. R. e Gomez, J. D.** 3, s.l. : American Society of Civil Engineering (ASCE), 2013, Journal of Civil Engineering, Vol. 17, p. 556-567.

23. *Evaluation of shear design procedures for concrete structures.* **Collins, M. P.** s.l. : CSA Technical Committee on RC Design, 2001.

24. **Nowak, A. S. and Collins, K. R.** *Reliability of Structures, Second Edition.* 2nd. s.l. : CRC Press, 2012.

25. **European Committee for Standardization (CEN).** Eurocode 1: Action on Structures - Traffic Loads on Bridges. Brussels : s.n., 2003. EN1991-2:2003.

26. —. Eurocode 2: Design of concrete structures. Brussels : s.n., 2004. EN1992:2004.

Annex A

Design of the bridges according to CNR-DT 203/2006

The bridges object of study, already introduced in Section, are here described in detail. Are specified the characteristics of the materials, both of concrete and FRP bars used for the flexural design, as well as the loads acting on the bridges. Traffic loads are calculated according to EN 1991-2 (*Eurocode 1: Actions on structures - Part 2: Traffic loads on bridges.*). Acting moment and shear force for continuous bridges are determined by means of a software FEM.

A-I. Materials

A-I-I. Concrete

	Symbols	*Values*	*Units*
Characteristic compressive strength	f_{ck}	20,00	MPa
Partial factor	α	0,85	
Partial safety factor	γ_c	1,5	
Design value	f_{cd}	11,33	MPa
Mean value of compressive strength	f_{cm}	28,00	MPa
Mean value of tensile strength	f_{ctm}	2,21	MPa
Characteristic tensile strength	$f_{ctk(0,05)}$	1,55	MPa
Design value of tensile strength	f_{ctd}	1,03	MPa
Secant modulus of elasticity	E_{cm}	29962	MPa
Design value of the elastic modulus	E_{cd}	24968	MPa
Specific weight	ρ	25,00	kN/m^3

Table 0-1: *Characteristics of concrete, calculated according NTC 08*

A-I-II. CFRP Carbon Fiber Reinforced Polymer bars

Carbon Fiber Reinforced Polymer bars are utilized as longitudinal reinforcement of the bridges analyzed. The CFRP characteristics are taken from a manufacturer factsheet.

	Symbols	*Values*	*Units*
Nominal diameter	Φ	15,9	mm
Nominal cross-section area	A_b	199	mm^2
Ultimate tensile strength	f_{fk}	1103	MPa
Tensile modulus of elasticity	*Ef*	124	GPa
Elongation at ultimate strain	ε_{fk}	0,89	%
Partial factor	γ_f	1,5	
Environmental conversion factor	η_a	1,0	
Conversion factor for long-term effects	η_l	1,0	
Maximum tensile strain	ε_{fd}	0,53	%
Design value of tensile strain	f_{fd}	662,16	MPa

Table 0-2: *Characteristics of CFRP bars: nominal values are taken from manufacturer factsheet, design values are calculated according CNR-DT 203.*

A-I-III. Paving

In order to calculate the permanent load acting on the bridges, it is assumed a value of the specific weight of the road paving:

Specific weight	ρ	20,00	kN/m^3

A-II. Bridges

A-II-I. B10RC

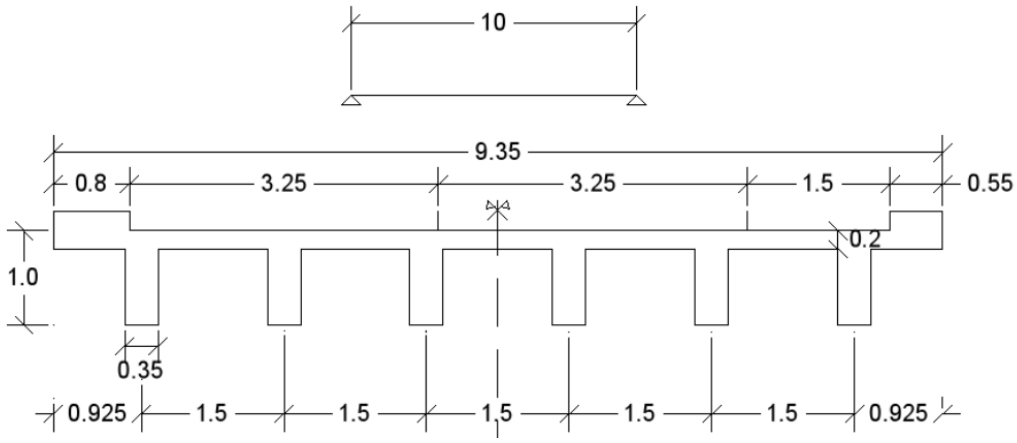

Fig. 0-1: *B10RC cross-section (dimensions in m).*

A-II-I-I. Geometric characteristics of the cross sections

	Symbols	Values	Units
Span length	L	10,00	m
Total bridge width	B	9,35	m
Carriageway width	l_c	8,00	m
Left sidewalk width	b_l	0,80	m
Right sidewalk width	b_r	0,55	m
Beams width	b	0,35	m
Beams depth	h	0,80	m
N° of beams	n	6	
Slab depth	t_s	0,20	m
Sidewalk depth	h_s	0,20	m
Paving depth	t_p	0,08	m
Total area of the cross section	A_t	3,82	m^2

A-II-I-II. Loads

- **Permanent Loads**

DEAD LOADS	*Symbols*	*Values*	*Units*
Reinforced concrete	g_{RC}	95,50	kN/m
Paving	g_p	12,80	kN/m
Guard Rail	g_{gr}	3,00	kN/m
Total distributed Dead Load	g	111,30	kN/m

Partial factor	γ_G	1,35	

- **Variable Loads: Road Traffic Actions**

Notional lanes	*Symbols*	*Values*	*Units*
Carriageway width	l_c	8,00	m
Width of notional lanes	w_c	3,00	m
n° of notional lanes	n_i	2,00	
Width of the remaining area	w_r	2,00	m

	TS	*UDL*
Load Model 1	Q_{ik} *[kN]*	q_{ik} *[kN/m^2]*
Lane 1	300,00	9,00
Lane 2	200,00	2,50
Remaining area	0,00	2,50

Load Model 4		
Crowd loading	q_{fk} *[kN/m^2]*	2,50

TRAFFIC LOADS (UDL)		
Symbols	*Values*	*Units*
q_{1k}	27,00	kN/m
q_{2k}	7,50	kN/m
q_{rk}	5,00	kN/m
q_{fk}	3,38	kN/m
q	42,88	kN/m

TRAFFIC LOADS (TS)		
Symbols	*Values*	*Units*
Q	500,00	kN

Partial factor	γ_Q	1,35	

A-II-I-III. Actions

- **Acting moment**

Characteristic values	*mid span*
Acting moment due to *g [kNm]*	1391,25
Acting moment due to *q [kNm]*	535,94
Acting moment due to *Q [kNm]*	2200,00
Total acting moment *Msd [kNm]*	4127,19

Total factored moment M_{tot}	5571,70	kNm
n° of beams *n*	6,00	
Average moment for each beam M_{sd}	**928,62**	**kNm**

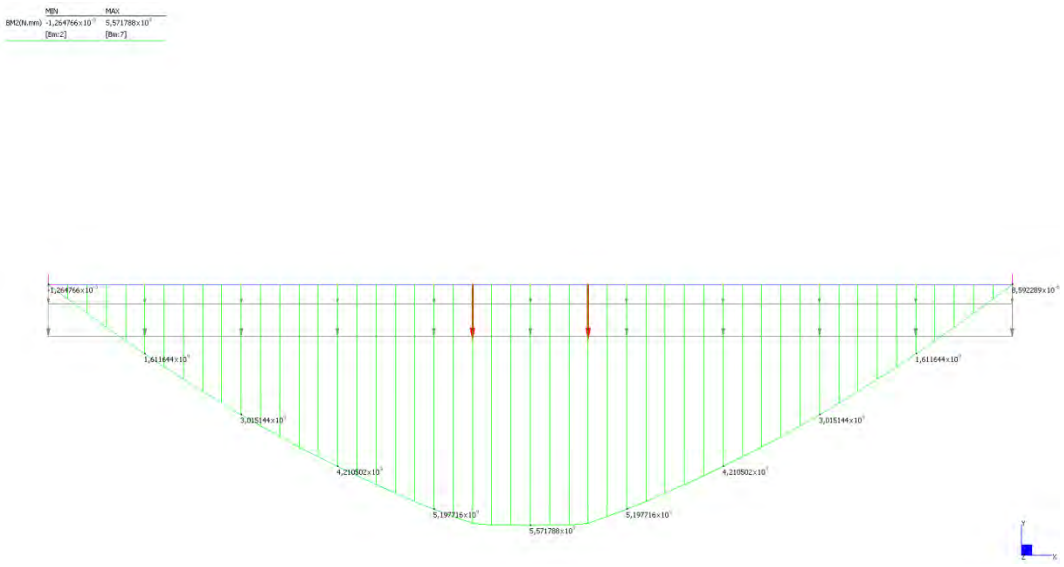

Fig. 0-2: *Maximum acting moment at mid span.*

- **Acting shear force**

Characteristic values	*lateral support*
Acting shear force due to *g [kN]*	556,50
Acting shear force due to *q [kN]*	214,38
Acting shear force due to *Q [kN]*	890,00
Total shear force *Vsd [kN]*	1660,88

Total factored moment V_{tot}	2242,18	kN
n° of beams *n*	6,00	
Average moment for each beam V_{sd}	**373,70**	**kN**

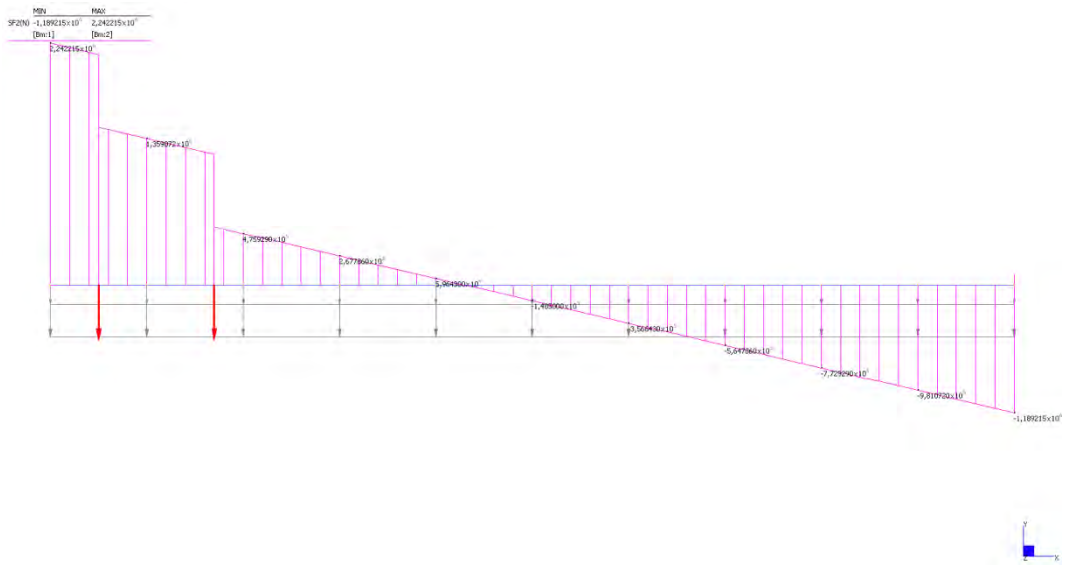

Fig. 0-3: *maximum shear force acting at the support.*

A-II-I-IV. Flexure design

In order to design the flexural reinforcement, it will be considered the single T shape beam:

Depth of the web	h_w	800,00	mm
Width of the web	b_w	350,00	mm
Depth of the flange	h_f	200,00	mm
Width of the flange	b_f	1500,00	mm
Total height	h	1000,00	mm
Effective depth	d	920,00	mm

FLEXURAL REINFORCEMENT	*n° of bars*	*reinforcement area [mm²]*	*neutral axis depth [mm]*	*Resisting Moment [kNm]*
mid span	10	1990	77,51	1161,21

According to CNR-DT 203/06, for elements without shear reinforcement, sufficient longitudinal FRP reinforcement in tension shall be provided that $\rho = A_f/(b \cdot d) \geq 0{,}01$.

MINIMUM REINFORCEMENT	*n° of bars*	*reinforcement area [mm²]*	*neutral axis depth [mm]*	*Resisting Moment [kNm]*
mid span	18	3582	139,52	2016,65

A-II-I-V. Shear strength

		flexural reinforcement [kN]	*minimum reinforcement (CNR-DT203) [kN]*
lateral support	*CNR DT-203*	120,05	136,45
	ACI440.1 R-06	96,18	123,65
	MODEL	211,35	284,53

A-II-II. B12RC

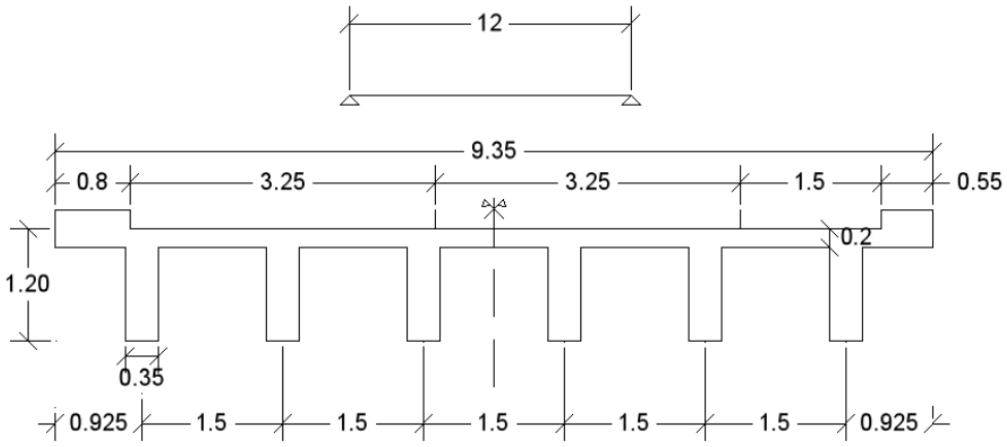

Fig. 0-4: *B12RC cross-section (dimensions in m).*

A-II-II-I. Geometric characteristics of the cross sections

	Symbols	Values	Units
Span length	L	12,00	m
Total bridge width	B	9,35	m
Carriageway width	l_c	8,00	m
Left sidewalk width	b_l	0,80	m
Right sidewalk width	b_r	0,55	m
Beams width	b	0,35	m
Beams depth	h	1,00	m
N° of beams	n	6	
Slab depth	t_s	0,20	m
Sidewalk depth	h_s	0,20	m
Paving depth	t_p	0,08	m
Total area of the cross section	A_t	4,24	m^2

A-II-II-II. Loads

- **Permanent Loads**

DEAD LOADS	*Symbols*	*Values*	*Units*
Reinforced concrete	g_{RC}	106,00	kN/m
Paving	g_p	12,80	kN/m
Guard Rail	g_{gr}	3,00	kN/m
Total distributed Dead Load	g	121,80	kN/m

Partial factor	γ_G	1,35	

- **Variable Loads: Road Traffic Actions**

Notional lanes	*Symbols*	*Values*	*Units*
Carriageway width	l_c	8,00	m
Width of notional lanes	w_c	3,00	m
n° of notional lanes	n_i	2,00	
Width of the remaining area	w_r	2,00	m

	TS	*UDL*
Load Model 1	Q_{ik} *[kN]*	q_{ik} *[kN/m^2]*
Lane 1	300,00	9,00
Lane 2	200,00	2,50
Remaining area	0,00	2,50

Load Model 4		
Crowd loading	q_{fk} *[kN/m^2]*	2,50

TRAFFIC LOADS (UDL)		
Symbols	*Values*	*Units*
q_{1k}	27,00	kN/m
q_{2k}	7,50	kN/m
q_{rk}	5,00	kN/m
q_{fk}	3,38	kN/m
q	42,88	kN/m

TRAFFIC LOADS (TS)		
Symbols	*Values*	*Units*
Q	500,00	kN

Partial factor	γ_Q	1,35	

A-II-II-III. Actions

- **Acting moment**

Characteristic values	*mid span*
Acting moment due to *g [kNm]*	2192,40
Acting moment due to *q [kNm]*	771,75
Acting moment due to *Q [kNm]*	2700,00
Total acting moment *Msd [kNm]*	5664,15

Total factored moment M_{tot}	7646,60	kNm
n° of beams *n*	6,00	
Average moment for each beam M_{sd}	**1274,43**	**kNm**

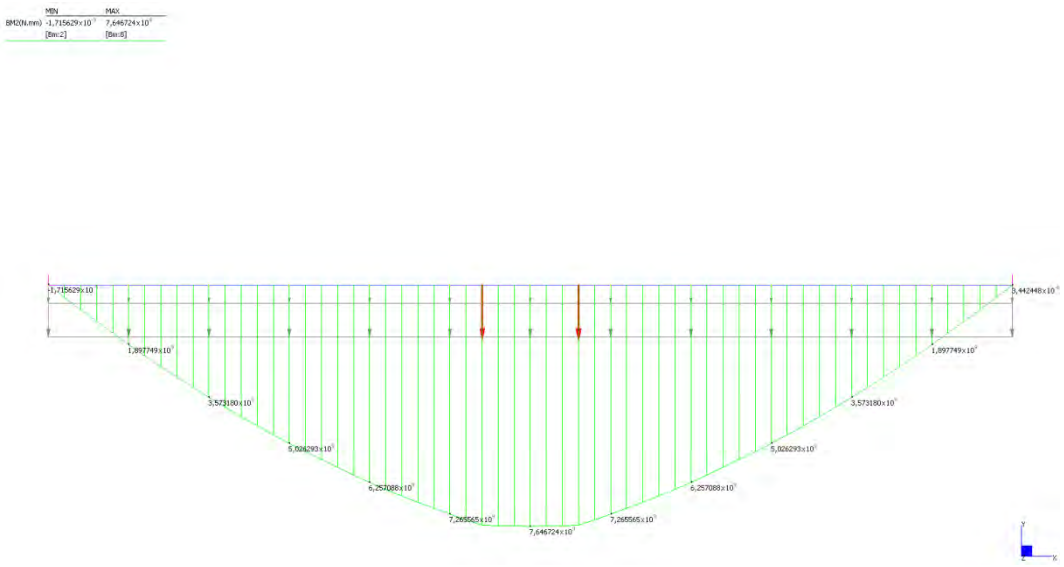

Fig. 0-5: *Maximum acting moment at mid span.*

- **Acting shear force**

Characteristic values	*lateral support*
Acting shear force due to *g [kN]*	730,80
Acting shear force due to *q [kN]*	257,25
Acting shear force due to *Q [kN]*	908,33
Total shear force *Vsd [kN]*	1896,38

Total factored moment V_{tot}	2560,11	kN
n° of beams *n*	6,00	
Average moment for each beam V_{sd}	**426,69**	**kN**

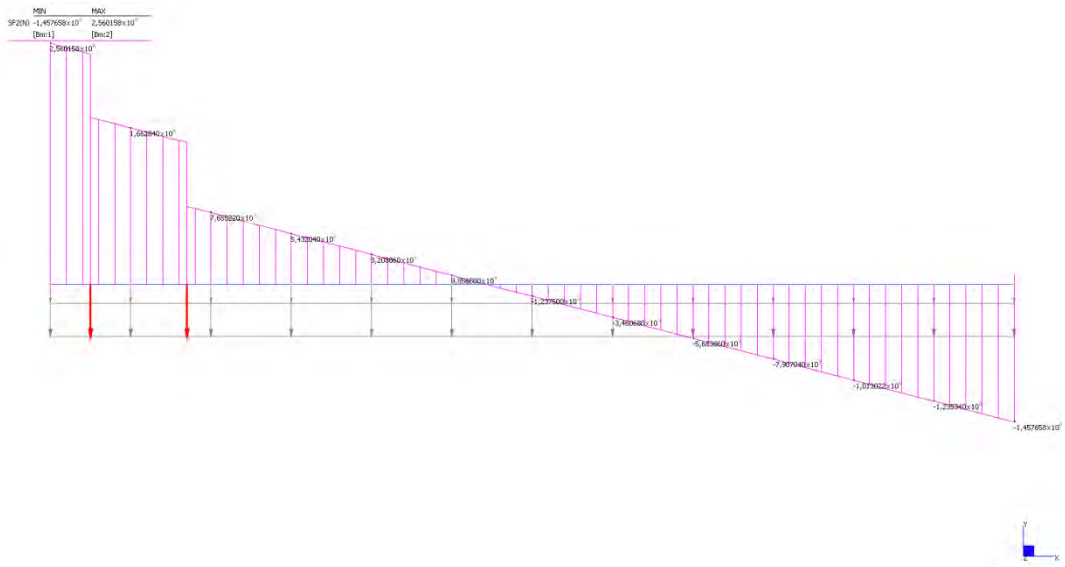

Fig. 0-6: *maximum shear force acting at the support.*

A-II-II-IV. Flexure design

In order to design the flexural reinforcement, it will be considered the single T shape beam:

Depth of the web	h_w	1000,00	mm
Width of the web	b_w	350,00	mm
Depth of the flange	h_f	200,00	mm
Width of the flange	b_f	1500,00	mm
Total height	h	1200,00	mm
Effective depth	d	1120,00	mm

FLEXURAL REINFORCEMENT	*n° of bars*	*reinforcement area [mm²]*	*neutral axis depth [mm]*	*Resisting Moment [kNm]*
mid span	10	1990	77,51	1424,75

According to CNR-DT 203/06, for elements without shear reinforcement, sufficient longitudinal FRP reinforcement in tension shall be provided that $\rho = A_f/(b \cdot d) \geq 0{,}01$.

MINIMUM REINFORCEMENT	*n° of bars*	*reinforcement area [mm²]*	*neutral axis depth [mm]*	*Resisting Moment [kNm]*
mid span	20	3980	155,02	2747,37

A-II-II-V. Shear strength

		flexural reinforcement [kN]	*minimum reinforcement (CNR-DT203) [kN]*
lateral support	*CNR DT-203*	141,69	162,19
	ACI440.1 R-06	107,37	144,88
	MODEL	233,97	330,30

A-II-III. B16RC

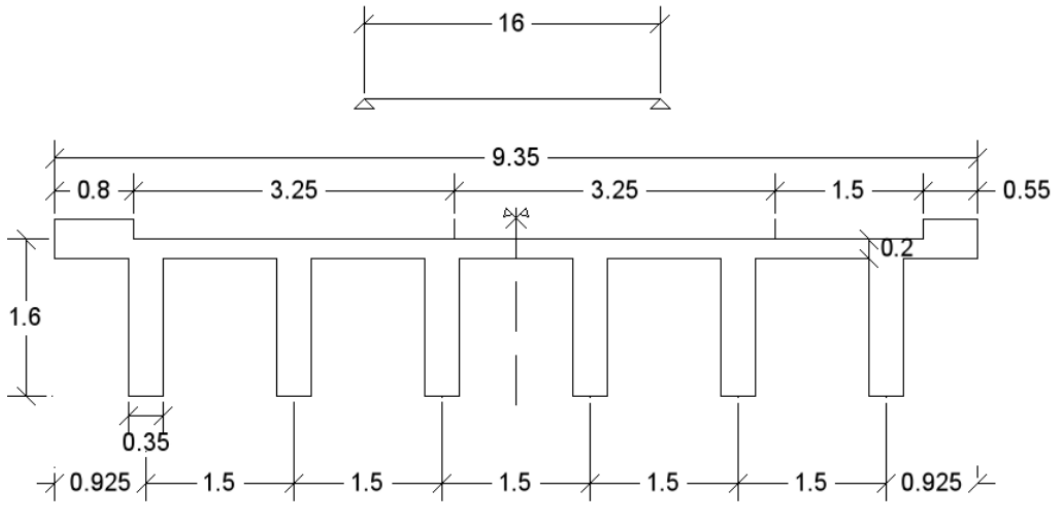

Fig. 0-7: *B16RC cross-section (dimensions in m).*

A-II-III-I. Geometric characteristics of the cross sections

	Symbols	Values	Units
Span length	L	16,00	m
Total bridge width	B	9,35	m
Carriageway width	l_c	8,00	m
Left sidewalk width	b_l	0,80	m
Right sidewalk width	b_r	0,55	m
Beams width	b	0,35	m
Beams depth	h	1,40	m
N° of beams	n	6	
Slab depth	t_s	0,20	m
Sidewalk depth	h_s	0,20	m
Paving depth	t_p	0,08	m
Total area of the cross section	A_t	5,08	m^2

A-II-III-II. Loads

- **Permanent Loads**

DEAD LOADS	*Symbols*	*Values*	*Units*
Reinforced concrete	g_{RC}	127,00	kN/m
Paving	g_p	12,80	kN/m
Guard Rail	g_{gr}	3,00	kN/m
Total distributed Dead Load	g	142,80	kN/m

Partial factor	γ_G	1,35	

- **Variable Loads: Road Traffic Actions**

Notional lanes	*Symbols*	*Values*	*Units*
Carriageway width	l_c	8,00	m
Width of notional lanes	w_c	3,00	m
n° of notional lanes	n_i	2,00	
Width of the remaining area	w_r	2,00	m

	TS	*UDL*
Load Model 1	Q_{ik} *[kN]*	q_{ik} *[kN/m^2]*
Lane 1	300,00	9,00
Lane 2	200,00	2,50
Remaining area	0,00	2,50

Load Model 4		
Crowd loading	q_{fk} *[kN/m^2]*	2,50

TRAFFIC LOADS (UDL)		
Symbols	*Values*	*Units*
q_{1k}	27,00	kN/m
q_{2k}	7,50	kN/m
q_{rk}	5,00	kN/m
q_{fk}	3,38	kN/m
q	42,88	kN/m

TRAFFIC LOADS (TS)		
Symbols	*Values*	*Units*
Q	500,00	kN

Partial factor	γ_Q	1,35	

A-II-III-III. Actions

- **Acting moment**

Characteristic values	*mid span*
Acting moment due to *g [kNm]*	4569,60
Acting moment due to *q [kNm]*	1372,00
Acting moment due to *Q [kNm]*	3700,00
Total acting moment *Msd [kNm]*	9641,60

Total factored moment M_{tot}	13016,16	kNm
n° of beams *n*	6,00	
Average moment for each beam M_{sd}	**2169,36**	**kNm**

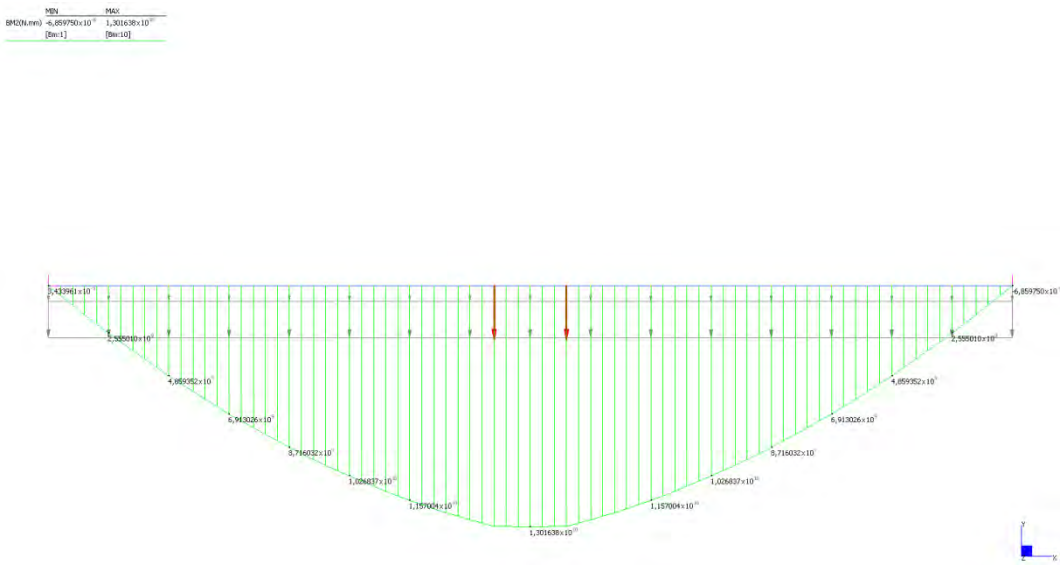

Fig. 0-8: *Maximum acting moment at mid span.*

- **Acting shear force**

Characteristic values	*lateral support*
Acting shear force due to *g [kN]*	1142,40
Acting shear force due to *q [kN]*	343,00
Acting shear force due to *Q [kN]*	931,25
Total shear force *Vsd [kN]*	2416,65

Total factored moment V_{tot}	3262,48	kN
n° of beams *n*	6,00	
Average moment for each beam V_{sd}	**543,75**	**kN**

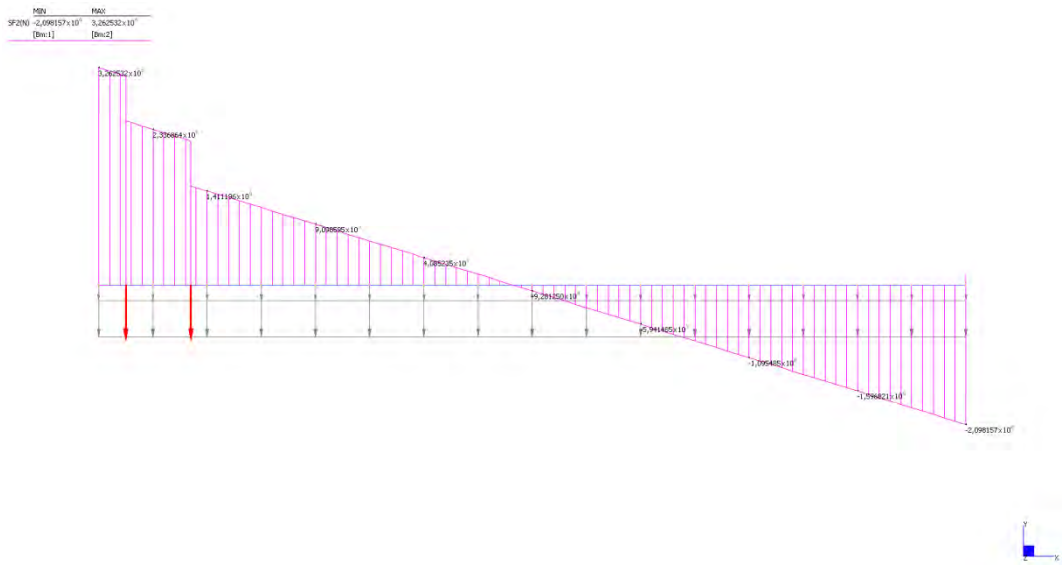

Fig. 0-9: *Maximum shear force acting at the support.*

A-II-III-IV. Flexure design

In order to design the flexural reinforcement, it will be considered the single T shape beam:

Depth of the web	h_w	1400,00	mm
Width of the web	b_w	350,00	mm
Depth of the flange	h_f	200,00	mm
Width of the flange	b_f	1500,00	mm
Total height	h	1600,00	mm
Effective depth	d	1520,00	mm

FLEXURAL REINFORCEMENT	*n° of bars*	*reinforcement area [mm²]*	*neutral axis depth [mm]*	*Resisting Moment [kNm]*
mid span	12	2388	93,01	2329,94

According to CNR-DT 203/06, for elements without shear reinforcement, sufficient longitudinal FRP reinforcement in tension shall be provided that $\rho = A_f/(b \cdot d) \geq 0{,}01$.

MINIMUM REINFORCEMENT	*n° of bars*	*reinforcement area [mm²]*	*neutral axis depth [mm]*	*Resisting Moment [kNm]*
mid span	28	5572	217,03	5076,44

A-II-III-V. Shear strength

		flexural reinforcement [kN]	*minimum reinforcement (CNR-DT203) [kN]*
lateral support	*CNR DT-203*	193,17	221,88
	ACI440.1 R-06	147,74	199,21
	MODEL	322,29	455,55

A-II-IV. B20RC

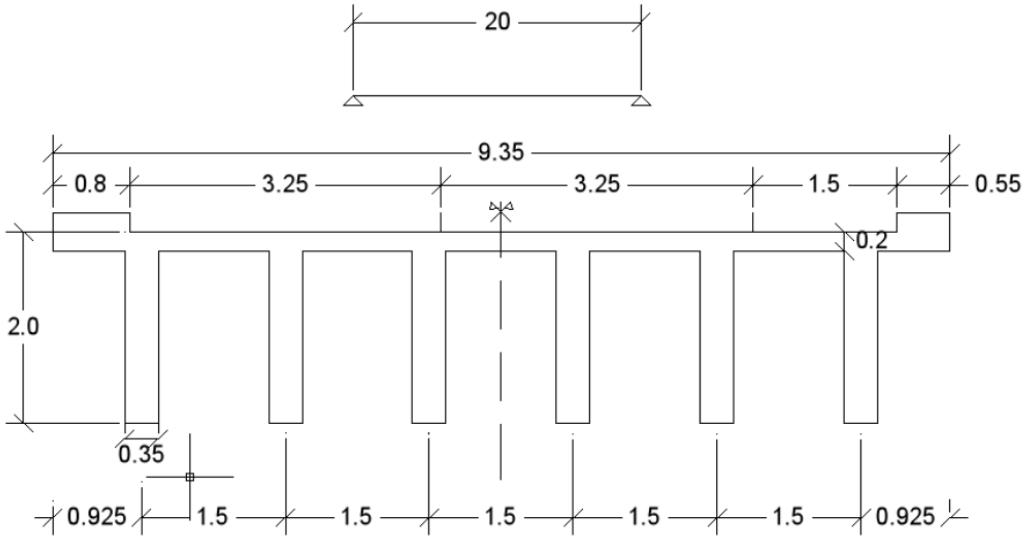

***Fig. 0-10: B20RC** cross-section (dimensions in m).*

A-II-IV-I. Geometric characteristics of the cross sections

	Symbols	*Values*	*Units*
Span length	L	20,00	m
Total bridge width	B	9,35	m
Carriageway width	l_c	8,00	m
Left sidewalk width	b_l	0,80	m
Right sidewalk width	b_r	0,55	m
Beams width	b	0,35	m
Beams depth	h	1,80	m
N° of beams	n	6	
Slab depth	t_s	0,20	m
Sidewalk depth	h_s	0,20	m
Paving depth	t_p	0,08	m
Total area of the cross section	A_t	5,92	m^2

A-II-IV-II. Loads

- **Permanent Loads**

DEAD LOADS	*Symbols*	*Values*	*Units*
Reinforced concrete	g_{RC}	148,00	kN/m
Paving	g_p	12,80	kN/m
Guard Rail	g_{gr}	3,00	kN/m
Total distributed Dead Load	g	163,80	kN/m

Partial factor	γ_G	1,35	

- **Variable Loads: Road Traffic Actions**

Notional lanes	*Symbols*	*Values*	*Units*
Carriageway width	l_c	8,00	m
Width of notional lanes	w_c	3,00	m
n° of notional lanes	n_i	2,00	
Width of the remaining area	w_r	2,00	m

	TS	*UDL*
Load Model 1	Q_{ik} *[kN]*	q_{ik} *[kN/m^2]*
Lane 1	300,00	9,00
Lane 2	200,00	2,50
Remaining area	0,00	2,50

Load Model 4		
Crowd loading	q_{fk} *[kN/m^2]*	2,50

TRAFFIC LOADS (UDL)		
Symbols	*Values*	*Units*
q_{1k}	27,00	kN/m
q_{2k}	7,50	kN/m
q_{rk}	5,00	kN/m
q_{fk}	3,38	kN/m
q	42,88	kN/m

TRAFFIC LOADS (TS)		
Symbols	*Values*	*Units*
Q	500,00	kN

Partial factor	γ_Q	1,35	

A-II-IV-III. Actions

- **Acting moment**

Characteristic values	*mid span*
Acting moment due to *g [kNm]*	8190,00
Acting moment due to *q [kNm]*	2143,75
Acting moment due to *Q [kNm]*	4700,00
Total acting moment *Msd [kNm]*	15033,75

Total factored moment M_{tot}	20295,56	kNm
n° of beams *n*	6,00	
Average moment for each beam M_{sd}	**3382,59**	**kNm**

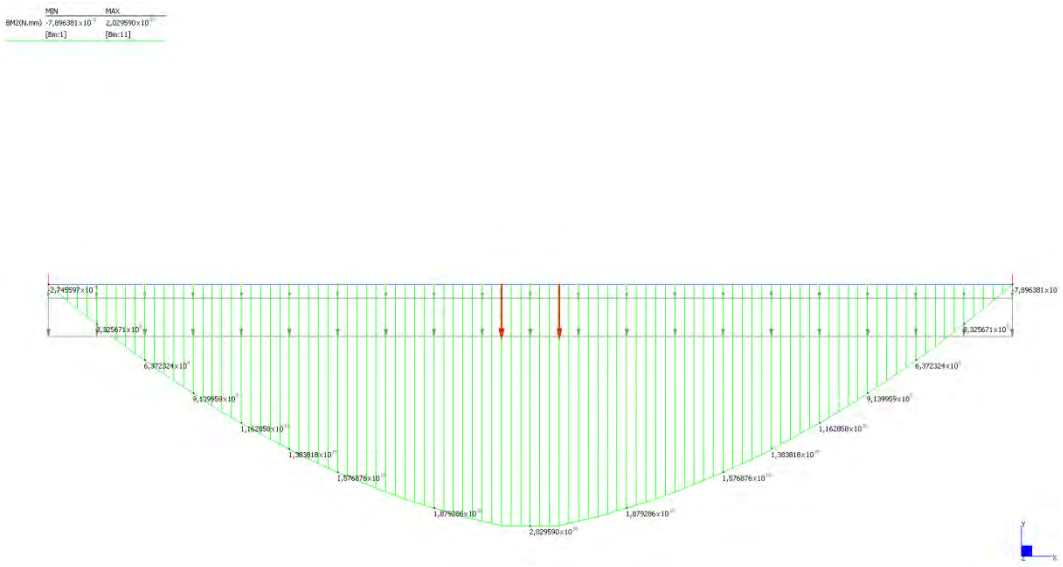

Fig. 0-11: *Maximum acting moment at mid span.*

- **Acting shear force**

Characteristic values	*lateral support*
Acting shear force due to *g [kN]*	1638,00
Acting shear force due to *q [kN]*	428,75
Acting shear force due to *Q [kN]*	945,00
Total shear force *Vsd [kN]*	3011,75

Total factored moment V_{tot}	4065,86	kN
n° of beams *n*	6,00	
Average moment for each beam V_{sd}	**677,64**	**kN**

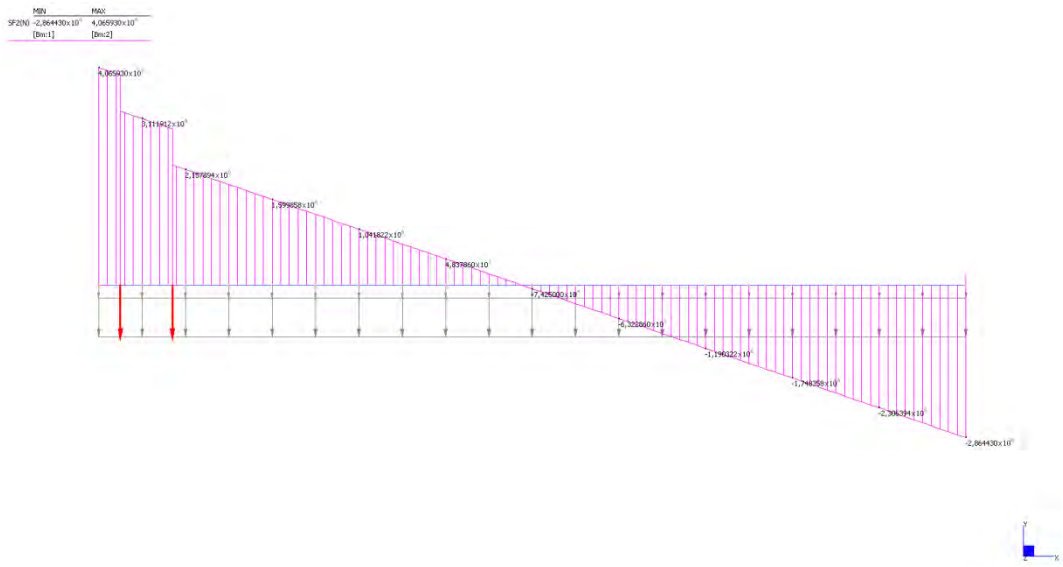

Fig. 0-12: *Maximum shear force acting at the support.*

A-II-IV-IV. Flexure design

In order to design the flexural reinforcement, it will be considered the single T shape beam:

Depth of the web	h_w	1800,00	mm
Width of the web	b_w	350,00	mm
Depth of the flange	h_f	200,00	mm
Width of the flange	b_f	1500,00	mm
Total height	h	2000,00	mm
Effective depth	d	1920,00	mm

FLEXURAL REINFORCEMENT	*n° of bars*	*reinforcement area [mm²]*	*neutral axis depth [mm]*	*Resisting Moment [kNm]*
mid span	16	3184	124,02	3917,23

According to CNR-DT 203/06, for elements without shear reinforcement, sufficient longitudinal FRP reinforcement in tension shall be provided that $\rho = A_f/(b \cdot d) \geq 0{,}01$.

MINIMUM REINFORCEMENT	*n° of bars*	*reinforcement area [mm²]*	*neutral axis depth [mm]*	*Resisting Moment [kNm]*
mid span	34	6766	263,54	7375,39

A-II-IV-V. Shear strength

		flexural reinforcement [kN]	*minimum reinforcement (CNR-DT203) [kN]*
lateral support	*CNR DT-203*	244,88	285,89
	ACI440.1 R-06	180,57	256,56
	MODEL	392,38	586,53

A-II-V. S10RC

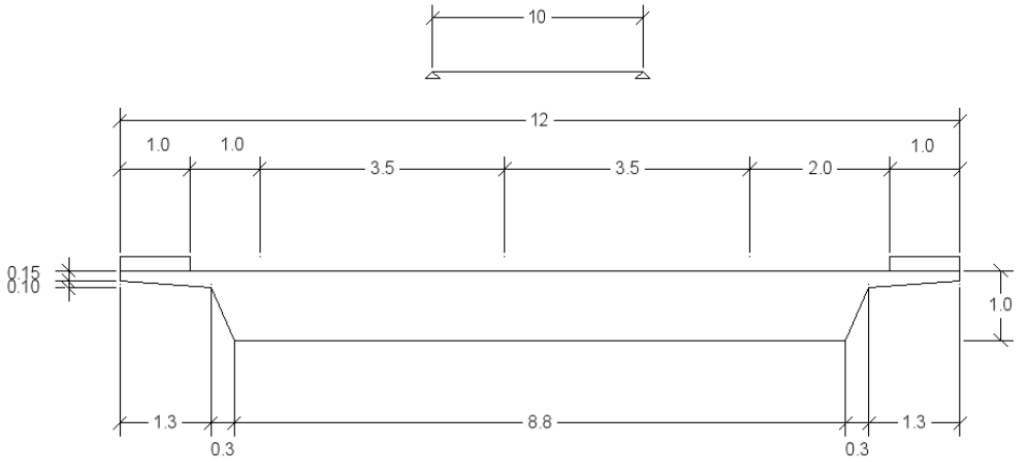

Fig. 0-13: *S10RC cross-section (dimensions in m).*

A-II-V-I. Geometric characteristics

	Symbols	*Values*	*Units*
Span length	L	10,00	m
Total bridge width	B	12,00	m
Carriageway width	l_c	10,00	m
Left sidewalk width	b_l	1,00	m
Right sidewalk width	b_r	1,00	m
Slab depth	h	0.85	m
Sidewalk depth	h_s	0,15	m
Paving depth	t_p	0,08	m
Total area of the cross section	A_t	10,07	m^2

A-II-V-II. Loads

- **Permanent Loads**

DEAD LOADS	*Symbols*	*Values*	*Units*
Reinforced concrete	g_{RC}	252,38	kN/m
Paving	g_p	16,00	kN/m
Guard Rail	g_{gr}	3,00	kN/m
Total distributed Dead Load	g	271,38	kN/m

Partial factor	γ_G	1,35	

- **Variable Loads: Road Traffic Actions**

Notional lanes	*Symbols*	*Values*	*Units*
Carriageway width	l_c	10,00	m
Width of notional lanes	w_c	3,00	m
n° of notional lanes	n_i	3,00	
Width of the remaining area	w_r	1,00	m

	TS	*UDL*
Load Model 1	Q_{ik} *[kN]*	q_{ik} *[kN/m^2]*
Lane 1	300,00	9,00
Lane 2	200,00	2,50
Lane 3	100,00	2,50
Remaining area	0,00	2,50

Load Model 4		
Crowd loading	q_{fk} *[kN/m^2]*	2,50

TRAFFIC LOADS (UDL)		
Symbols	*Values*	*Units*
q_{1k}	27,00	kN/m
q_{2k}	7,50	kN/m
q_{3k}	7,50	kN/m
q_{rk}	2,50	kN/m
q_{fk}	5,00	kN/m
q	49,50	kN/m

TRAFFIC LOADS (TS)		
Symbols	*Values*	*Units*
Q	600,00	kN

Partial factor	γ_Q	1,35	

A-II-V-III. Actions

- **Acting moment**

	mid span
Acting moment due to *g [kNm]*	4579,45
Acting moment due to *q [kNm]*	835,31
Acting moment due to *Q [kNm]*	3564,00
Total acting moment *Msd [kNm]*	8978,77

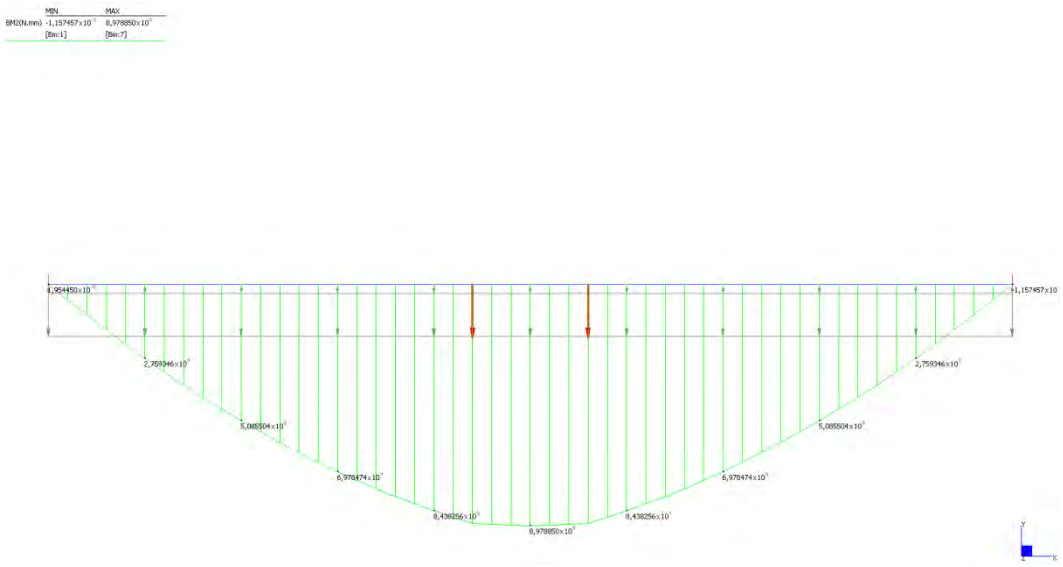

Fig. 0-14: *Maximum acting moment at mid span.*

- **Acting shear force**

	lateral support
Acting shear force due to *g [kN]*	1831,78
Acting shear force due to *q [kN]*	334,13
Acting shear force due to *Q [kN]*	1201,50
Total shear force *Vsd [kN]*	3367,41

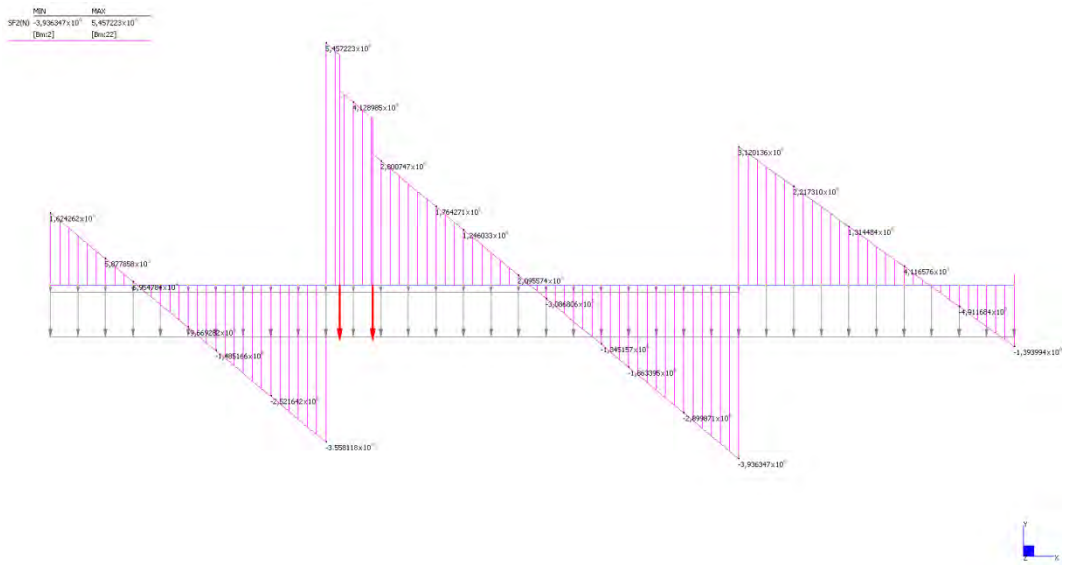

Fig. 0-15: *Maximum shear force acting at the support.*

A-II-V-IV. Flexure design

A simplified T shape section is considered:

Depth of the web	h_w	800,00	mm
Width of the web	b_w	9000,00	mm
Depth of the flange	h_f	200,00	mm
Width of the flange	b_f	12000,00	mm
Total height	h	1000,00	mm
Effective depth	d	920,00	mm

FLEXURAL REINFORCEMENT	*n° of bars*	*reinforcement area [mm²]*	*neutral axis depth [mm]*	*Resisting Moment [kNm]*
mid span	78	15522	75,57	9067,43

According to CNR-DT 203/06, for elements without shear reinforcement, sufficient longitudinal FRP reinforcement in tension shall be provided that $\rho = A_f/(b \cdot d) \geq 0{,}01$.

MINIMUM REINFORCEMENT	*n° of bars*	*reinforcement area [mm²]*	*neutral axis depth [mm]*	*Resisting Moment [kNm]*
mid span	18	83182	404,99	38143,22

A-II-V-V. Shear strength

		flexural reinforcement [kN]	*minimum reinforcement (CNR-DT203) [kN]*
lateral support	*CNR DT-203*	2731,88	3416,78
	ACI440.1 R-06	1491,71	3046,73
	MODEL	3259,90	6938,65

A-II-VI. S1015RC

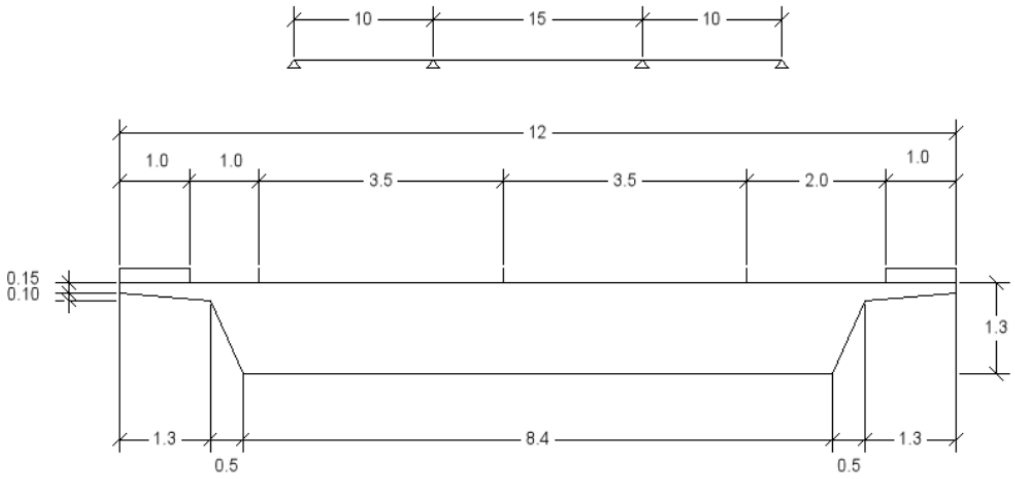

Fig. 0-16: *S1015RC cross-section (dimensions in m).*

A-II-VI-I. Geometric characteristics

	Symbols	*Values*	*Units*
Span length	L	35,00	m
Total bridge width	B	12,00	m
Carriageway width	l_c	10,00	m
Left sidewalk width	b_l	1,00	m
Right sidewalk width	b_r	1,00	m
Slab depth	h	1,15	m
Sidewalk depth	h_s	0,15	m
Paving depth	t_p	0,08	m
Total area of the cross section	A_t	12,62	m^2

A-II-VI-II. Loads

- **Permanent Loads**

DEAD LOADS	*Symbols*	*Values*	*Units*
Reinforced concrete	g_{RC}	315,38	kN/m
Paving	g_p	16,00	kN/m
Guard Rail	g_{gr}	3,00	kN/m
Total distributed Dead Load	g	334,38	kN/m

Partial factor	γ_G	1,35	

- **Variable Loads: Road Traffic Actions**

Notional lanes	*Symbols*	*Values*	*Units*
Carriageway width	l_c	10,00	m
Width of notional lanes	w_c	3,00	m
n° of notional lanes	n_i	3,00	
Width of the remaining area	w_r	1,00	m

	TS	*UDL*
Load Model 1	Q_{ik} *[kN]*	q_{ik} *[kN/m^2]*
Lane 1	300,00	9,00
Lane 2	200,00	2,50
Lane 3	100,00	2,50
Remaining area	0,00	2,50

Load Model 4		
Crowd loading	q_{fk} *[kN/m^2]*	2,50

TRAFFIC LOADS (UDL)		
Symbols	*Values*	*Units*
q_{1k}	27,00	kN/m
q_{2k}	7,50	kN/m
q_{3k}	7,50	kN/m
q_{rk}	2,50	kN/m
q_{fk}	5,00	kN/m
q	49,50	kN/m

TRAFFIC LOADS (TS)		
Symbols	*Values*	*Units*
Q	600,00	kN

Partial factor	γ_Q	1,35	

A-II-VI-III. Actions

- **Acting moment**

	mid span	*middle support*	*lateral span*
Acting moment due to *g [kNm]*	5550,18	7788,75	3013,28
Acting moment due to *q [kNm]*	1011,94	1234,52	711,69
Acting moment due to *Q [kNm]*	3499,57	2089,43	2984,99
Total acting moment *Msd [kNm]*	10061,69	11112,70	6709,96

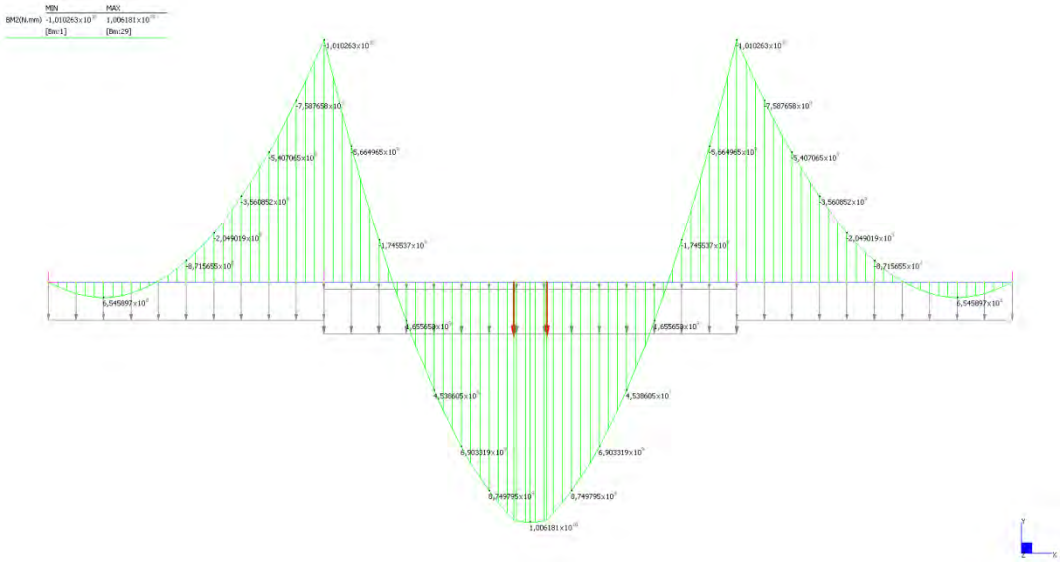

Fig. 0-17: *Maximum acting moment at mid span.*

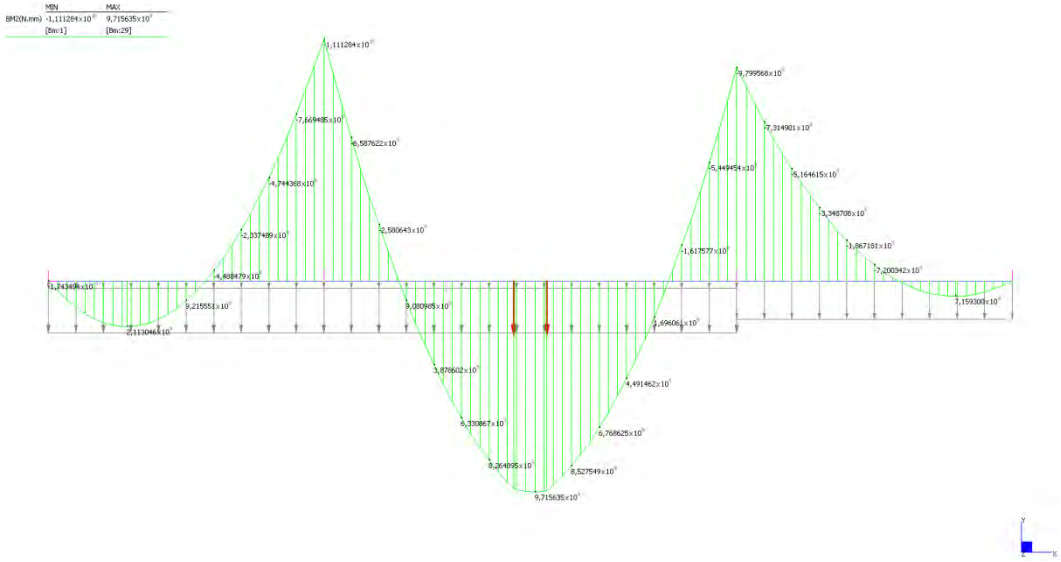

Fig. 0-18: *Maximum acting moment at the middle support (negative moment).*

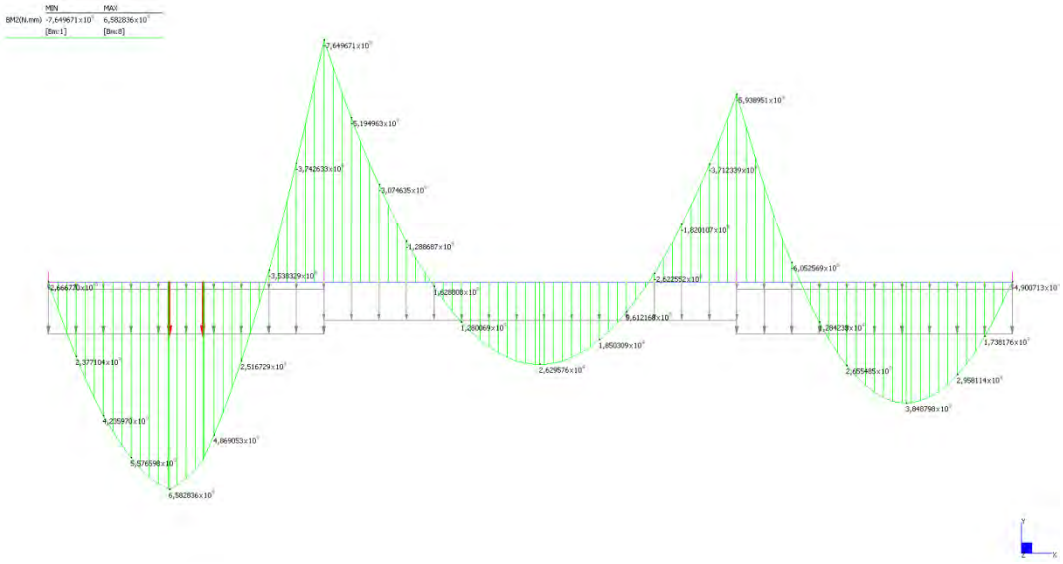

Fig. 0-19: *Maximum acting moment at the lateral span.*

- **Acting shear force**

	middle support	*lateral support*
Acting shear force due to *g [kN]*	3385,60	1497,48
Acting shear force due to *q [kN]*	533,01	308,40
Acting shear force due to *Q [kN]*	1538,62	1403,53
Total shear force *Vsd [kN]*	5457,23	3209,41

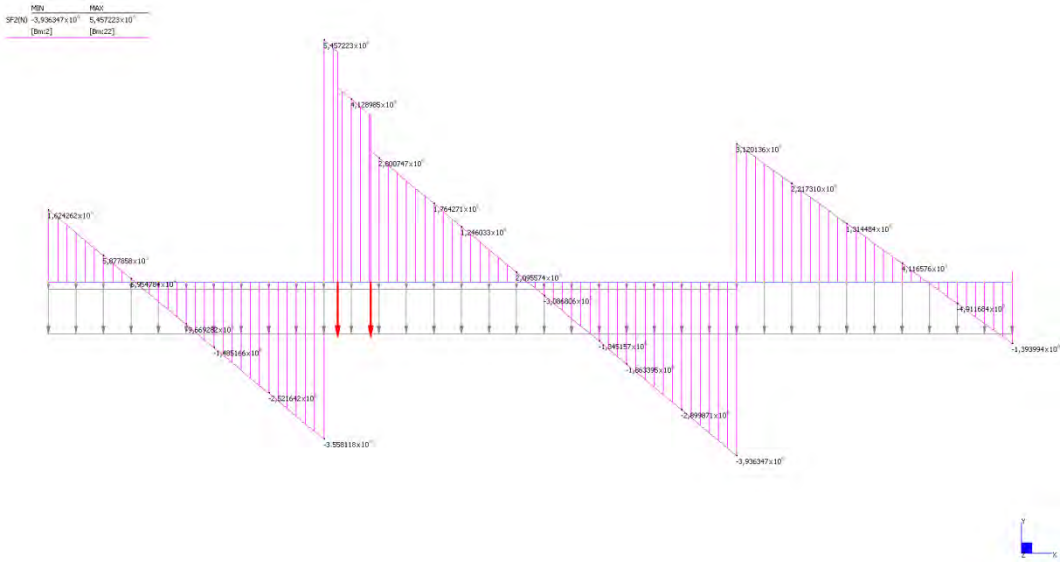

Fig. 0-20: *maximum shear force acting at the middle support.*

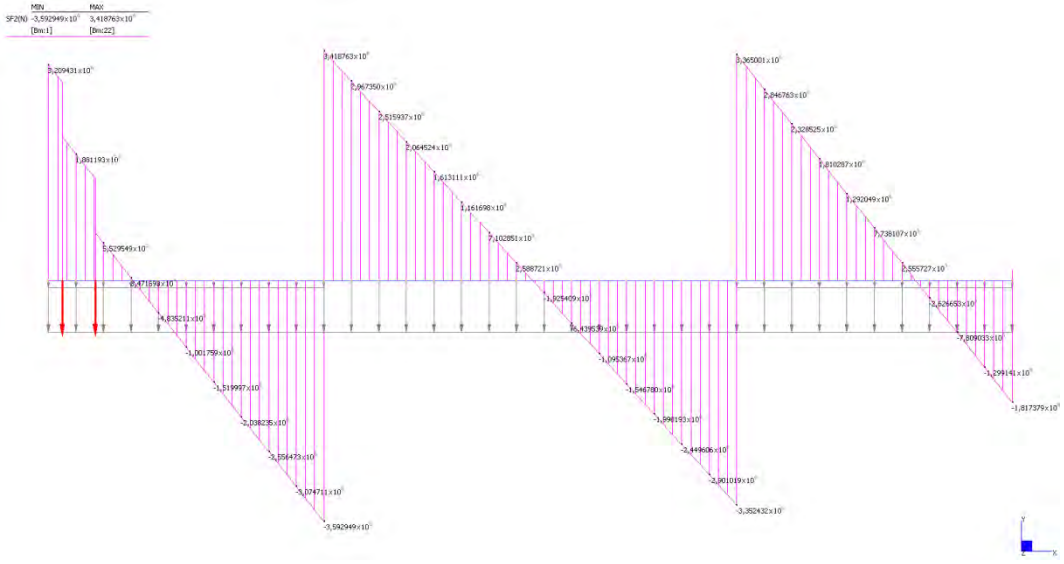

Fig. 0-21: *Maximum shear force acting at the lateral support.*

A-II-VI-IV. Flexure design

A simplified T shape section is considered:

Depth of the web	h_w	1100,00	mm
Width of the web	b_w	8900,00	mm
Depth of the flange	h_f	200,00	mm
Width of the flange	b_f	12000,00	mm
Total height	h	1300,00	mm
Effective depth	d	1220,00	mm

FLEXURAL REINFORCEMENT	*n° of bars*	*reinforcement area [mm²]*	*neutral axis depth [mm]*	*Resisting Moment [kNm]*
mid span	68	13532	65,88	10636,45
middle support	74	14726	96,67	11424,86
lateral span	44	8756	42,63	6949,82

According to CNR-DT 203/06, for elements without shear reinforcement, sufficient longitudinal FRP reinforcement in tension shall be provided that $\rho = A_f/(b \cdot d) \geq 0{,}01$.

MINIMUM REINFORCEMENT	*n° of bars*	*reinforcement area [mm²]*	*neutral axis depth [mm]*	*Resisting Moment [kNm]*
mid span	546	108654	529,02	65443,97
middle support	546	108654	713,28	62115,53
lateral span	546	108654	529,02	65443,97

A-II-VI-V. Shear strength

		flexural reinforcement [kN]	*minimum reinforcement (CNR-DT203) [kN]*
lateral support	*CNR DT-203*	3455,01	4476,20
	ACI440.1 R-06	1323,30	3988,76
	MODEL	3066,74	9080,59
middle support	*CNR DT-203*	3516,53	4476,20
	ACI440.1 R-06	1664,98	3988,76
	MODEL	3705,01	9080,59

A-II-VII. S1520RC

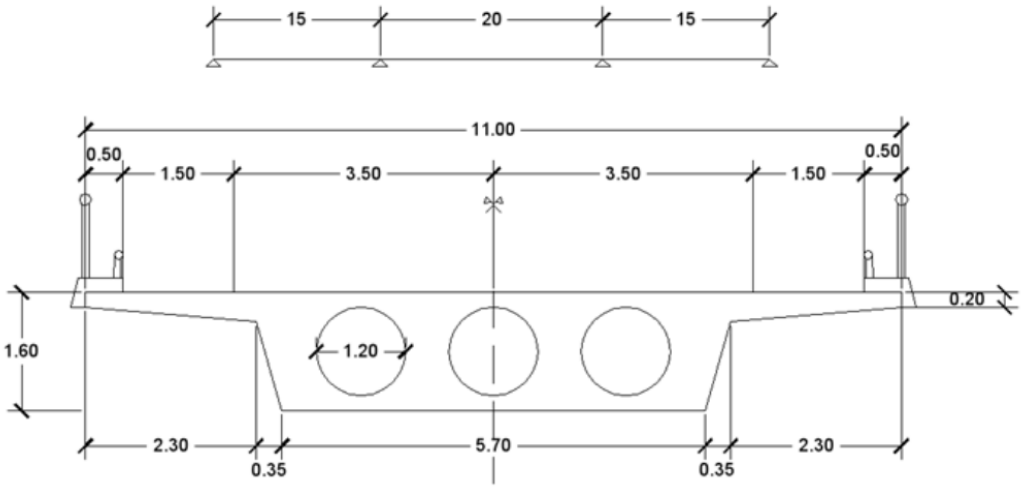

Fig. 0-22: *S1520RC cross-section (dimensions in m).*

A-II-VII-I. Geometric characteristics

	Symbols	*Values*	*Units*
Span length	L	50,00	m
Total bridge width	B	11,00	m
Carriageway width	l_c	10,00	m
Left sidewalk width	b_l	0,50	m
Right sidewalk width	b_r	0,50	m
Slab depth	h	1,40	m
Sidewalk depth	h_s	0,20	m
Paving depth	t_p	0,08	m
Total area of the cross section	A_t	8,14	m^2

A-II-VII-II. Loads

- **Permanent Loads**

DEAD LOADS	*Symbols*	*Values*	*Units*
Reinforced concrete	g_{RC}	203,50	kN/m
Paving	g_p	16,00	kN/m
Guard Rail	g_{gr}	3,00	kN/m
Total distributed Dead Load	g	222,50	kN/m

Partial factor	γ_G	1,35	

- **Variable Loads: Road Traffic Actions**

Notional lanes	*Symbols*	*Values*	*Units*
Carriageway width	l_c	10,00	m
Width of notional lanes	w_c	3,00	m
n° of notional lanes	n_i	3,00	
Width of the remaining area	w_r	1,00	m

	TS	*UDL*
Load Model 1	Q_{ik} *[kN]*	q_{ik} *[kN/m^2]*
Lane 1	300,00	9,00
Lane 2	200,00	2,50
Lane 3	100,00	2,50
Remaining area	0,00	2,50

Load Model 4		
Crowd loading	q_{fk} *[kN/m^2]*	2,50

TRAFFIC LOADS (UDL)		
Symbols	*Values*	*Units*
q_{1k}	27,00	kN/m
q_{2k}	7,50	kN/m
q_{3k}	7,50	kN/m
q_{rk}	2,50	kN/m
q_{fk}	2,50	kN/m
q	47,00	kN/m

TRAFFIC LOADS (TS)		
Symbols	*Values*	*Units*
Q	600,00	kN

Partial factor	γ_Q	1,35	

A-II-VII-III. Actions

- **Acting moment**

	mid span	*middle support*	*lateral span*
Acting moment due to *g [kNm]*	6257,81	9783,05	4823,42
Acting moment due to *q [kNm]*	1762,50	2242,78	1499,48
Acting moment due to *Q [kNm]*	4923,72	2690,28	4617,18
Total acting moment *Msd [kNm]*	12944,03	14716,11	10940,08

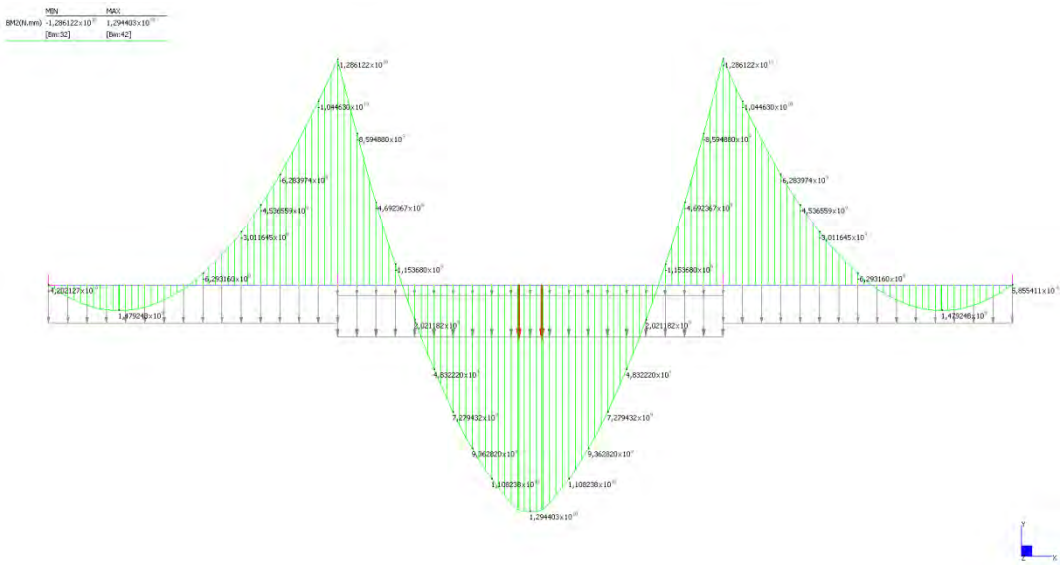

Fig. 0-23: *Maximum acting moment at mid span.*

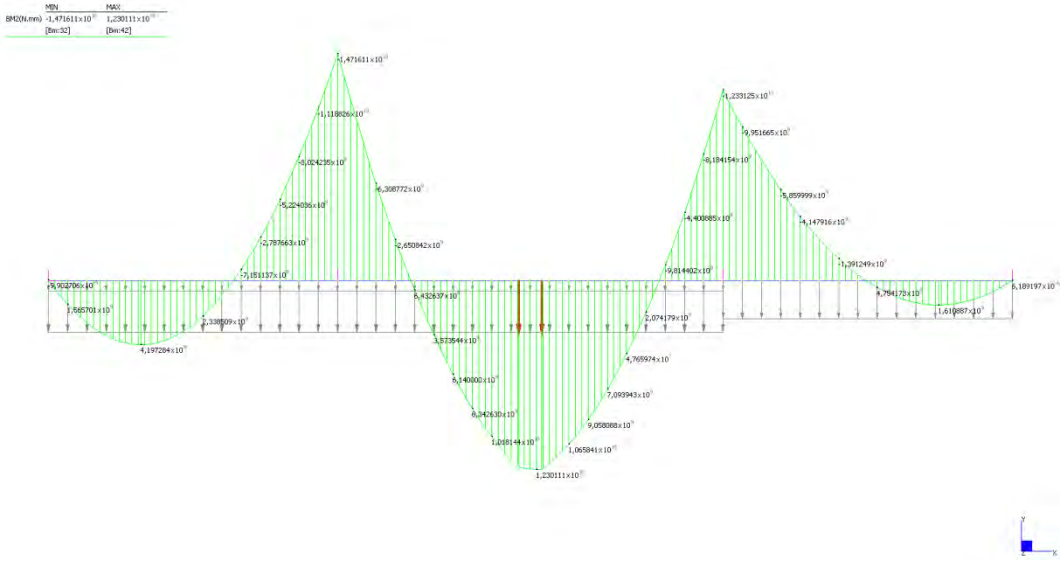

Fig. 0-24: *Maximum acting moment at the middle support (negative moment).*

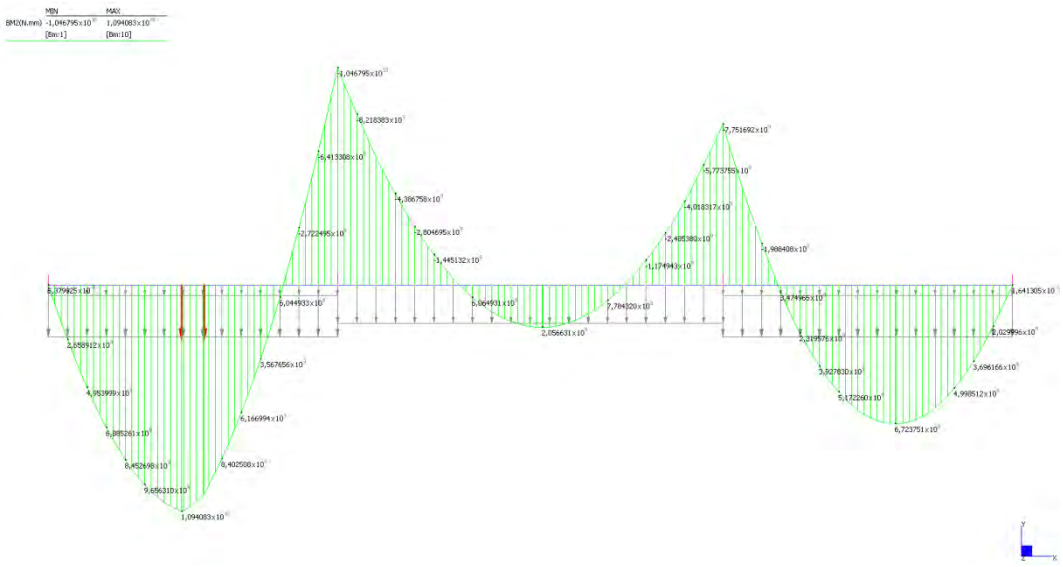

Fig. 0-25: *Maximum acting moment at the lateral span.*

- **Acting shear force**

	middle support	*lateral support*
Acting shear force due to *g [kN]*	3003,75	1620,08
Acting shear force due to *q [kN]*	688,04	436,22
Acting shear force due to *Q [kN]*	1559,32	1473,26
Total shear force *Vsd [kN]*	5251,11	3529,56

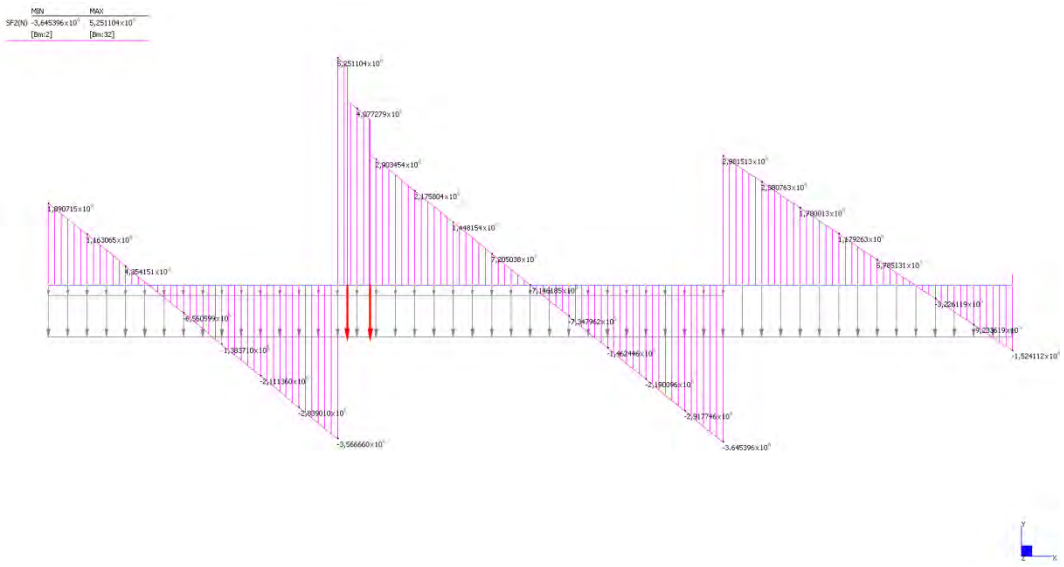

Fig. 0-26: *Maximum shear force acting at the middle support.*

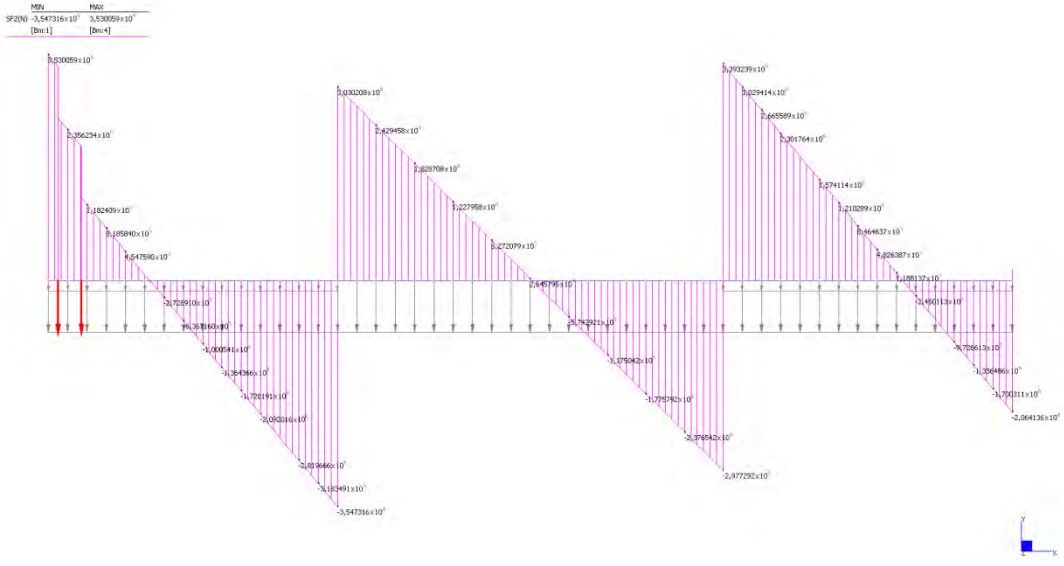

Fig. 0-27: *Maximum shear force acting at the lateral support.*

A-II-VII-IV. Flexure design

A simplified T shape section is considered:

Depth of the web	h_w	1350,00	mm
Width of the web	b_w	2450,00	mm
Depth of the flange	h_f	250,00	mm
Width of the flange	b_f	11000,00	mm
Total height	h	1600,00	mm
Effective depth	d	1520,00	mm

FLEXURAL REINFORCEMENT	*n° of bars*	*reinforcement area [mm²]*	*neutral axis depth [mm]*	*Resisting Moment [kNm]*
mid span	68	13532	71,87	13297,72
middle support	86	17114	408,12	14912,49
lateral span	58	11542	61,30	11382,56

According to CNR-DT 203/06, for elements without shear reinforcement, sufficient longitudinal FRP reinforcement in tension shall be provided that $\rho = A_f/(b \cdot d) \geq 0{,}01$.

MINIMUM REINFORCEMENT	*n° of bars*	*reinforcement area [mm²]*	*neutral axis depth [mm]*	*Resisting Moment [kNm]*
mid span	188	37412	198,71	35193,23
middle support	188	37412	892,18	26603,74
lateral span	188	37412	198,71	35193,23

A-II-VII-V. Shear strength

		flexural reinforcement [kN]	*minimum reinforcement (CNR-DT203) [kN]*
lateral support	*CNR DT-203*	1278,35	1536,73
	ACI440.1 R-06	842,27	1370,30
	MODEL	1822,35	3120,73
middle support	*CNR DT-203*	1319,36	1536,73
	ACI440.1 R-06	955,37	1370,30
	MODEL	2073,15	3120,73